This is to certify that the
dissertation entitled

SYNTHESIS, ENHANCED FUSOGENICITY, AND SOLID STATE NMR MEASUREMENTS OF OLIGOMERIC HIV-1 FUSION PEPTIDE CONSTRUCTS

presented by

RONG YANG

has been accepted towards fulfillment
of the requirements for the

Ph.D. degree in Chemistry

David P. Weliky
Major Professor's Signature

April 27, 2005
Date

SYNTHESIS, ENHANCED FUSOGENICITY, AND SOLID STATE NMR MEASUREMENTS OF OLIGOMERIC HIV-1 FUSION PEPTIDE CONSTRUCTS

By

Rong Yang

A DISSERTATION

Submitted to
Michigan State University
In partial fulfillment of the requirements
For the degree of

DOCTOR OF PHILOSOPHY

Department of Chemistry

2005

ABSTRACT

SYNTHESIS, ENHANCED FUSOGENICITY, AND SOLID STATE NMR MEASUREMENTS OF OLIGOMERIC HIV-1 FUSION PEPTIDE CONSTRUCTS

By

Rong Yang

The HIV-1 fusion peptide (FP) is a ~20 residue sequence at the N-terminus of the viral protein gp41 and plays a key role in catalyzing fusion between viral and target cell membranes. Peptides composed of the FP sequence serve as useful model systems for understanding some aspects of fusion catalysis. The gp41 protein is trimeric and during viral/cell fusion, it is thought that three FPs interact with target cell membranes with their C-termini in close proximity. In an effort to mimic this oligomeric topology in a peptide model system, an FP construct (FPtr) was synthesized with three FP strands chemically bonded at their C-termini through lysine sidechains. The yield is ~1μmol for a 10μmol synthesis. Analytical ultracentrifugation demonstrated that FPtr does not self-associate in aqueous solution and therefore models the expected FP topology of gp41. To assess the effect of the oligomeric strand topology on fusion, comparative functional fusion assays were carried out using FPtr, FPdm (a cross-linked FP dimer construct), and FPmn (FP monomer). The fusion rates (k) varied significantly among the constructs with $k_{tr}>k_{dm}>k_{mn}$ and $k_{tr} \sim 40k_{mn}$. Thus, there is a strong correlation of the fusion rate with C-terminal cross-linking and with the number of strands in the construct.

We applied solid state NMR techniques to characterize the membrane-inserted structure of FPtr, FPdm, and FPmn. The N-terminal secondary structures of these peptides are determined by rotational-echo double-resonance (REDOR) chemical shift

measurements. Our NMR results suggest that HIV-1 fusion peptides may adopt parallel β strand arrangement in the virus' host cell membrane, which is consistent with the existing high-resolution structure of gp41 soluble ectodomain. We proposed that the parallel strand arrangement could be part of the reason for the enhanced fusion rate in FPtr and FPdm because of (1) greater membrane perturbation due to placement of the apolar N-terminal regions of FP strands on one end of the oligomer; and (2) greater local free energy released when multiple FP strands bind to the membrane in close proximity. For fusion peptide constructs inserted into a membrane with different lipid headgroup and cholesterol composition, we observed helical structure in the vicinity of Phe-8, which suggest that secondary structure of fusion peptide is lipid-dependent.

In addition, deuterium NMR is used to probe the specific effect of fusion peptide on lipid motion and structure. Our findings are consistent with a model in which the addition of fusion peptide promotes the formation of curvature in the lipid membranes.

Dedicated to my husband, Guangming Wang.

ACKNOWLEDGMENTS

The guidance and sponsorship from my advisor, Dr. David P. Weliky, is essential for this work. His intelligence and experience have helped me through many difficulties in research. He is very supportive of independent thinking and always encourages me to try out new ideas. His passion for truth is the most precious quality of a scientist. I would also like to thank my committee members, Drs. John L. McCracken, Merling Bruening, Timothy Watson, and John Allison for their support throughout my graduate study.

I am grateful of the generosity of Drs. James Geiger, Honggao Yan, Babak Borhan, David L. DeWitt, and Francis J. Castellino, who have allowed me to use their instruments. I also want to thank Drs. Mary Prorok and Qiuyun Dai who have kindly assisted me in the analytical ultracentrifugation experiments. I am particularly thankful for the help from Dr. Joseph Lecom who rescued our peptide synthesizer numerous times. I appreciate the help from Dr. Alicia Pastor at the MSU Center for Advanced Microscopy. Assistance from the MSU Mass Spectrometry Facility and the Max T. Rogers NMR Facility are also appreciated.

I want to thank my family, particularly my husband, Guangming, for their love and support. My husband came from China to join me, for this reason he gave up his own business and had to start over from learning English and attending school. I cherished the sacrifice and effort he made for the sake of love. After my daughter Shimiao was born, Guangming helped me take care of her for half a year. I also want to thank my parents, who have been taking care of Shimiao in Beijing for two years. Their selfless care for Shimiao provided me a worry-free time to focus on research. I feel guilty with my

daughter since I was not able to accompany her in her early ages. Her leaving pained me very much. However, it also motivated me to work harder in order to complete my degree in order to reunite with her sooner. My mom has brought Shimiao to the U.S a week ago. I am so happy to see them again.

Finally, I would like to thank every former and current member in Dr. Weliky's research team: Dr. Charles Gabrys, Bhagyashree Khunte, Paul Parkanzky, Christian Canlas, Chris Wasniewski, Michele Bonder, Zhaoxiong Zheng, Jason Criscione, Vamshi Cotla, and Qiang Wei. Their collaboration and friendship are very important for me to complete this work.

TABLE OF CONTENTS

LIST OF TABLES

Page

LIST OF FIGURES

Page

CHAPTER III

CHAPTER VIII

LIST OF SYMBOLS AND ABBREVIATIONS

AAA	Amino Acid Analysis
CD	Circular Dichroism
DMAP	4-Dimethylaminopyridine
ESR	Electron Spin Resonance
FID	Free Induction Decay
FMOC	9-Fluorenylmethoxycarbonyl
FP	Fusion Peptide;
FPdm	Fusion Peptide Dimer
FPmn	Fusion Peptide Monomer
FPtr	Fusion Peptide Trimer
FRET	Fluorescence Resonance Energy Transfer
HEPES	*N*-2-hydroxyethylpiperazine-*N*'-2-ethanesulfonic acid
HIV	Human Immunodeficiency Virus
HPLC	High Performance Liquid Chromatography
LM	Lipid Mixture
LUV	Large Unilamellar Vesicles
MALDI	Matrix-Assisted Laser Desorption Ionization
MAS	Magic Angle Spinning
NMR	Nuclear Magnetic Resonance
N-NBD-PE	*N*-(7-nitro-2,1,3-benzoxadiazol-4-yl)-phosphatidylethanolamine
N-Rh-PE	*N*-(lissamine rhodamine B sulfonyl)-phosphatidylethanolamine

PI	Phosphatidylinositol
POPC	1-Palmitoyl-2-oleoyl-sn-glycero-3-phosphocholine
POPE	1-Palmitoyl-2-oleoyl-sn-glycero-3-phosphoethanolamine
POPS	1-Palmitoyl-2-oleoyl-sn-glycero-3-[phospho-L-serine]
REDOR	Rotational Echo Double Resonance
RFDR	Radio Frequency-driven Dipolar Coupling
SDS	Sodium Dodecyl Sulfate
TFA	Trifluoroacetic Acid
TEM	Transmission Electron Microscopy
TPPM	Two Pulse Phase Modulation

CHAPTER I

INTRODUCTION

BACKGROUND

Membrane fusion is an essential process in life. It underlies many physiological functions including egg fertilization, synaptic transmission, insulin secretion, and intracellular protein transport. It is also a key step in the infectious process of enveloped animal viruses. All these functions require transport of materials across the membranes of cells, transport vesicles, organelles, and viruses.

Infection of mammalian cells requires the delivery of the viral gene to host cells, which is made possible when the viral membrane fuses with its target cell membrane, forming a fusion pore, which allows the viral gene to enter its host (cf. Figure 1). Fusion between viral and target cell membranes is mediated by viral envelope proteins, which undergoes conformational changes that bring the two membranes into apposition. It has been hypothesized that the free energy released by the protein's conformational changes is transferred into membrane fusion activation energy and facilitates the merging of two bilayer membranes [1].

Among the many viral infectious diseases, AIDS has been a serious threat to human health in the past three decades. Its infection and spread are dependent on the delivery of the HIV-1 viral RNA to two types of white blood cells: the *T*4 lymphocyte cell and the macrophage cell [2].

HIV-1 viral/host cell fusion is mediated by the viral envelope glycoproteins gp120 and gp41. In particular, the N-terminal region of gp41 (cf. Figure 2), termed the fusion peptide (FP), plays an important role in initiating fusion. Synthetic fusion peptide analogs have been reported to induce vesicle fusion and red blood cell fusion in the absence of the

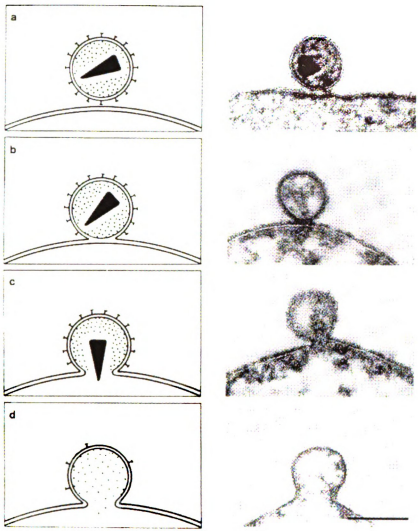

Figure 1 [7]. HIV Infection: (Left) Model of infection process. (Right) Freeze fracture electron micrography of a virion (a) binding to, (b-d) fusing with, and infecting host cell.

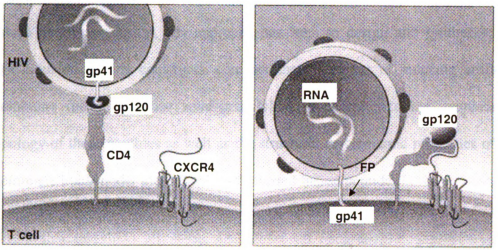

Figure 2 [20]. Model of HIV Infection. FP = fusion peptide region. Time Sequence: left panel, right panel.

rest of gp41 [3-5]. The site-directed mutation/fusion activity relationships are similar for viral/cell fusion and fusion peptide-induced vesicle fusion [6-9]. Information about the HIV-1 fusion peptide-induced membrane fusion is important for understanding HIV infection and for the design of therapeutic and prophylactic strategies. In addition, the fusion protein of many other viruses including influenza and moloney murine leukemia viruses have the similar N-terminal fusion peptide region [10-12], so understanding the HIV-1 fusion peptide should be generally useful for understanding the fusion peptide from these viruses. Furthermore, the mechanism of viral/host cell fusion induced by fusion proteins resembles that of intracellular vesicle fusion mediated by the SNARE proteins [13], so investigating the function of viral fusion proteins may provide additional insight into the understanding of cellular transport processes.

The overall goal of our research is to understand some aspects of the fusion peptide-induced viral/target cell fusion. And my specific aim is to study how the

oligomerization state and secondary structure of HIV-1 fusion peptide affect its ability to induce membrane fusion. My approach has been to design and synthesize oligomeric HIV-1 fusion peptide constructs, compare their activities of inducing artificial bilayer membrane fusion, and use solid-state NMR to characterize the membrane-insertion topology of these peptides as well as the structural and dynamic properties of the bilayer membrane lipids under the influence of inserted fusion peptide.

1. Structural Biology of Viral Envelope Proteins

A biomembrane consists of a fluid phospholipid bilayer intercalated with proteins, carbohydrates, and their complexes. Membrane fusion requires the viruses' and host cells' lipid bilayer to merge into one united whole membrane. There are four steps in viral/host cell membrane fusion [1]: (1) Viral/host cell binding; (2) formation of small fusion pores through which electrolytes can pass; (3) mixing of viral and host cell lipids; (4) formation of a large fusion pore through which larger molecules can pass and creation of a single virus/host cell moiety. In Figure 1[14], step (1), (3), and (4) are illustrated in a series of freeze fracture/electron micrographs which follow the time evolution of HIV virion infection of a host cell. The fusion process is controlled on a temporal and molecular basis such that the host cell remains intact and can serve to the virus.

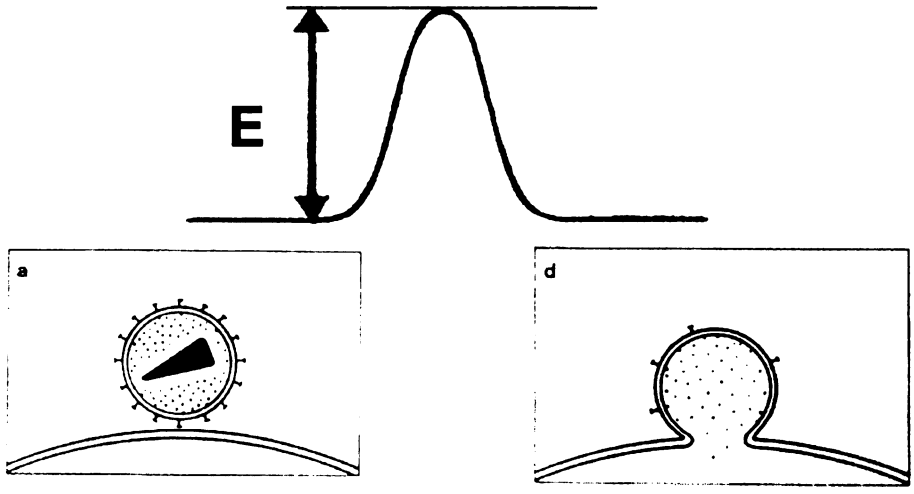

Figure 3. Energy barrier (E) for viral/host cell membrane fusion.

Looking at the fusion process (cf. Figure 1), one would wonder how it start with two membranes and end up with one membrane. The energy of the starting and ending point are approximately the same, whereas there is an energy barrier to cross if the lipids from the two bilayers are going to mix together (cf. Figure 3). It is generally believed that the triggered conformational changes of the viral envelope glycoproteins gp120 and gp41 provide the free energy for the two membranes to merge [15, 16].

On the surface of the HIV-1 virion, gp120 and gp41 form non-covalently bond complexes, with three sets of gp120-gp41 complexes associating as trimer [17]. During the initial step of HIV infection, the gp41-gp120 complex associates with the CD4 receptor and the chemokine receptor (CXCR-4) proteins of target human T or macrophage cells [18, 19]. This interaction is followed by a series of undetermined conformational changes that expose the N-terminus of gp41, termed the fusion peptide, which then inserts into the target cell membrane and catalyzes fusion (cf. Figure 2) [10,

21]. This highly conserved ~ 20 amino acid region is named the "fusion peptide" because mutations or deletions in this region greatly disrupt viral/host cell membrane fusion and infection [6-8]. Additionally, radioactive labeling has demonstrated that the fusion peptide is the only region of the influenza viral fusion protein which inserts deeply into the membrane during fusion [22].

A commonly accepted model [10] predicted that during the conformational change, receptor binding to the gp120 envelope protein moves the gp120 away from gp41 (cf. Figure 4). The fusion peptide of gp41 is exposed and inserted into the target cell membrane. The target cell membrane is drawn towards the host cell membrane by a putative gp41 conformational change from an undetermined structure to the observed coiled-coil gp41 structure. The close proximity of the viral and host cell membranes at a cluster of envelope protein trimers is then believed to lead to viral/host cell membrane fusion. Recent models suggest that there are at least six trimers at the fusion site [23]. This number is in approximate agreement with a recent model of influenza fusion, in which a minimum of eight HAs were predicted at the fusion site [24].

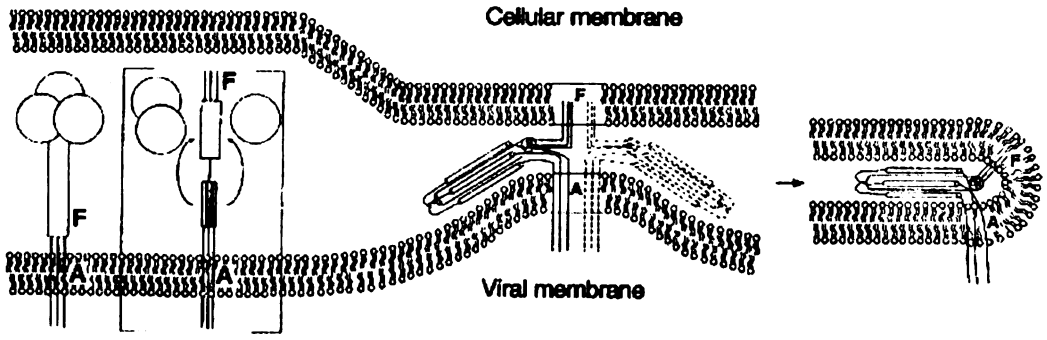

Figure 4 [10]. A model for the interaction with membranes of gp41 and other viral fusion subunits, during membrane fusion. Left, before fusion, viral glycoproteins project their receptor-binding domains (spheres) towards the cellular membrane. Brackets, a conformational change extends the N-terminal fusion peptide (**F**) towards the cellular membrane. Center, after the outer layer of the fusion conformation has assembled, the N-terminal fusion peptides (**F**) and the C-terminal transmembrane anchors (**A**) lie near each other at a site of close apposition of the prefusion membranes. Flexible links between the central rod and the **F** and **A** segments allow variable orientations of the rod with respect to the two membranes. A second trimer, shown in dotted lines, indicates how such trimers might aggregate at their hydrophobic ends at initial sites of fusion. Right, after membrane fusion, both the fusion peptides (**F**) and transmembrane anchors (**A**) are shown in the same membrane, as suggested previously [25-27].

This model is supported by recent high-resolution structural data [10, 28, 29]. Figure 5 [29] displays the ribbon diagram of SIV (simian immunodeficiency virus) and HIV-1 gp41 soluble ectodomain determined by solution NMR and X-ray crystallography. The SIV gp41 is a good model system because its amino acid sequence is highly similar to that of HIV-1 [29]. These structures are believed to correspond to the protein conformations after fusion has occurred and perhaps during fusion as well. The ectodomain of an individual gp41 molecule folds back on itself and the molecules associate as very stable coiled coil trimers [10, 28]. The inferred proximity of the gp41 transmembrane and fusion peptide domains suggests that gp41 may catalyze membrane fusion by bringing the virus and host cell close together [10, 29].

In each of these structures, the proteins are trimeric and the three N-termini (corresponding to about residue 30 in the whole envelope protein) are in close proximity at the end of an in-register helical coiled-coil. Due to the hydrophobicity of the fusion peptide region, it was not included in these soluble constructs. However, these structures end just several residues to the C-terminus of the fusion peptide and they imply that the C-termini of three fusion peptide strands are in close proximity. Therefore it has been hypothesized that at least three fusion peptides insert into the target cell membrane during fusion with their C-termini close to each other.

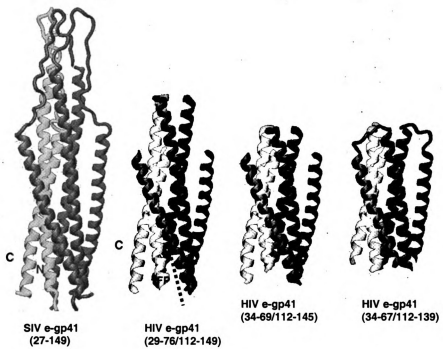

Figure 5 [29]. Comparison of the soluble structure of SIV e-gp41 (ectodomain of gp41) with the X-ray structures of truncated versions of HIV-1 e-gp41. The residue numbering corresponds to that of SIV gp41. The X-ray structures were taken from Weissenhorn et al. [10], Chan et al. [30], and Tan et al. [31].

The gp41 trimeric coiled-coil motif was also observed in the structure of the low pH influenza haemagglutinin and many other viruses [11, 32-34]. This shared motif, together with evidence from mutational studies and findings of multiple trimers/high local fusion peptide concentration at the fusion site[1, 7, 10, 23, 24, 29], suggest a similar membrane fusion mechanism for all of these viruses in which fusion peptide trimerization may be a structural requirement for viral/target cell fusion.

There have been various experiments to investigate fusion peptide trimerization and its effect on the membrane fusion. Recently, enhanced fusion has been observed with

influenza fusion protein constructs which have a similar trimer motif to gp41 and likely contain fusion peptides in the biologically relevant trimeric topology [35, 36]. In addition, solid-state NMR measurements suggested an oligomeric β sheet structure for the HIV-1 fusion peptides associated with phospholipid membrane whose lipid headgroup and cholesterol composition resembles that of the host cell of HIV-1 virus [37, 38]. Jointly, these experiments support the hypothesis that an oligomeric fusion peptide topology may plan an important role in fusion.

Therefore, we thought that it would be useful to study the fusion peptide domain of HIV-1 gp41 as a trimer with the C-termini of three strands chemically cross-linked. We also thought that it would be interesting to compare the fusogenicity of the cross-linked trimer and the previously studied non-cross-linked monomeric fusion peptide.

In our research, we chose to study the free fusion peptide (H-AVGIGALFLGFLGAAGSTMGARS-NH_2) derived from the fusogenic region of the HIV-1 envelope glycoprotein gp41. The free fusion peptide is a good model to study viral/host cell fusion because it causes fusion of lipid vesicles and erythrocytes and because its site-directed mutagenesis/fusion activity relationships are comparable to those of the fusion peptide domain in the intact protein [6-9]. We designed C-terminal cross-linked fusion peptide trimers, which are very likely the lowest order oligomerization state of gp41 during fusion [29]. We also synthesized monomeric and dimeric fusion peptides and compared these peptides' capacity of mediating fusion in an intervesicular lipid mixing assay and examined their structures by solid-state NMR. My studies showed that the trimeric peptide has a 15-40 fold enhanced fusion rate relative to the monomer and also has a reduced activation energy of vesicle fusion. These data suggest that

trimerization of the fusion peptide is important in viral/cell fusion. Our solid state NMR measurements provide further insights into the fusion-active topology of HIV-1 fusion peptide.

2. Solid state NMR measurements of the structure of oligomeric membrane-bound HIV-1 fusion peptide (FP) and the FP-induced membrane bilayer curvature

Solid state nuclear magnetic resonance (NMR) spectroscopy is a novel approach to determine atomic-level structure and dynamics in biological systems. It is particularly applicable to systems which are difficult to characterize with X-ray or solution NMR including membrane, aggregated, and partially ordered proteins. There are two principal advantages of solid state NMR over the more established techniques of X-ray crystallography and solution NMR spectroscopy: (1) crystals are not required and (2) large (>30,000 molecular weight) systems can be studied [39, 40]. Recently, systems including the β-amyloid fibrils implicated in Alzheimer's disease [41, 42], the E. *coli* serine receptor [43], and a HIV-1 peptide/neutralizing antibody complex [44] have been studied by solid state NMR.

The techniques I used include: (1) Rotational-echo double-resonance (REDOR) measurements [45] to probe the secondary structure of membrane associated fusion peptide oligomers; and (2) Deuterium-NMR relaxation measurement to characterize the dynamic properties of membrane lipids. In collaboration with Zhaoxiong Zheng and Michele Bodner, our REDOR experiments revealed predominantly β strand conformation for FPs associated with LM3 (a lipid mixture containing POPC, POPE, POPS, sphingomyelin, PI, and cholesterol in a mol ratio of 10:5:2:2:1:10, which resembles the

lipid headgroup and cholesterol composition in the host cell of HIV-1 [46]) and helical conformation for FPs associated with PC/PG (a lipid mixture containing POPC and POPG in a 4:1 mol ratio). My deuterium-NMR results indicated that the fusion peptide promotes more curvature in the membrane system.

REFERENCE

1. Bentz, J. (2000) *Biophys. J. 78*, 886-900.
2. Haseltine, W. A. and Wong-Stall, F. (1988) in *The Science of AIDS* (Piel, J., Eds.) pp 13-25, W. H. Freeman and Company, New York.
3. Durell, S. R., Martin, I., Ruysschaert, J. M., Shai, Y., and Blumenthal, R. (1997) *Mol. Membr. Biol. 14*, 97-112.
4. Rafalski, M., Lear, J. D., and DeGrado, W. F. (1990) *Biochemistry 29*, 7917-22.
5. Slepushkin, V. A., Melikyan, G. B., Sidorova, M. S., Chumakov, V. M., Andreev, S. M., Manulyan, R. A., and Karamov, E. V. (1990) *Biochem. Biophys. Res. Commun. 172*, 952-7.
6. Freed, E. O., Myers, D. J., and Risser, R. (1990) *Proc. Natl. Acad. Sci. U. S. A. 87*, 4650-4.
7. Freed, E. O., Delwart, E. L., Buchschacher, G. L., Jr., and Panganiban, A. T. (1992) *Proc. Natl. Acad. Sci. U. S. A. 89*, 70-4.
8. Schaal, H., Klein, M., Gehrmann, P., Adams, O., and Scheid, A. (1995) *J. Virol. 69*, 3308-14.
9. Delahunty, M. D., Rhee, I., Freed, E. O., and Bonifacino, J. S. (1996) *Virology 218*, 94-102.
10. Weissenhorn, W., Dessen, A., Harrison, S. C., Skehel, J. J., and Wiley, D. C. (1997) *Nature 387*, 426-30.
11. Fass, D., Harrison, S. C., and Kim, P. S. (1996) *Nat. Struct. Biol. 3*, 465-9.
12. Hernandez, L. R., Hoffman, T. R., Wolfsberg, T. G., and White, J. M. (1996) *Annu. Rev. Cell Dev. Biol. 12*, 965-974.
13. Weber, T., Zemelman, B. V., McNew, J. A., Westermann, B., Gmachl, M., Parlati, F., Sollner, T. H., and Rothman, J. E. (1998) *Cell 92*, 759-772.
14. Grewe, C., Beck, A., and Gelderblom, H. R. (1990) *J. Acquir. Immune. Defic. Syndr. 3*, 965-74.
15. Bentz, J. (2000) *Biophys. J. 78.*
16. Rothman, J. E., and Wieland, F. T. (1996) *Science 272*, 227-34.
17. Kwong, P. D., Wyatt, R., Sattentau, Q. J., Sodroski, J., and Hendrickson, W. A. (2000) *J. Virol. 74*, 1961-1972.

18. Blumenthal, R., and Dimitrov, D. S. (1997) in *Handbook of Physiology, Section 14: Cell Physiology* (Hoffman, J. F., and Jamieson, J. C., Eds.) pp 563-603, Oxford, New York.

19. Lapham, C. K., Ouyang, J., Chandrasekar, N. Y., Dimitrov, D. S., and Golding, H. (1996) *Science 274*, 602-605.

20. Balter, M. (1996) *Science 274*, 1988-1991.

21. Wyatt, R., and Sodroski, J. (1998) *Science 280*, 1884-8.

22. Durrer, P., Galli, C., Hoenke, S., Corti, C., Gluck, R., Vorherr, T., and Brunner, J. (1996) *J. Biol. Chem. 271*, 13417-21.

23. Munoz-Barroso, I., Durell, S., Sakaguchi, K., Appella, E., and Blumenthal, R. (1998) *J. Cell. Biol. 140*, 315-23.

24. Bentz, J. (2000) *Biophys. J. 78*, 227-45.

25. Bullough, P. A., Hughson, F. M., Skehel, J. J., and Wiley, D. C. (1994) *Nature 371*, 37-43.

26. Wharton, S. A., Calder, L. J., Ruigrok, R. W. H., Skehel, J. J., Steinhauer, D. A., and Wiley, D. C. (1995) *EMBO J. 14*, 240-246.

27. Skehel, J. J., Bizebard, T., Bullough, P. A., Hughson, F. M., Knossow, M., Steinhauer, D. A., Wharton, S. A., and Wiley, D. C. (1995) *Cold Spring Harbor Symposia on Quantitative Biology 60*, 573-580.

28. Lu, M., Blacklow, S. C., and Kim, P. S. (1995) *Nat. Struct. Biol. 2*, 1075-82.

29. Caffrey, M., Cai, M., Kaufman, J., Stahl, S. J., Wingfield, P. T., Covell, D. G., Gronenborn, A. M., and Clore, G. M. (1998) *EMBO J. 17*, 4572-84.

30. Chan, D. C., Fass, D., Berger, J. M., and Kim, P. S. (1997) *Cell 89*, 263-73.

31. Tan, K., Liu, J., Wang, J., Shen, S., and Lu, M. (1997) *Proc. Natl. Acad. Sci. U. S. A. 94*, 12303-8.

32. Kobe, B., Center, R. J., Kemp, B. E., and Poumbourios, P. (1999) *Proc. Natl. Acad. Sci. U. S. A. 96*, 4319-24.

33. Baker, K. A., Dutch, R. E., Lamb, R. A., and Jardetzky, T. S. (1999) *Mol. Cell 3*, 309-19.

34. Weissenhorn, W., Carfi, A., Lee, K. H., Skehel, J. J., and Wiley, D. C. (1998) *Mol. Cell 2*, 605-16.

35. Epand, R. F., Macosko, J. C., Russell, C. J., Shin, Y. K., and Epand, R. M. (1999) *J. Mol. Biol. 286*, 489-503.

36. Lau, W. L., Ege, D. S., Lear, J. D., Hammer, D. A., and DeGrado, W. F. (2004) *Biophys. J. 86*, 272-284.

37. Yang, J., Gabrys, C. M., and Weliky, D. P. (2001) *Biochemistry 40*, 8126-37.

38. Yang, J., and Weliky, D. P. (2003) *Biochemistry 42*, 11879-11890.

39. Griffin, R. G. (1998) *Nat. Struct. Biol. NMR Suppl.* 508-12.

40. Marassi, F. M., and Opella, S. J. (1998) *Curr. Opin. Struct. Biol. 8*, 640-8.

41. Lansbury, P. T., Jr., Costa, P. R., Griffiths, J. M., Simon, E. J., Auger, M., Halverson, K. J., Kocisko, D. A., Hendsch, Z. S., Ashburn, T. T., Spencer, R. G., and et al. (1995) *Nat. Struct. Biol. 2*, 990-8.

42. Benzinger, T. L., Gregory, D. M., Burkoth, T. S., Miller-Auer, H., Lynn, D. G., Botto, R. E., and Meredith, S. C. (1998) *Proc. Natl. Acad. Sci. U. S. A. 95*, 13407-12.

43. Wang, J., Balazs, Y. S., and Thompson, L. K. (1997) *Biochemistry 36*, 1699-703.

44. Weliky, D. P., Bennett, A. E., Zvi, A., Anglister, J., Steinbach, P. J., and Tycko, R. (1999) *Nat. Struct. Biol. 6*, 141-5.

45. Gullion, T., and Schaefer, J. (1989) *J. Magn. Reson. 81*, 196-200.

46. Aloia, R. C., Tian, H., and Jensen, F. C. (1993) *Proc. Natl. Acad. Sci. U. S. A. 90*, 5181-5.

CHAPTER II

DESIGN AND SYNTHESIS OF OLIGOMERIC HIV-1 FUSION PEPTIDE CONSTRUCTS

BACKGROUND

In HIV-1 envelope protein gp41, the N-terminal fusion peptide is a key motif in initiating membrane fusion. This hydrophobic region is believed to penetrate into the target cell membrane and initiate fusion. To function properly, the fusion peptide may need to insert into the target membrane with a precise structure. Specifically, formation of a correctly assembled fusion peptide oligomer has been postulated to be a requirement in membrane fusion catalysis [1, 2]. In order to understand how the membrane insertion topology contributes to the perturbations of the lipid bilayer that are necessary for two membranes to fuse, the relevant oligomerization state of FP must be known.

The structure of the truncated HIV-1 gp41 soluble ectodomain has been determined by X-ray crystallography and solution NMR [3, 4] (cf. Figure 6).

Figure 6 [4]. Ribbon diagram of SIV e-gp41 (soluble ectodomain of gp41) viewed from the side with respect to the viral membrane.

These structures end ~ 10 residues C-terminal of the fusion peptide. Due to the bulky, nonpolar residues in the fusion peptide sequence, the peptide fragments that contain it would have significantly increased hydrophobicity. Such peptides tend to aggregate and are difficult to crystallize. Also, when the fusion peptide is bound with bilayer membrane, it is nearly immobilized in the lipids and therefore does not have the fast molecular tumbling property required by solution NMR for line-narrowing. As a result, neither X-ray crystallography nor solution NMR techniques could resolve the structure of membrane bound fusion peptide.

Although the fusion peptide region is not included in the established trimeric structures of the gp41 ectodomain (cf. Figure 6), its likely topology can be imagined, since the C-termini of the fusion peptides are just a few amino acids away from the N-termini of the gp41 soluble ectodomain. In the trimeric coiled-coil structure of the gp41 soluble ectodomain, the close proximity of the N-termini of the three molecules implies that at least three fusion peptides insert into the target cell membrane with their C-termini near each other.

In addition to evidence from envelope protein trimerization, experiments and modeling studies have shown that the fusion site contains multiple trimers and a corresponding high fusion peptide concentration [3-7], which indicate the importance of fusion peptide oligomerization. An important piece of evidence is that the functional disruptive V2E mutation in the gp41 fusion peptide is trans-dominant, i. e. cells expressing 10% mutant protein and 90% wild-type protein exhibit only 40% of the fusion activity of cells with 100% wild-type protein [8]. These data are consistent with a model

in which the mutant peptide disrupts the correct assembly of a functionally essential fusion peptide oligomer [1, 2].

Recently, enhanced fusion has been observed with influenza fusion protein constructs which have a similar trimer motif to gp41 and likely contain fusion peptides in the biologically relevant trimeric topology [9] [10]. In addition, solid state NMR measurements suggest an oligomeric β strand structure for the HIV-1 fusion peptide [11, 12]. Jointly, these experiments support the proposition that an oligomeric topology of the fusion peptide may plan an important role in fusion.

Synthetic peptides are good models for investigating some aspects of the full protein-mediated fusion process. By comparing the effects of similar point mutations in isolated fusion peptides to those studied in intact viruses, many investigators have found direct correlations between the properties of the isolated fusion peptides and the intact fusion proteins [13]. For example, the wild-type HIV-1 fusion peptide was compared with a V2E mutant in which the Val-2 was replaced by Glu-2 [1]. This single substitution in gp41 abolished the fusion activity of the virus, and substantially reduced activity when coexpressed with excess wild type protein [8, 14]. Similarly, while the synthetic wild-type fusion peptide was very fusogenic, the V2E mutant was totally non-fusogenic. In addition, a mixture of the mutant and wild-type peptide was also non-fusogenic.

The advantage of working with small synthetic peptides is that a relatively large quantity of these peptides can be acquired. Also, in spectroscopy there will be no background from the remaining larger portions of the protein.

In most fusion peptide studies to date, the peptides were synthesized as monomers. Aiming at mimicking the biologically relevant trimeric topology of the HIV-1

fusion peptide in its membrane inserted form, we designed and synthesized a fusion peptide analogue composed of three HIV-1 fusion peptide strands cross-linked at their C-termini. We characterized the synthetic peptides' conformation, aggregation, and interaction with membranes.

Our synthetic approach has greatly benefited from incorporating 3 to 6 C-terminal lysine residues to increase the fusion peptide analogues' solubility in aqueous solution. This approach was originally invented by Tamm et al. [15]. The additional positively charged C-terminal lysines significantly increase the hydrophilicity of the fusion peptide. In addition, the lysines minimize self-association of the peptides, which is essential for interpreting their oligomerization-fusogenicity relationship (cf. chapter III).

The trimeric fusion peptide synthetic approach is described in this chapter. In order to delineate the correlation between oligomerization state of fusion peptide and its fusion catalyzing activity, monomeric and dimeric fusion peptide analogues are also synthesized. The solution oligomerization state, fusogenicity and solid state NMR structural measurements on these model peptides will be addressed in Chapters III – VIII.

MATERIALS AND METHODS

Materials. Rink amide resin was purchased from Advanced Chemtech (Louisville, KY). Fmoc-β-Ala-Wang resin, N-α-Fmoc-N-ε-t-butoxycarbonyl-L-lysine (Fmoc-Lys(Boc)), and other 9-fluorenylmethoxycarbonyl (FMOC)-amino acids were obtained from Peptides International (Louisville, KY). N-α-Fluorenylmethoxycarbonyl-N-ε-4-methyltrityl-L-lysine (Fmoc-Lys(Mtt)) was purchased from Calbiochem-Novabiochem (La Jolla, CA). All other reagents were analytical grade.

Fusion Peptide Monomer (FPmn). Monomeric fusion peptides are denoted as FPmn. Several different constructs were synthesized: FP (AVGIGALFLGFLGAAGSTMGARS), FPW (AVGIGALFLGFLGAAGSTMGARSW) FPK3 (AVGIGALFLGFLGAAGSTMGARSKKK), FPCK3 (AVGIGALFLGFLGAAGSTMGARSCKKK), FPCCK3 (AVGIGALFLGFLGAAGSTMGARSCCKKK), FPK3W (AVGIGALFLGFLGAAGSTMGARSKKKW), FPK6W (AVGIGALFLGFLGAAGSTMGARSKKKKKKW), FPCK3W (AVGIGALFLGFLGAAGSTMGARSCKKKW), FPCK6W (AVGIGALFLGFLGAAGSTMGARSCKKKKKKW), and FPCCK3W (AVGIGALFLGFLGAAGSTMGARSCCKKKW). These peptides were synthesized as their C-terminal amides using a peptide synthesizer (ABI 431A, Foster City, CA) equipped for FMOC chemistry. The sequences all contain the 23 N-terminal residues of the LAV_{1a} strain of HIV-1 gp41 and were sometimes followed by cysteine(s) for cross-linking and/or three to six lysines for enhanced solubility and/or a tryptophan as a uv/vis chromophore [15]. Peptides were cleaved from the resin in a three hour reaction using a mixture of TFA:H_2O:phenol:thioanisole:ethanedithiol in a 33:2:2:2:1 volume ratio. Peptides were subsequently purified by reversed-phase HPLC using a preparative C_{18} column (Vydac, Hesperia, CA) and a water/acetonitrile gradient containing 0.1% TFA. Mass spectroscopy was used to verify peptide purity. Isotopically labeled forms of the peptides FP23K3W and FP23CK3W were also synthesized with a ^{13}C carbonyl label at Phe-8 and a ^{15}N label at Leu-9.

Fusion Peptide Dimer (FPdm). Figure 7 (a) displays the cross-linking reaction

schemes. Peptides at ~ 5 mM concentration were cross-linked in 10 mM pH 8.2 DMAP buffer which was open to the atmosphere. Cross-linking was completed within one day. FPdm dimers were formed in a solution containing monocysteine peptide. Cross-linked FPdm were purified by reversed-phase HPLC with higher mass peptides eluting at higher acetonitrile concentrations. Cross-linked peptide masses were checked using SDS gels and mass spectrometry.

(a)

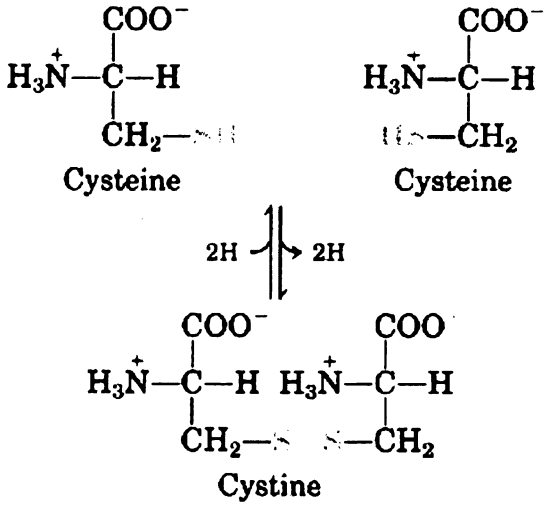

(b)

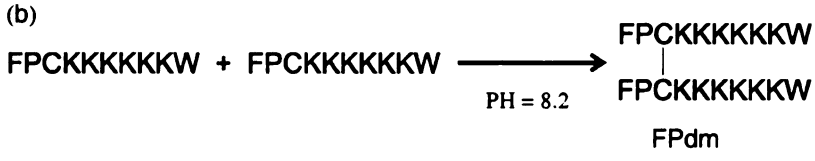

Figure 7. (a) The Cysteine cross-linking reaction [16]. (b) Formation of FPdm by Cysteine cross-linking.

Fusion Peptide Trimer (FPtr)

Method 1. By Cysteine Cross-linking (with one strand out of register). As displayed in Figure 8, the first version of FPtr was formed in a solution containing dicysteine peptide and monocysteine peptide in a 1: 4 ratio.

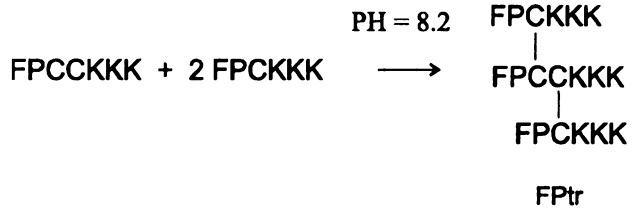

Figure 8. Cysteine cross-linking reaction to form FPtr (with one strand out of register).

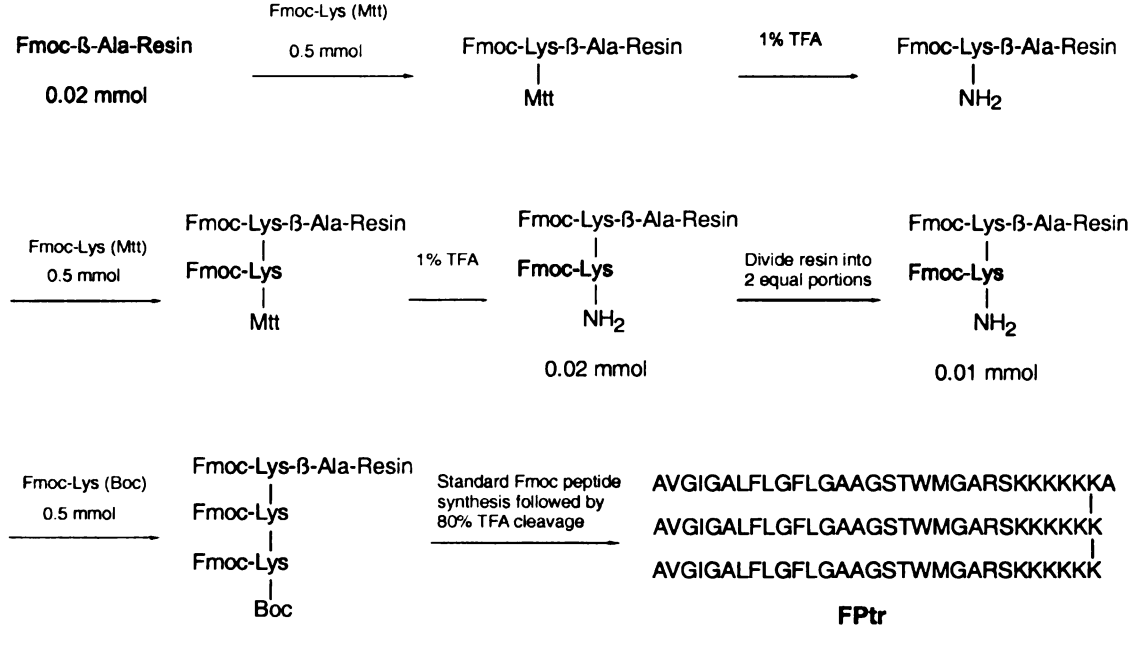

Figure 9. FPtr synthesis scheme (in-register trimer).

Method 2. By Lysine Scaffold (all strand in register). Figure 9 displays the scheme for creating the trimer scaffold with coupling through amino groups on lysine sidechains [17, 18]. Each Fmoc-Lys(Mtt) was added in a two hour coupling step using a peptide synthesizer and the standard Fmoc chemistry for the instrument. After each

addition, the resin was taken out of the synthesizer reaction vessel and the Mtt protecting group on the lysine sidechain was removed by gentle mixing in 4 mL of a 1:5:94 mixture of trifluoroacetic acid (TFA):triisopropylsilane (TIS):dichloromethane (DCM). The mixing in the 1% TFA solution was done for two minutes and was followed by removal of the solution by filtration and a resin wash with DCM. The 1% TFA reaction/filtration/DCM wash cycle was repeated six times. The clear TFA solution became yellow when added to the resin and this yellow color was less intense with each subsequent cycle.

After addition of each Fmoc-Lys(Mtt) and removal of its Mtt group, the trimer scaffold was completed by addition of Fmoc-Lys(Boc) on the peptide synthesizer with standard Fmoc chemistry and two hour coupling time. FPtr synthesis was then continued on the synthesizer using standard chemistry and included addition of non-native lysines to improve aqueous solubility and tryptophans as 280 nm chromophores for peptide quantitation. Each amino acid was coupled for four hours and coupling was followed by acetylation of free NH_2 groups to terminate any unreacted strands. The isotopically labeled amino acids 1-^{13}C Fmoc-Phe and ^{15}N Fmoc-Leu were incorporated into the peptide at Phe-8 and Leu-9, respectively. After completion of the synthesis, peptides were cleaved from the resin in a three hour reaction using a mixture of TFA:H_2O:phenol:thioanisole:ethanedithiol in a 33:2:2:2:1 ratio. Peptides were subsequently purified by reversed-phase HPLC using a C_{18} column and a water:acetonitrile gradient which varied from 80:20 to 20:80 ratios. FPtr mass was checked using mass spectrometry and analytical ultracentrifugation.

RESULTS AND DISCUSSION

FPmn. Figure 10 (a) displays the 280-nm detected chromatogram of FPCK3W.

FPdm. Figure 10 (b) displays the 280-nm detected reversed-phase chromatogram of the products formed by cross-linking of FPCK3W. The main peak corresponds to the FPdm dimer. Peak identification was made by mass spectrometry (cf. Figure 10) with supporting evidence that under the same chromatographic conditions, the FPCK3W eluted at lower acetonitrile concentration than FPdm.

FPtr (one strand out of register). Figure 10 (c) displays the 220-nm detected chromatogram of the cross-linking products formed from the reaction of FPCCK3W and FPCK3 in a 1:4 ratio. The largest peak corresponds to the FPdm dimmer, and the last peak corresponds to FPtr trimer. In terms of increasing hydrophobicity, the molecules can be ordered FPmn, FPdm, and FPtr, and this also matches the ordering of the acetonitrile concentration at elution. Additional evidence for the trimer assignment was by detection of the chromatogram at 280 nm, as displayed in Figure 10 (d). In this chromatogram, the FPdm and FPtr peaks have approximately equal intensity. The peak intensities in panels (c) and (d) are qualitatively consistent with 220-nm detection of all FPtr and FPdm and 280-nm detection of all FPtr and only FPdm containing at least one FPCCK3W strand.

The identification of FPtr was also made by mass spectrometry (cf. Figure 12). Figure 13 illustrates the assignment of multiple peaks in Figure 12. There are several possible reactions in the cross-linking of FPCCK3W and FPCK3, resulting in the desired trimer **A** (FPtr) and undesired dimers **B**, **C**, and **D**. Peak **B1, D1** correspond to FPCK3, which was generated by the laser power breaking the disulfide bond in **B** and **D**. The double protonated species $(\mathbf{BH_2})^{2+}$ also contribute to Peak **B1**. Peak **C1** correspnds to the

FPCCKKKW monomer and the double protonated species $(\mathbf{CH_2})^{2+}$. **D2** arises from the double prononated species $(\mathbf{DH_2})^{2+}$. **D3** corresponds to the FPCKKKW monomer, resulting from breaking of the disulfide bond in **D**. The signal intensity of peak **A** is relatively small comparing to the other two major peaks. This is possibly due to signal suppression, which is a common phenomenon in MALDI. The experimental mass of the various products differs from their theoretical mass by 0.1-0.2 %.

As evidenced in Figure 10 (b), FPdm was the major product formed in cross-linking of either pure FPCK3W or FPCK3. Using 6 mg of monomer starting material, ~ 3 mg of FPdm could be obtained after HPLC purification. FPtr was not the major product of cross-linking (cf. Figure 10 (c)), and after HPLC purification and repurification, ~ 0.2 mg of FPtr was obtained from a cross-linking reaction that began with 15 mg of monomer starting material.

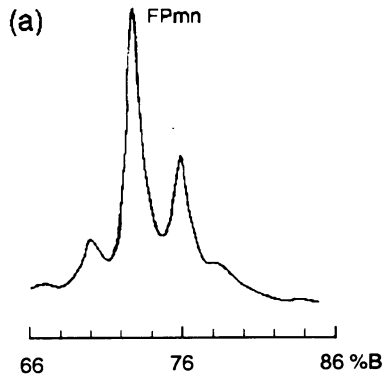
(a)
FPmn
66
76
86 %B

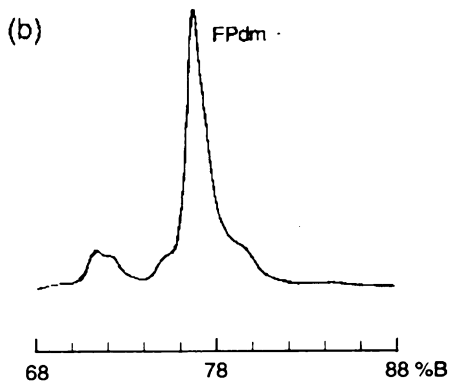
(b)
FPdm
68
78
88 %B

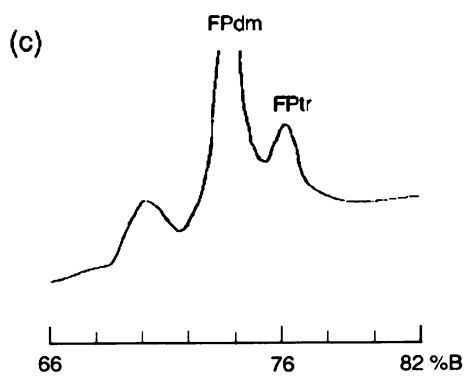
(c)
FPdm
FPtr
66
76
82 %B

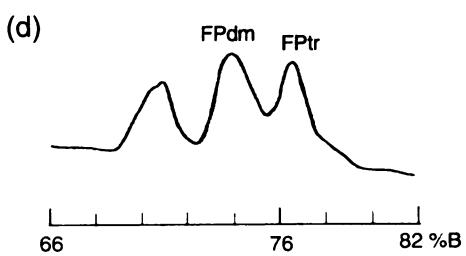
(d)
FPdm
FPtr
66
76
82 %B

Figure 10. HPLC chromatograms of FPmn, FPdm, and FPtr (one strand out of register). The gradient was between two solvents A and B, 90/10 water/acetonitrile and 10/90 water/acetonitrile, respectively. (a) 280-nm detected chromatogram of FPCK3W. (b) 280-nm detected chromatogram of cross-linking of FPCK3W. The main product is the cross-linked FPdm dimer. (c) 220-nm detected and (d) 280-nm detected chromograms of cross-linking of FPCCK3W and FPCK3 at 1:4 mol ratio. In panel c, the largest peak that goes off-scale corresponds to cross-linked FPdm, and the following peak corresponds to cross-linked FPtr trimer. In panel d, the FPtr and FPdm peaks have comparable intensities because at 280 nm, all FPtr is detected whereas only FPdm with at least one FPCCK3W strand is detected. For panel c-d, the beginning and end of the chromatograms correspond to 66 and 82 % acetonitrile, respectively.

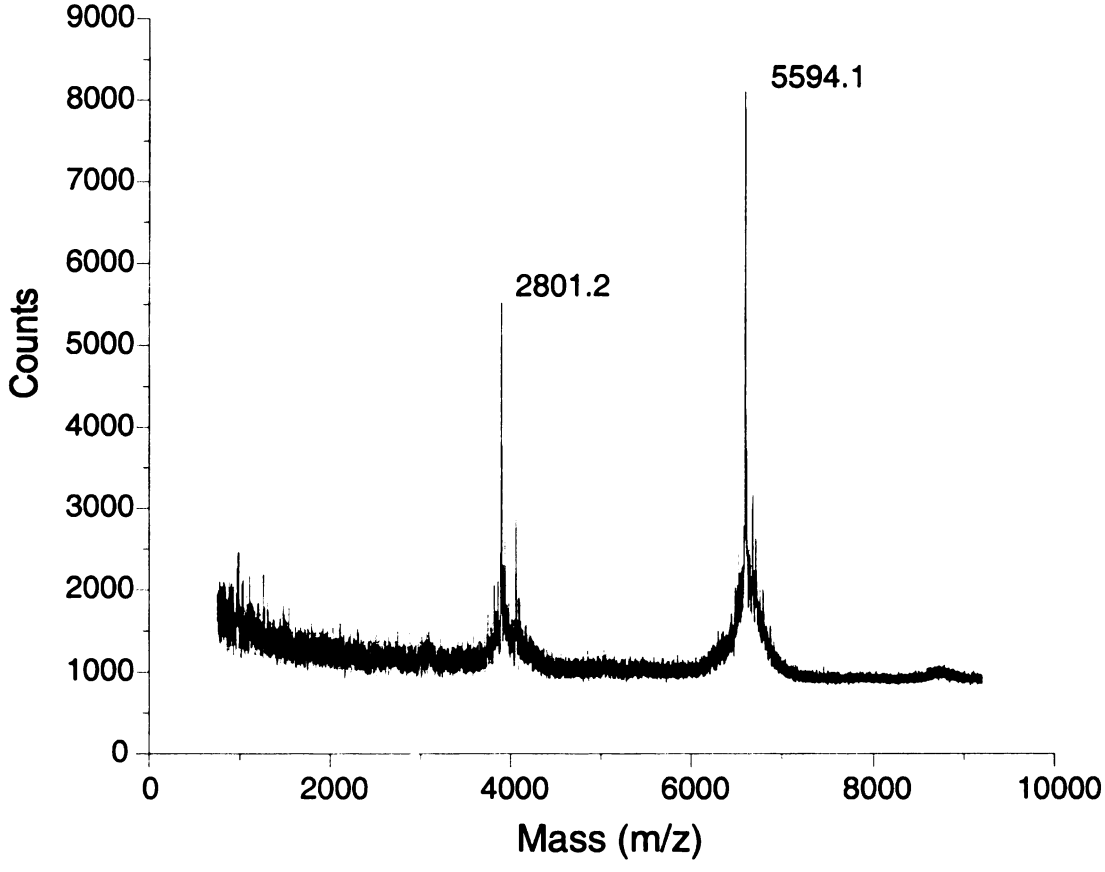

Figure 11. MALDI spectrum for $(FPCK3W)_2$ dimer. The peak of 5594.1 corresponds to FPdm, which has a theoretical molecular mass of 5594.6 g/mol. The peak of 2801.2 arises from the double protonated species and FPCK3W monomer formed by breaking of disulfide bond in FPdm.

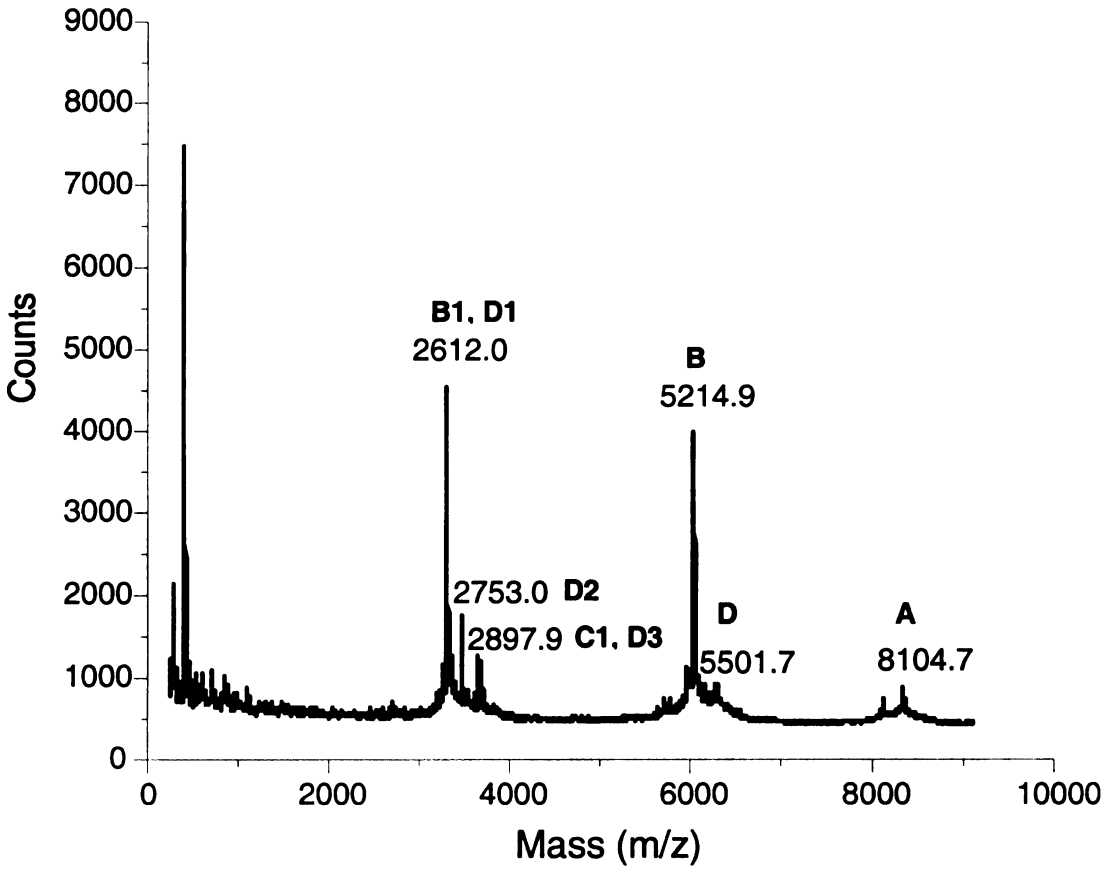

Figure 12. MALDI spectrum for FPtr (cross-linked product of FPCCK3W and FPCK3 in a 1:4 mol ratio). Peak **A** (8104.7) corresponds to FPtr, which has a theoretical molecular mass of 8121.7 g/mol. Due to the fact that the instrument was neither internally calibrated nor recently externally calibrated, there was a disagreement of ~ 17 mass unit. The other peaks arise from a variety of sources as indicated in Figure 13.

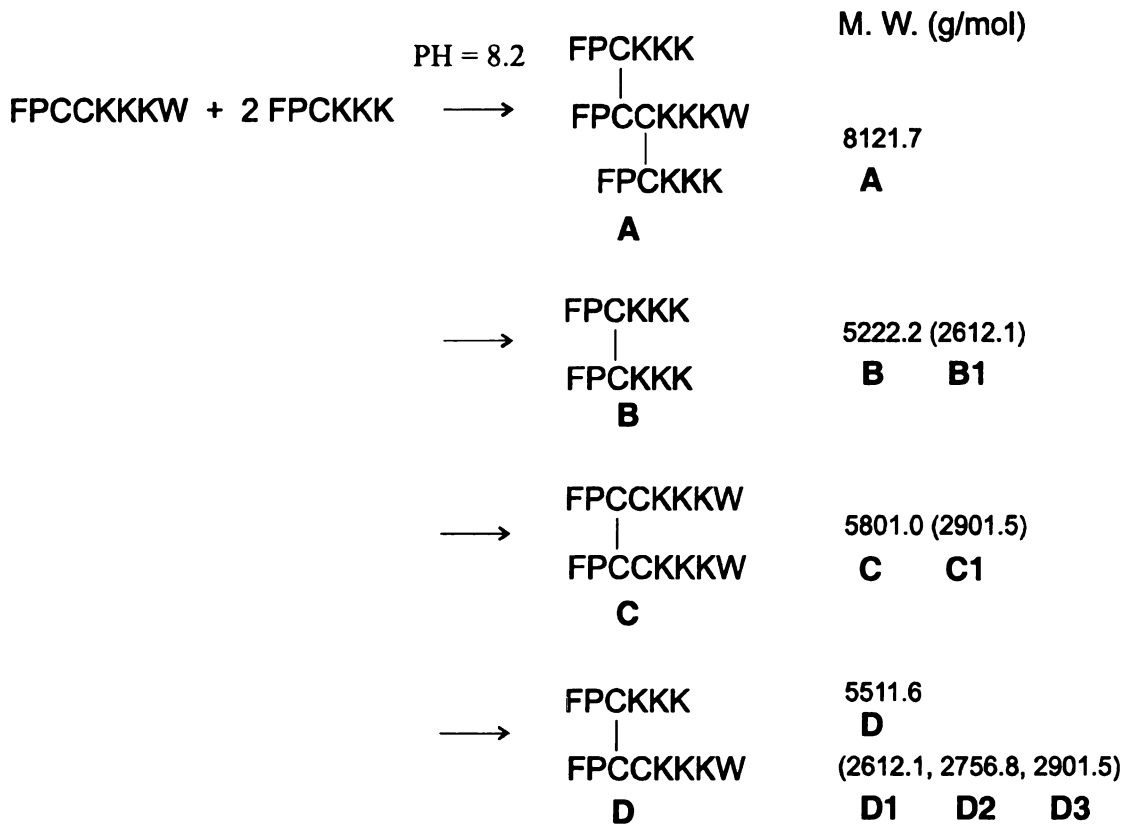

Figure 13. Possible reactions in the cross-linking of FPCCK3W and FPCK3, resulting in the desired product **A** and undesired products **B**, **C**, and **D**. The theoretical molecular masses of the products are listed on the right. **B1** correspnds to the FPCKKK monomer due to breaking of disulfide bond under laser and the double prononated species $(\mathbf{BH_2})^{2+}$. **C1** correspnds to the FPCCKKKW monomer and the double protonated species $(\mathbf{CH_2})^{2+}$. **D1** corresponds to the FPCKKK monomer, **D2** corresponds to the double prononated species $(\mathbf{DH_2})^{2+}$, and **D3** corresponds to the FPCKKKW monomer.

FPtr (in register). Using a water:acetonitrile gradient varying from 80:20 to 20:80 ratios in HPLC purification, FPtr eluted at ~30:70 ratio and was identified by mass spectroscopy (cf. Figure 14). An additional peak with +128 mass units was also observed in the FPtr mass spectrum. We believe that this peak was due to peptides which had an additional lysine on one strand. It has recently been reported that the free ε-NH_2 group of a Lys residue can catalyze the removal of the Lys Fmoc group, and in the FPtr synthesis, this premature Fmoc removal could allow coupling of an additional Lys on the first or second strand [19]. Premature removal of the Fmoc group on the first Lys might also lead to formation of a peptide tetramer but there was at most a minor (<15%) peak in the tetramer region of the FPtr mass spectrum. In future FPtr syntheses, attempt will be made to minimize the premature removal of the Fmoc group using the straightforward Mtt deprotection and coupling protocol from the Albericio *et al.*[19].

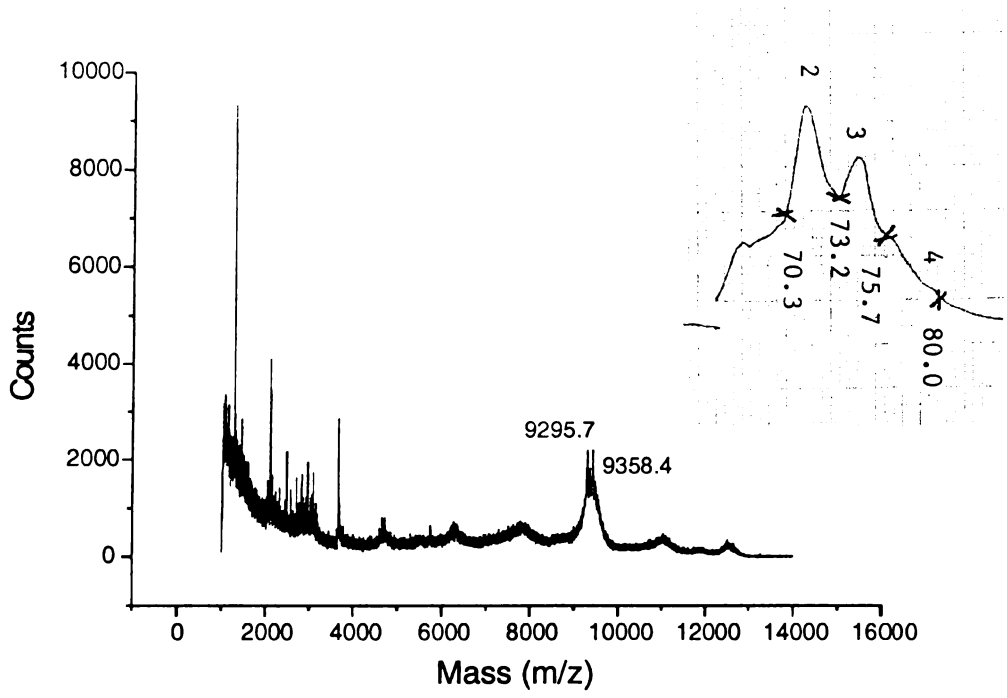

Figure 14. MALDI spectrum and 280-nm detected chromatogram for FPtr (in-register). The peak labeled "3" in the HPLC corresponds to FPtr with a theoretical molecular mass of 9274.0 g/mol.

REFERENCE

1. Kliger, Y., Aharoni, A., Rapaport, D., Jones, P., Blumenthal, R., and Shai, Y. (1997) *J. Biol. Chem. 272*, 13496-505.

2. Pritsker, M., Rucker, J., Hoffman, T. L., Doms, R. W., and Shai, Y. (1999) *Biochemistry 38*, 11359-71.

3. Weissenhorn, W., Dessen, A., Harrison, S. C., Skehel, J. J., and Wiley, D. C. (1997) *Nature 387*, 426-30.

4. Caffrey, M., Cai, M., Kaufman, J., Stahl, S. J., Wingfield, P. T., Covell, D. G., Gronenborn, A. M., and Clore, G. M. (1998) *EMBO J. 17*, 4572-84.

5. Munoz-Barroso, I., Durell, S., Sakaguchi, K., Appella, E., and Blumenthal, R. (1998) *J. Cell. Biol. 140*, 315-23.

6. Bentz, J. (2000) *Biophys. J. 78*, 227-45.

7. Bentz, J. (2000) *Biophys. J. 78*, 886-900.

8. Freed, E. O., Delwart, E. L., Buchschacher, G. L., Jr., and Panganiban, A. T. (1992) *Proc. Natl. Acad. Sci. U. S. A. 89*, 70-4.

9. Epand, R. F., Macosko, J. C., Russell, C. J., Shin, Y. K., and Epand, R. M. (1999) *J. Mol. Biol. 286*, 489-503.

10. Lau, W. L., Ege, D. S., Lear, J. D., Hammer, D. A., and DeGrado, W. F. (2004) *Biophys. J. 86*, 272-284.

11. Yang, J., Gabrys, C. M., and Weliky, D. P. (2001) *Biochemistry 40*, 8126-37.

12. Yang, J., and Weliky, D. P. (2003) *Biochemistry 42*, 11879-11890.

13. Durell, S. R., Martin, I., Ruysschaert, J. M., Shai, Y., and Blumenthal, R. (1997) *Mol. Membr. Biol. 14*, 97-112.

14. Freed, E. O., Myers, D. J., and Risser, R. (1990) *Proc. Natl. Acad. Sci. U. S. A. 87*, 4650-4.

15. Han, X., and Tamm, L. K. (2000) *Proc. Natl. Acad. Sci. U. S. A. 97*, 13097-13102.

16. Lehninger, A. L., Nelson, D. L., and Cox, M. M. (1997) *Principles of Biochemistry*, 2nd Edition ed., Worth Publishers, New York, NY.

17. Aletras, A., Barlos, K., Gatos, D., Koutsogianni, S., and Mamos, P. (1995) *Int. J. Pept. Protein Res. 45*, 488-496.

18. In (1999) *Novabiochem Catalog and Peptide Synthesis Handbook* pp S 32-34, Calbiochem-Novabiochem Corp.

19. Farrera-Sinfreu, J., Royo, M., and Albericio, F. (2002) *Tetrahedron Lett. 43*, 7813-7815.

CHAPTER III

VERIFICATION OF THE SYNTHESIZED FUSION PEPTIDE CONSTRUCTS' SOLUTION AGGREGATION STATE

BACKGROUND

There are a significant number of bulky, nonpolar residues in the HIV-1 fusion peptide sequence. If synthetic fusion peptides are dissolved in aqueous solution, they tend to self-associate and form aggregates. In particular, our synthetic peptide analogues containing two or three fusion peptide strands would aggregated more than non-cross-linked monomeric peptides do.

In fusion assays, FPs bind to membranes from aqueous solution and the correlation of fusogenicity with numbers of strands could be confounded by prior self-association of FPs in aqueous solution. For example, analytical ultracentrifugation demonstrated that 75 μM FPK3W is monomeric in 5 mM pH 7 HEPES buffer. A mixture of monomer and higher order oligomerization states were observed for FPdm (cross-linked product of FPCK3W in a 1:1 ratio) and FPtr (cross-linked product of FPCCK3W and FPCK3 in a 1:4 ratio) at concentrations of 40 and 20 μM, respectively [1]. Thus, the possibility exists that some part of the enhanced fusogenicity of FPdm and FPtr is related to their oligomeric state in aqueous solution. On the other hand, studies of different FPmn peptide constructs that were either monomeric or oligomeric in aqueous solution did not show a clear correlation between M_f and oligomeric state [2]. In addition, for the influenza fusion peptide, there does not appear to be a correlation between the peptide oligomeric state in aqueous solution and its final oligomerization state in the membrane, which suggests that oligomers can break up and/or (re)form at the membrane interface [3].

One goal of the present work is to determine the correlation between the different numbers of strands in FPmn, FPdm, and FPtr with their respective fusion catalyzing

activities. Therefore, it is crucial to obtain FPmn, FPdm, and FPtr constructs which do not self-associate in aqueous solution. In order to specifically address the effect of oligomerization, we have synthesized cross-linked fusion peptides with longer (6) C-terminal lysine sequences. Analytical ultracentrifugation of influenza fusion peptides showed that additional lysines could change the peptide from an oligomeric to a monomeric state in solution [3]. Here, we observed similar effect for the cross-linked HIV-1 fusion peptides.

Analytical ultracentrafugation experiments were performed on synthetic fusion peptide constructs in order to assess their self-association. Our results indicated that FPmn, FPdm, and FPtr do not self-associate at FP concentrations comparable to those in stock solutions of the functional assays.

MATERIALS AND METHODS

Peptides. The amino acid sequences of FPmn, FPdm, and FPtr tested by analytical ultra-centrifugation are displayed in Figure 15. Their synthetic protocols were described in Chapter II. The peptides were dissolved in 5 mM pH 7 HEPES buffer. Their concentrations were ~100 μM for FPmn, 40 μM for FPdm, and 25 μM for FPtr. These concentrations were chosen so that they were comparable to those in stock solutions for the functional assays. The 280-nm absorbance of these solutions were ~ 0.5 – 0.6.

Figure 15. Amino acid sequences of FP constructs in the analytical ultracentrifugation experiment.

Sedimentation Equilibrium. Sedimentation equilibrium experiments at room temperature were performed on an analytical ultracentrifuge (Beckman XL-I, Palo Alto, CA) using an An-60 Ti rotor. The instrument was operated in absorbance mode at 280 nm. Samples were loaded into six-channel epon charcoal-filled centerpieces equipped with quartz windows and were equilibrated at rotor speeds of 32000, 45000, or 52000 rpm. Data were fitted using the analysis software supplied by Beckman to a single molar mass (M) using:

$$(A/A_0) = \exp[M(1-v\rho)(r^2 - r_0^2)(\omega^2/2RT)] \quad (1)$$

where A and A_0 are the experimental absorbencies at radius r and reference radius r_0, respectively, v is the partial specific volume of FPmn, FPdm, or FPtr, ρ is the buffer density, ω is the angular velocity, R is the ideal gas constant, and T is the temperature [4]. This equation assumes no baseline offset and a single value of M, i.e. a single self-association state for all peptides in solution. The values of v for each peptide were calculated from the mass average of the partial specific volumes of the individual amino acids in FPmn, FPdm, and FPtr [5]. The value of ρ was set to 1.0 g/ml.

RESULTS AND DISCUSSION

Figure 16 displays the results of the sedimentation equilibrium experiment at 20 °C for a sample made with 100 μM FPK6W peptide in 5 mM pH 7 buffer. The rotor speed was 45000 rpm. The top panel shows that the differences between the experimental and fitted absorbance were small (< 0.02) and random as a function of r, which indicates that a single-species model is reasonable. The bottom panel displays 280 nm absorbance (proportional to peptide concentration) as a function of centrifugal radius. With a partial specific volume of 0.7703 ml/g and a solvent density of 1.0 g/ml, the optimal fit the data set, determined by a non-linear least square method, was a molecular weight of ~ 3000, which is close to the monomeric FPK6W mass of 3080 g/mol. Data were also acquired at 52000 rpm and could be fit well to equation (1) with values of M between 2560 and 2810 g/mol. Thus these results indicate that FPK6W at ~ 100 μM concentration is predominantly monomeric in 5 mM pH 7 HEPES buffer.

Figure 17 and 18 display the sedimentation equilibrium data and fittings for 40 μM FPdm, and 25 μM FPtr, respectively. The rotor speeds were 32000 rpm for both samples. Using a single molar mass model according to equation (1), and with specific volume of 0.7657 for FPdm and 0.7700 for FPtr, the fitted molecular mass was ~ 5700 g/mol for FPdm, and ~ 11000 g/mol for FPtr, which are close to the actual non-associated peptide masses of 6364 and 9274 for FPdm and FPtr, respectively. For both fits, the residual differences between the calculated and fitted absorbances were randomly distributed around zero with typical magnitudes less than 0.02. For FPdm, data were also obtained at rotor speed of 45000 and 52000 rpm with the result of 4800 and 4500 g/mol, respectively. For FPtr, result of 11600 and 10400 g/mol were respectively obtained at

rotor speeds of 32000 and 45000 rpm. These results demonstrate that FPdm and FPtr are predominantly monomeric under conditions similar to that of the lipid mixing assay. Figure 19 compares the results of the sedimentation equilibrium experimental curves at 20°C for the sample made with 104.3 μM FPmn, 41.6 μM FPdm, and 27.8 μM FPtr. The fitted masses of the three peptides are 3000, 5700, and 11000 g/mol, respectively, and are close to the actual non-associated peptide masses of 3080, 6364, and 9274 g/mol.

CONCLUSION

In conclusion, the analytical ultra-centrifugation results suggest that for fusion peptide concentrations close to the stock peptide concentration used in fluorescence assay and solid state NMR measurements, our synthesized fusion peptide constructs do not aggregate in aqueous solution. This information is essential for the later interpretation of the impact of fusion peptide oligomerization on membrane fusion catalysis.

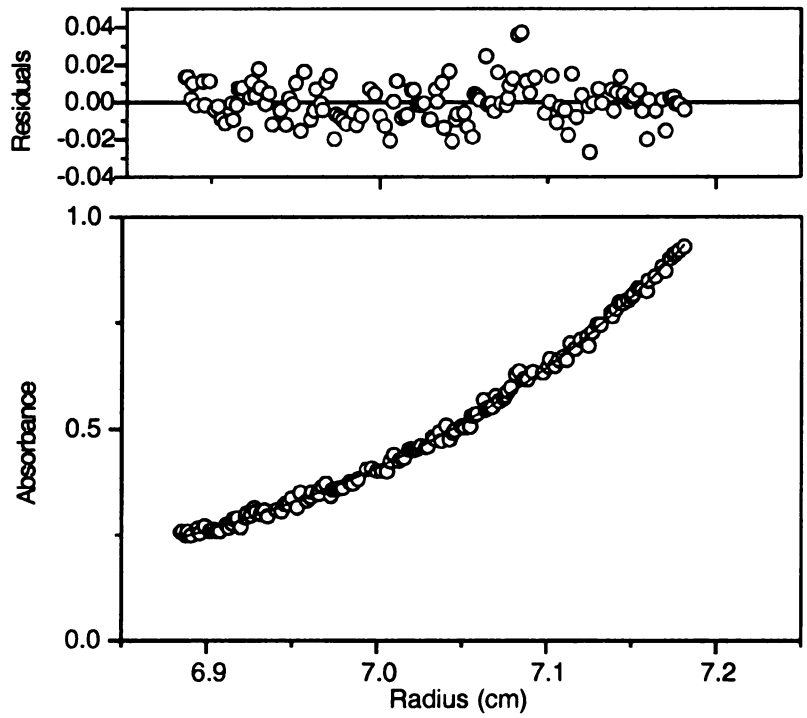

Figure 16. Sedimentation equilibrium experiments of 100 μM FPmn. The main panel shows the absorbance at 280 nm as a function of the centrifugal radius after reaching the equilibrium in 20 hours at 45,000 rpm. The best fit to the model for a single species was obtained with a molecular weight of ~3026 (shown as a solid line through the experimental points). The upper panel shows the residuals between the data and the fit.

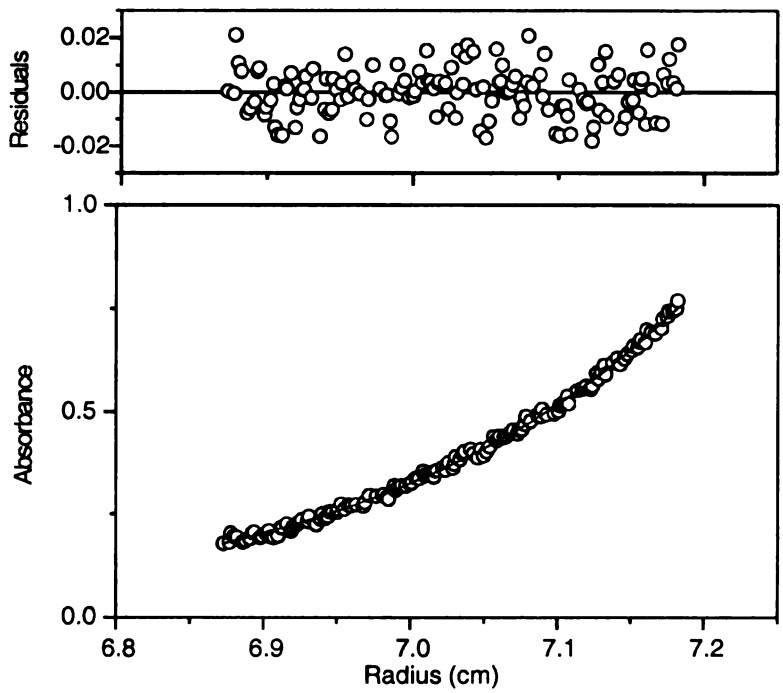

Figure 17. Sedimentation equilibrium experiments of 40 μM FPdm. The main panel shows the absorbance at 280 nm as a function of the centrifugal radius after reaching the equilibrium in 20 hours at 32,000 rpm. The best fit to the model for a single species was obtained with a molecular weight of ~5729 (shown as a solid line through the experimental points). The upper panel shows the residuals between the data and the fit.

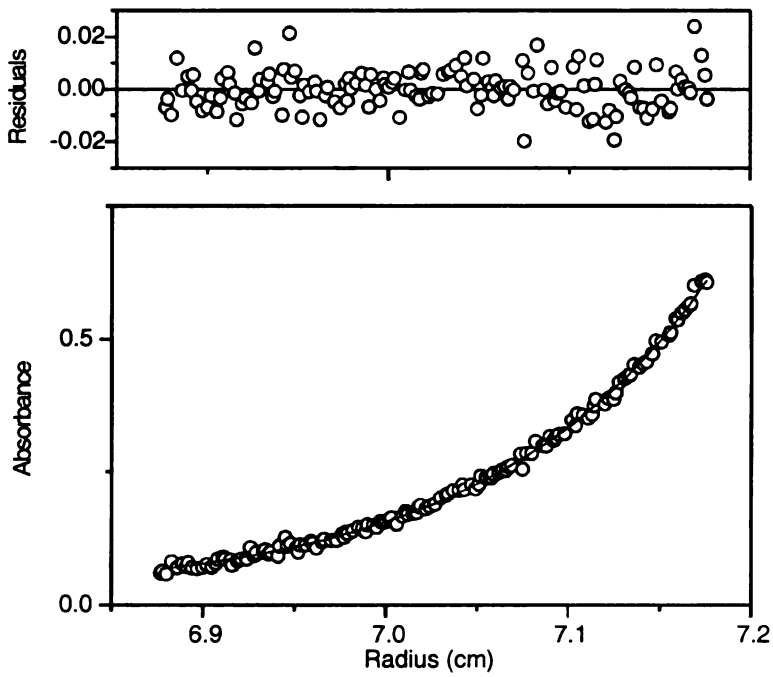

Figure 18. Sedimentation equilibrium experiments of 25 μM FPtr. The main panel shows the absorbance at 280 nm as a function of the centrifugal radius after reaching the equilibrium in 20 hours at 32,000 rpm. The best fit to the model for a single species was obtained with a molecular weight of ~10863 (shown as a solid line through the experimental points). The upper panel shows the residuals between the data and the fit.

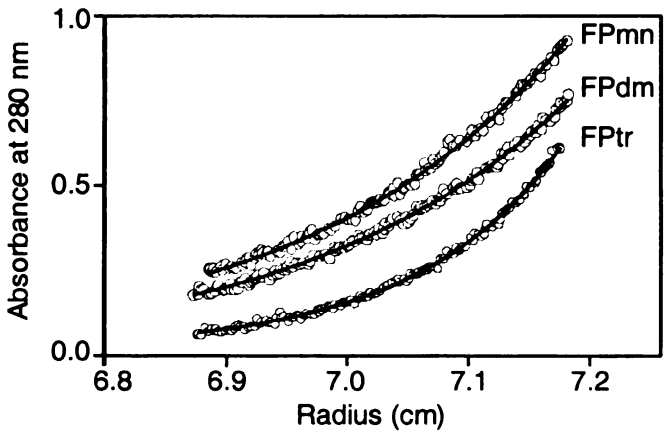

Figure 19. Comparison of sedimentation equilibrium experimental fitting curves of FPmn, FPdm, and FPtr.

REFERENCE

1. Yang, R., Yang, J., and Weliky, D. P. (2003) *Biochemistry 42*, 3527-3535.

2. Yang, J., Prorok, M., Castellino, F. J., and Weliky, D. P. (2004) *Biophys. J. 87*, 1951-1963.

3. Parkanzky, P. D., Prorok, M., Castellino, F. J., and Weliky, D. P., unpublished experiments.

4. Cantor, C. R., and Shimmel, P. R. (1980) *Biophysical Chemistry*, W. H. Freeman and Company, New York.

5. Laue, T. M., Shah, B. D., Ridgeway, T. M., and Pelletier, S. L. (1992) in *Analytical Ultracentrifugation in Biochemistry and Polymer Science* (Harding, S. E., Rowe, A. J., and Horton, J. C., Eds.), Royal Society of Chemistry, Cambridge, UK.

CHAPTER IV

COMPARISON OF THE FUSOGENICITY BETWEEN DIFFERENT FUSION PEPTIDE OLIGOMERS BY FLUORESCENCE ASSAY

BACKGROUND

In this chapter, a resonance energy transfer (RET) assay is employed to compare the fusogenicity among different fusion peptide oligomeric constructs. The RET assay was designed by Struck et al. (1981) [1] to measure lipid mixing during membrane fusion. It relies on the resonance energy transfer between N-(7-nitro-2,1,3,-benaoxadiazol-4-yl)phosphatidylethanolamine (*N*-NBD-PE), the energy donor, and *N*-(lissamine Rhodamine B sulfonyl)phosphatidylethanolamine (*N*-Rh-PE), the energy acceptor (cf. Figure 20). In the assay, if fusion occurs, the labeled lipids are diluted in the unlabeled membranes. Since RET depends significantly on the distance between the donor and acceptor [2], the fusion-associated dilution leads to an increase in fluorescence.

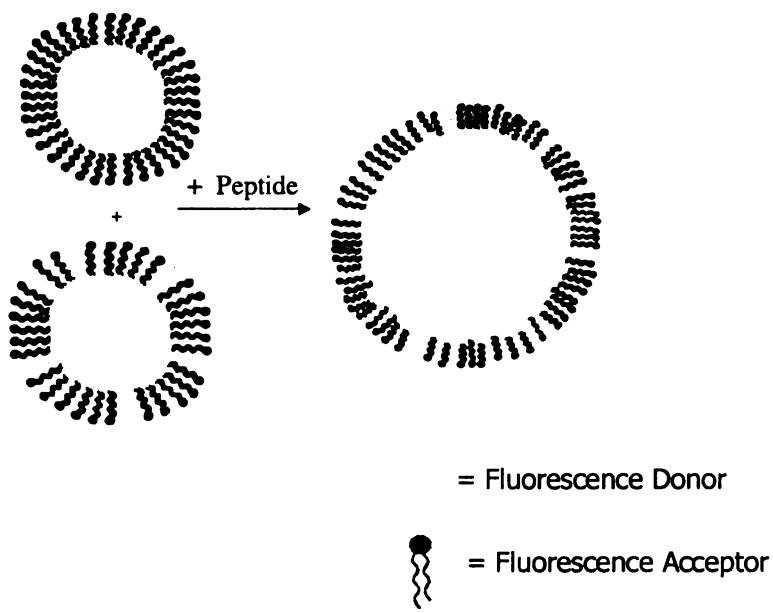

Figure 20. Resonance energy transfer (RET) assay.

Because of its sensitivity and the ability to continuously monitor the events of fusion from the very beginning stage [3], RET assay is well suited to probe fusogenic peptides and proteins. This approach has been commonly used in the study of phospholipid bilayer fusion promoted by viral fusion proteins and synthetic analogues [4, 5].

Recently, fusion assays on influenza fusion protein constructs have demonstrated that oligomerization of fusion peptide considerably enhances lipid mixing. Epand et al. has studied a 127-residue FHA2 protein construct including both the fusion peptide domain as well as the ~ 100-residues C-terminal of the peptide [4-10]. Glutaraldehyde cross-linking showed that this construct is predominantly trimeric in either 2% n-octyl β-D-glucoside or 0.5% Triton X-100 detergent. When a solution of 100 μM FHA2 in 0.1% Triton was added to a lipid vesicle solution, the induced lipid mixing was significantly higher than that induced by the original influenza fusion peptide. In another experiment, DeGrado et al. [11] synthesized a peptide that incorporates the wild-type influenza fusogenic peptide sequence (ccX31) followed by a V_aL_d peptide sequence that self-assembles into a coiled-coil trimer at neutral pH and aggregates at acidic pH [12]. At acidic pH, the fusogenicity of ccX31 is higher than that of the flu peptide by itself. Collectively, these results are consistent with the hypothesis that oligomerization of fusogenic peptides promotes membrane fusion.

In this chapter, we compared the fusogenicity of the three synthetic HIV-1 fusion peptide constructs: FPmn, FPdm, and FPtr in an intervesicle lipid mixing assay. At peptide strand/lipid mol ratios between 0.0050 and 0.010, the final extent of lipid mixing for the dimer and trimer was 2-3 times greater than for the monomer. These data suggest

that the higher local concentration of peptide strand in the cross-linked peptides enhances fusogenicity and that oligomerization of the fusion peptide in gp41 may enhance the rate of viral/target cell membrane fusion. This effect is in addition to the role of gp41 trimerization in stabilizing the gp41 coiled-coil structure which may aid fusion catalysis by bringing the viral and target cell membrane into apposition [13, 14]. The fusion enhancement effect of C-terminal cross-linking observed in the present study suggests that a higher local peptide concentration is an additional factor for gp41's fusion catalyzing activity.

It should be noted that the cysteine cross-linked FPtr employed in this chapter has one strand out of register. In the next Chapter, the fusion assay of an in-register FPtr is performed on a stopped-flow spectrofluorimeter and demonstrates a dramatically enhanced fusion rate relative to the monomeric and dimeric fusion peptides.

MATERIALS AND METHODS

Materials. 1-palmitoyl-2-oleoyl-sn-glycero-3-phosphocholine (POPC), 1-palmitoyl-2-oleoyl-sn-glycero-3-phosphoethanolamine (POPE), 1-palmitoyl-2-oleoyl-sn-glycero-3-[phospho-L-serine] (POPS), phosphatidylinositol (PI), sphingomyelin, *N*-(7-nitro-2,1,3-benzoxadiazol-4-yl)-phosphatidylethanolamine (*N*-NBD-PE), *N*-(lissamine Rhodamine B sulfonyl)-phosphatidylethanolamine (*N*-Rh-PE) were purchased from Avanti Polar Lipids, Inc. (Alabaster, AL). The Micro BCA™ protein assay was obtained from Pierce (Rockford, IL). N-2-hydroxyethylpiperazine-N'-2-ethanesulfonic acid (HEPES) and Triton X-100 were obtained from Sigma. All other reagents were analytical grade.

Peptides. Monomer peptides are denoted as FPmn. Several different constructs were synthesized according to the procedure described in Chapter II: FP (AVGIGALFLGFLGAAGSTMGARS), FPW (AVGIGALFLGFLGAAGSTMGARSW) FPK3 (AVGIGALFLGFLGAAGSTMGARSKKK), FPCK3 (AVGIGALFLGFLGAAGSTMGARSCKKK), FPCCK3 (AVGIGALFLGFLGAAGSTMGARSCCKKK), FPK3W (AVGIGALFLGFLGAAGSTMGARSKKKW), FPCK3W (AVGIGALFLGFLGAAGSTMGARSCKKKW), and FPCCK3W (AVGIGALFLGFLGAAGSTMGARSCCKKKW). FPdm ($(FPCK3)_2$ or $(FPCK3W)_2$) are the cross-linking product of monocysteine fusion peptide. FPtr are the product from cross-linking monocystein and dicystein fusion peptide at 4 to 1 mol ratio. The cross-linking schemes are described in Chapter II. The FPtr used here has one FP strand out of register with the other two.

Lipid Preparation. A "LM-3" lipid/cholesterol mixture was used which approximately reflects the lipid and cholesterol content of the HIV-1 virus and its target T-cells [15, 16]. The LM-3 mixture had POPC, POPE, POPS, sphingomyelin, PI and cholesterol in a 10:5:2:2:1:10 mole ratio. Lipid and cholesterol powders were dissolved together in chloroform. The chloroform was removed under a stream of nitrogen followed by overnight vacuum pumping. Lipid dispersions were then formed with addition of pH 7 buffer containing 5 mM N-2-hydroxyethylpiperazine-N'-2-ethanesulfonic acid (HEPES) and 0.01% NaN_3 preservative. After homogenization of the dispersion with ten freeze-thaw cycles, LUVs were prepared by extrusion through a polycarbonate filter with 100 nm diameter pores [17].

Peptide Concentration Quantitation. Peptide concentrations were quantitated in three different ways: (1) BCA assay; (2) 280 nm absorbance; and (3) quantitative amino acid analysis (AAA). The calibration of the BCA assay was done by comparison with weights of FP. Reproducibility of the BCA assay is ± 10%. Quantitation from 280 nm absorbance was made using an extinction coefficient of 6000 $M^{-1}cm^{-1}$ for FPmn (FPK3W), 12200 $M^{-1}cm^{-1}$ for FPdm (made from cross-linking FPCK3W), and 7200 $M^{-1}cm^{-1}$ for FPtr (made from cross-linking FPCCK3W and FPCK3). The reproducibility of an absorbance measurement was ± 0.010 a.u. or typically ± 2%. When 280 nm absorbance gave FPmn, FPdm, and FPtr concentrations of 100 μM, 50 μM, and 25 μM, respectively, AAA typically gave concentrations of ~ 90, 40, and 20 μM, respectively. Because AAA was considered to be the most accurate technique for absolute quantitation, concentrations determined by 280 nm absorbance for FPmn, FPdm, and FPtr solutions were multiplied by 0.9, 0.8, and 0.8, respectively. As will be presented in Figure 21 and table 1, similar fusion results were obtained when peptide was quantified by AAA and by BCA assay.

Lipid Mixing Assay for Membrane Fusion. The resonance energy transfer assay of Struck, *et al.* was used to monitor membrane fusion [1]. Two types of 100 nm diameter LM-3 LUV were prepared. One set contained two mol % of the fluorescent lipid *N*-NBD-PE and two mol % of the quenching lipid *N*-Rh-PE while the other set only contained unlabeled lipids. Fluorescently labeled and unlabeled vesicles were mixed in a 1:9 ratio. Following addition of peptide, lipid mixing between labeled and unlabeled vesicles caused dilution of the labeled lipids with a resulting increase of fluorescence. Fluorescence was recorded using 4 nm bandwidth on an Instruments S. A. Fluoromax-2

(Edison, NJ) spectrofluorimeter operating at excitation and emission wavelengths of 465 nm and 530 nm, respectively. A siliconized glass cuvette was used with continuous stirring in a thermostated cuvette holder. Measurements were carried out at 37 °C with 2 ml of 150 μM LUV in 5 mM pH 7 HEPES buffer. Peptide solution was added to the liposome solution to achieve the desired peptide:lipid mol ratio and the change in fluorescence of the sample was monitored following this addition. The initial residual fluorescence intensity, F_0, referenced zero lipid mixing. After addition of peptide, the fluorescence F(t) was monitored as a function of time (t). The maximum fluorescence intensity, F_{max}, was obtained following addition of 20 μl of 10% Triton X-100. Percent lipid mixing at time t is denoted as M(t) and was calculated using:

$$M(t) = [(F(t) - F_0)/(F_{max} - F_0)] \times 100 \quad (1)$$

When the peptide or Triton solution is added to the liposome solution, there are two competing effects on fluorescence: (1) increase due to lipid mixing; and (2) decrease due to larger solution volume and corresponding lower fluorophore concentration. The largest added peptide solution volume was 60 μl which increased the liposome solution volume by 3%. Experimentally, a 3% decrease in fluorescence was also observed when 60 μl of pure buffer was added to the liposome solution. In calculating M(t), F(t) and F_{max} values were adjusted to take into account the small volume change which occurs upon addition of peptide and detergent, respectively. With sufficient time, M(t) reached a constant value that is denoted as M_f, the final extent of lipid mixing. M_f is used as a measure of peptide fusogenicity.

In order to make meaningful comparisons between the lipid mixing abilities of different peptides, the following protocols were developed: (1) the same sets of unlabeled

and labeled liposomes were used for all of the peptides in each fusion assay; (2) peptide concentrations were adjusted so that the same volume of each peptide was added for a given peptide strand/lipid; and (3) for each peptide and peptide strand/lipid, two runs were made. The M_f values for the two runs were usually within 2% of each other. The stock peptide solution concentrations varied between 20 and 900 μM, and M_f appeared to be concentration-independent within this range. For most runs, peptide concentrations were ~90 μM for FPmn, ~40 μM for FPdm, and ~ 20 μM for FPtr.

RESULTS

Fusion of LM3 Vesicles. Figure 21 (a) displays one example of intervesicle lipid mixing by FPmn, FPdm, and FPtr at peptide strand:lipid = 0.010. In this case, FPmn was either FPK3 or FPCK3, FPdm was formed from cross-linking of FPCK3 and FPtr was formed from cross-linking of FPCCKKK and FPCKKK in a 1:4 mol ratio. Peptide concentrations were determined by the BCA assay. Because FPdm and FPtr have respectively twice and three times as many strands per molecule as FPmn, the peptide:lipid mol ratios for FPmn, FPdm, and FPtr are 0.010, 0.0050, and 0.0033, respectively. In these data, the M_f values for FPdm and FPtr are about two times greater than the M_f for FPmn. Figure 21 (b) displays more lipid mixing data for FPmn (FPK3W) and FPdm (made from cross-linking FPCK3W). In this case, peptide quantitation was made from AAA. At peptide strand:lipid = 0.0050 and 0.010, FPdm has 2 - 3 times the fusogenicity of FPmn, while at 0.020 ratio, the enhancement factor is about 1.3.

The final extent of lipid mixing, M_f, was used as a general measure of peptide fusogenicity. Figure 22 displays a plot of M_f as a function of peptide:lipid ratio for assays

using FPmn, FPdm, and FPtr with the same sets of liposomes. For these data, FPmn was FPK3W, FPdm was obtained from cross-linking FPCK3W and FPtr was obtained from cross-linking FPCCK3W and FPCK3 in a 1:4 mol ratio. The fusogenicity of FPdm and FPtr are comparable over the experimental range of peptide strand/lipid mol ratios. At lower ($\leq$ 0.010) peptide strand/lipid ratios, FPdm and FPtr are significantly more fusogenic than FPmn while at ratios closer to 0.020, the fusogenicities of the three peptides are much more comparable.

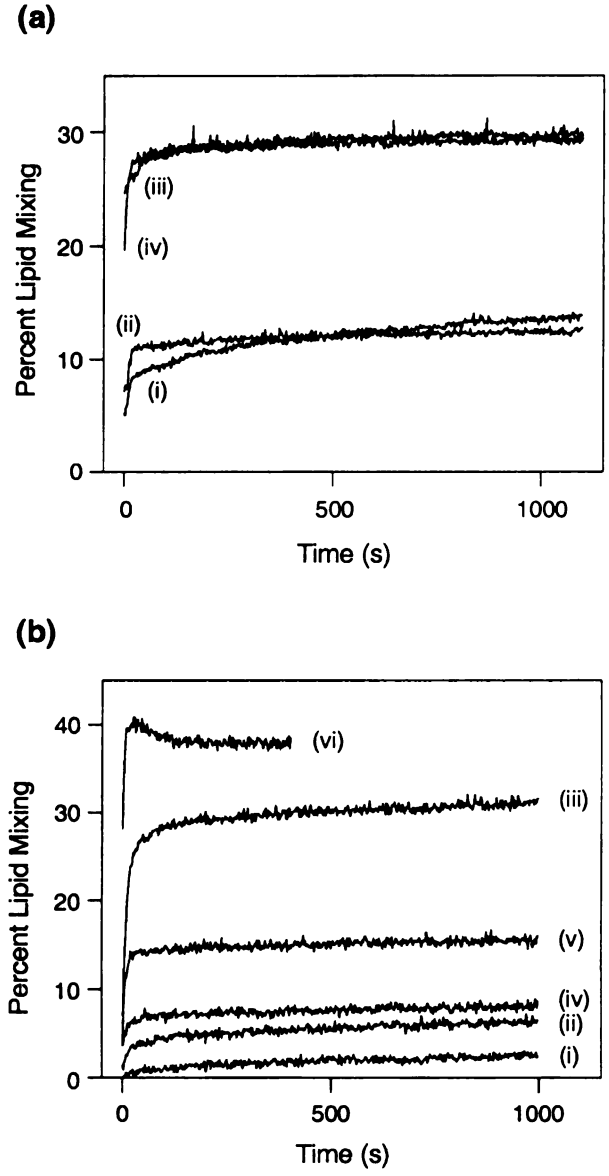

Figure 21. Lipid mixing assays. (a) Data for (i) FPmn (FPK3), (ii) FPmn (FPCK3), (iii) FPdm (cross-linked product of FPCK3), and (iv) FPtr (cross-linked product of FPCCK3 and FPCK3). For lines i – iv, the peptide strand/lipid mol ratio was 0.010, and peptide quantitation was made using the BCA assay. (b) Data for lines i – iii, FPmn (FPK3W) and lines iv – vi, FPdm (cross-linked product of FPCK3W). In lines i and iv, the peptide strand/lipid mol ratio was 0.0050; in lines ii and v, the ratio was 0.010; and in lines iii and vi, the ratio was 0.020. For panel b, peptide quantitation was made by AAA. For all of the runs in panel a, the same sets of liposomes were used, and for all of the runs in panel b, the same sets of liposomes were used.

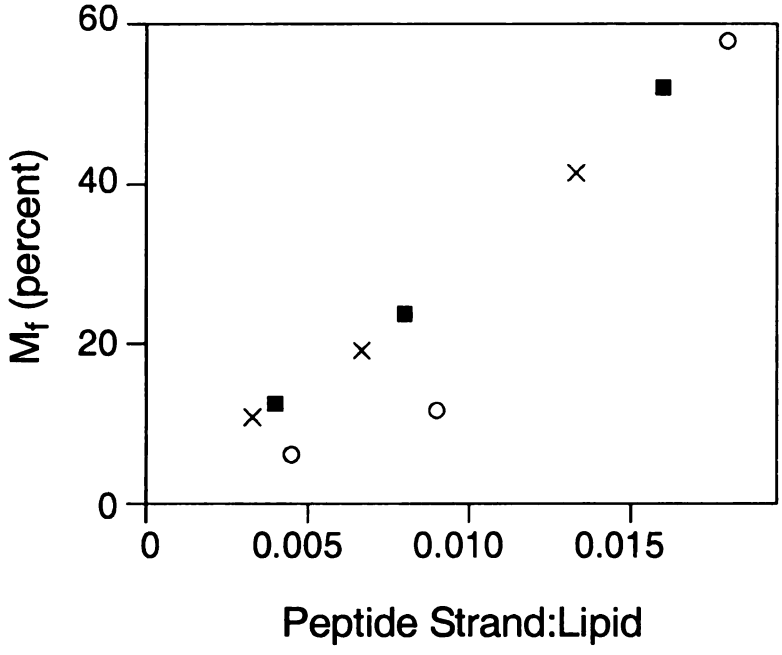

Figure 22. Fusogenicity M_f vs. peptide strand/lipid mol ratio. Open circles represent data for FPmn (FPK3W), closed squares represent data for FPdm (obtained from cross-linking FPCK3W), and crosses represent data for FPtr (obtained from cross-linking FPCCK3W and FPCK3). All of the data were obtained using the same sets of liposomes. The uncertainty in each M_f value is ± 1 %.

Table 1. Fusogenicity Ratios as a Function of Peptide Strand:lipid.

Peptide Strand:Lipid Mol Ratio	Fusogenicity Ratio[a]	
	FPdm/FPmn	FPtr/FPmn
0.0050	2.6 (0.5)	2.2 (0.3)
0.010	2.1 (0.3)	1.9 (0.4)
0.020	1.3 (0.1)	n.d.[b]

[a] This is calculated from the ratios of M_f values. The average fusogenicity ratio is followed by its standard deviation in parentheses.

[b] not determined.

When comparing runs using different sets of liposomes, there can be considerable variation in the M_f values, even for the same peptide and peptide strand/lipid. A more meaningful measure is the ratio of the M_f value of FPdm or FPtr to the M_f values of FPmn. For runs from the same sets of liposomes, these fusogenicity ratios were calculated at peptide strand/lipid mol ratios of 0.0050, 0.010, and 0.020. In some runs, the data had been obtained at peptide strand/lipid different than these three standard values so linear interpolation was used to calculate the fusogenicity ratios at the standard values. There was general consistency in the fusogenicity ratios among different liposome batches as evidenced in Table 1, which displays the average values and standard deviations of the fusogenicity ratios. For example, the FPdm/FPmn fusogenicity ratio at peptide strand/lipid = 0.010 represents the average of measurements taken with six different sets of liposomes. In addition, for a given peptide strand/lipid, the fusogenicity ratio is independent of the presence or absence of the C-terminal tryptophan in FPmn, FPdm, or FPtr and is also independent of the presence or absence of the cysteine in FPmn (cf. Figure 21 (a)).

DISCUSSION

The topology of insertion of the HIV-1 fusion peptide is strongly suggested from high-resolution structures of the soluble portion of the gp41 ectodomain [13, 14, 18-20]. In this topology, the C-termini of three fusion peptides are near one another and there is the possibility that the fusion peptides insert into the membrane in close proximity. In the present study, we have synthesized fusion peptides which are cross-linked at their C-termini with a topology close to that of the full protein. Relative to the monomer peptide,

these peptides enhance fusogenicity, at least to the lipid mixing stage of membrane fusion, which suggests that this topology may be a significant structural factor in catalyzing viral/target cell fusion. In the present chapter, we consider the final extent of lipid mixing as a measure of fusogenicity, but in the next chapter, we will carefully investigate the rates for buildup of lipid mixing. Preliminary analysis shows that these rates are generally larger for cross-linked peptides than for FPmn, and with further analysis and temperature-dependent studies, in Chapter V we attempted to quantify the effect of topology on the activation energy of membrane fusion.

The enhanced fusogenicities of cross-linked fusion peptide are consistent with the hypothesis that lipid mixing induced by fusion peptides requires some critical local concentration of peptide strands associated with the membrane. For FPdm and FPtr, the local concentration is elevated by cross-linking so that relative to FPmn, the cross-linked peptides allow greater lipid mixing at lower peptide strand/lipid. At higher peptide strand/lipid, FPmn, FPdm and FPtr would all have surpassed the critical concentration and would have more similar fusion activities, which is consistent with experimental observation (cf. Figure 22 and Table 1). The proposed correlation between local peptide concentration and fusogenicity has some similarity to an earlier hypothesis that fusion requires a critical number of fusion peptides per vesicle [21]. However, this latter hypothesis predicts that at constant peptide/lipid, fusion will be greater for larger vesicles, and we observed that for FPmn, M_f is independent of LM3 vesicle size [22].

In addition to the higher local peptide concentration achieved with cross-linking, the overall concentration of cross-linked peptide in LM3 could be higher than that of FPmn because of higher lipid affinity of the cross-linked peptide. However, there is some

experimental evidence that points against different affinity of different peptides. We will address this issue in Chapter IX.

In a more detailed molecular structural picture, there are at least two models that correlate cross-linking with enhanced fusogenicity. In one model, the main effect is greater peptide/lipid interactions that lead to larger membrane disruption. For example, a splayed helix model for oligomers has non-interacting helices that insert obliquely into the membrane [4]. In a trimer, each helix forms an edge of a trigonal pyramidal structure. In a second model, the topology correlates with a particular structural arrangement of interacting peptide strands, perhaps a parallel β sheet structure. For FPmn, solid state NMR measurements have demonstrated that in LM3 at peptide/lipid $\geq$ 0.010, the N-terminal and central regions of the peptides adopt a nonhelical β strand structure [16]. Additional solid state NMR REDOR studies have shown that there are both parallel and antiparallel arrangements of strands in LM-associated FPmn [23]. However, the C-terminal cross-linking topology of FPdm and FPtr suggests a parallel arrangement of strands. Furthermore, it is possible that the parallel alignment is more fusogenic than the antiparallel alignment. For parallel arrangement, the apolar N-terminal regions of two or more peptide strands could insert into the hydrophobic interior of the membrane, which could be more disruptive to the membrane than a single peptide strand. This particular insertion topology is less likely with the antiparallel arrangement in which the polar and apolar ends of strands would be on the same side of the oligomer. Thus, FPmn, which has a mix of both parallel and antiparallel alignments, would be less fusogenic than FPdm or FPtr. The actual strand arrangement of the membrane-associated cross-linked peptides will be investigated by solid state NMR (cf. Chapter VI) and other experimental methods.

In addition, our REDOR measurement demonstrated that LM3-associated FPmn, FPdm, and FPtr have similar chemical shifts of 171-173 ppm for the Phe-8 carbonyl carbon, which is consistent with predominantly β strand conformation for LM3-associated FPs. It is noted that in the solid state NMR experiments, the peptide structure is observed after vesicle fusion has occurred. It is also possible that fusion requires a transient structure that is different from the NMR structure that observed at the end state of fusion.

At peptide strand/lipid mol ratios between 0.004 and 0.015, FPdm and FPtr have approximately the same fusogenicity (cf. Figure 21, 22 and Table 1). This may be a general observation that the dimeric and trimeric topologies have approximately the same effect on lipid mixing. However, it is also noted that FPdm has an in-register strand alignment, whereas FPtr has one strand out of register with the other two strands (cf. Chapter II: Figure 7 and 8). In gp41, the three strands are likely in-register, and it is possible that this arrangement is a structural requirement for enhanced fusogenicity. In a further experiment, we find that vesicle fusion rate induced by an in-register FPtr is significantly faster than the FPdm (cf. Chapter V: Figure 26 and Table 2.). However, the final fluorescence for FPdm and the in-register FPtr are about the same. It appears that the third strand affects the rate but not the final amount of fusion.

Our results suggest that oligomeric fusion peptide topology may have also contributed to the enhanced fusogencity observed for the 127-residue FHA2 domain of influenza envelope protein [4-6] and for the construct containing residue 1-70 of gp41 [24]. In these systems, there is likely additional fusogenic enhancement because of the presence of other regions of the fusion protein. For the gp41 system, the overall fusogenicity of the 1-70 construct was about 10 times greater than that of the 1-23

construct, and this is a larger enhancement than we observed from cross-linking the 1-23 construct. In addition, although the 127-residue FHA2 induces cell-cell hemifusion, a 90-residue construct containing the fusion peptide and ~ 70 C-terminal residues does not induce cell-cell hemifusion [5]. One possible explanation for this observation is that the 37 extra residues in FHA2 contain a kinked loop region that is required for pH-dependent association of FHA2 trimers and for cell-cell hemifusion [4, 6, 9, 10].

In this study as well as lipid mixing studies from other groups, it is possible that the oligomerization of peptides in aqueous solution prior to interaction with the target membrane impacts the rate and extent of lipid mixing. For our work, analytical ultracentrifugation demonstrated that FPmn (FPK3W construct) is predominantly a monomer in the assay buffer, whereas FPdm and FPtr are mixtures of monomeric and oligomeric cross-linked peptides. Thus, the possibility exists that some part of the enhanced fusogenicity of FPdm and FPtr is related to their oligomeric state in aqueous solution. To address this question, we made FP constructs with more C-terminal lysines and assessed their self-association by analytical ultracentrifugation. Our data revealed that FPmn, FPdm, and FPtr with 6 C-terminal lysines are predominantly monomeric in the buffer solution used in fluorescence assay. The fusogenicities of these peptides with definite solution oligomeric state will be investigated in the next chapter.

In summary, we have shown a correlation between C-terminal cross-linking and enhanced fusogenicity of HIV-1 fusion peptides. The topology achieved through cross-linking is similar to the fusion peptide topology thought to exist in the fusogenic form of gp41. Thus, the topology may play a role in enhancing membrane fusion rates.

REFERENCE

1. Struck, D. K., Hoekstra, D., and Pagano, R. E. (1981) *Biochemistry 20*, 4093-9.

2. Fung, B. K.-K., and Stryer, L. (1978) *Biochemistry 17*, 5241-5248.

3. Duzgunes, N., and Bentz, J. (1988) in *Spectroscopic Membrane Probes* (Loew, L. M., Ed.) pp 117-159, CRC Press, Inc., Boca Raton, FL.

4. LeDuc, D. L., Shin, Y. K., Epand, R. F., and Epand, R. M. (2000) *Biochemistry 39*, 2733-9.

5. Leikina, E., LeDuc, D. L., Macosko, J. C., Epand, R., Shin, Y. K., and Chernomordik, L. V. (2001) *Biochemistry 40*, 8378-86.

6. Epand, R. F., Macosko, J. C., Russell, C. J., Shin, Y. K., and Epand, R. M. (1999) *J. Mol. Biol. 286*, 489-503.

7. Kim, C. H., Macosko, J. C., Yu, Y. G., and Shin, Y. K. (1996) *Biochemistry 35*, 5359-65.

8. Macosko, J. C., Kim, C. H., and Shin, Y. K. (1997) *J. Mol. Biol. 267*, 1139-48.

9. Kim, C. H., Macosko, J. C., and Shin, Y. K. (1998) *Biochemistry 37*, 137-44.

10. Epand, R. F., Yip, C. M., Chernomordik, L. V., LeDuc, D. L., Shin, Y. K., and Epand, R. M. (2001) *Biochim. Biophys. Acta 1513*, 167-175.

11. Lau, W. L., Ege, D. S., Lear, J. D., Hammer, D. A., and DeGrado, W. F. (2004) *Biophys. J. 86*, 272-284.

12. Ogihara, N. L., Weiss, M. S., DeGrado, W. F., and Eisenberg, D. (1997) *Protein Sci. 6*, 80-88.

13. Weissenhorn, W., Dessen, A., Harrison, S. C., Skehel, J. J., and Wiley, D. C. (1997) *Nature 387*, 426-30.

14. Caffrey, M., Cai, M., Kaufman, J., Stahl, S. J., Wingfield, P. T., Covell, D. G., Gronenborn, A. M., and Clore, G. M. (1998) *EMBO J. 17*, 4572-84.

15. Aloia, R. C., Tian, H., and Jensen, F. C. (1993) *Proc. Natl. Acad. Sci. U. S. A. 90*, 5181-5.

16. Yang, J., Gabrys, C. M., and Weliky, D. P. (2001) *Biochemistry 40*, 8126-37.

17. Hope, M. J., Bally, M. B., Webb, G., and Cullis, P. R. (1985) *Biochim. Biophys. Acta 812*, 55-65.

18. Chan, D. C., Fass, D., Berger, J. M., and Kim, P. S. (1997) *Cell 89*, 263-73.

19. Tan, K., Liu, J., Wang, J., Shen, S., and Lu, M. (1997) *Proc. Natl. Acad. Sci. U. S. A. 94*, 12303-8.

20. Yang, Z. N., Mueser, T. C., Kaufman, J., Stahl, S. J., Wingfield, P. T., and Hyde, C. C. (1999) *J. Struct. Biol. 126*, 131-44.

21. Nieva, J. L., Nir, S., and Wilschut, J. (1998) *J. Lipos. Res. 8*, 165-182.

22. Yang, J., and Weliky, D. P., unpublished experiments.

23. Yang, J., and Weliky, D. P. (2003) *Biochemistry 42*, 11879-11890.

24. Sackett, K., and Shai, Y. (2002) *Biochemistry 41*, 4678-85.

CHAPTER V

KINETIC ANALYSIS OF FUSION ASSAY

BACKGROUND

In Chapter IV, the final extent of lipid mixing (M_f) was used as a measure of fusogenicity. The M_f values associated with FPmn-, FPdm-, and FPtr-induced fusion were compared to demonstrate that oligomerized HIV-1 fusion peptides could induce more vesicle fusion than fusion peptides.

M_f values are representative of how much fusion has occurred. We are not only interested in the amount of fusion, but also interested in how fast the fusion has occurred, since an increased fusion rate is likely the most important fusion peptide effect on viral/target cell fusion,

Preliminary analysis showed that fusion rates are generally larger for cross-linked peptides than for FPmn. In this chapter, we analyzed the kinetics of stopped-flow fluorescence data to determine the variation of fusion rate with fusion peptide constructs. We also investigated the temperature dependence of fusion rates and derived the activation energy, pre-exponential factor, and change of entropy for LM3 and PC/PG vesicle fusion induced by FPmn, FPdm, and FPtr. A physical model is presented to explain the observed trends of these variables.

We noted that the FPtr used in Chapter IV induced a similar amount of fusion as FPdm (cf. Figure 21, 22 and Table 1 in Chapter IV). We speculated that this might be due to the fact that FPdm has an in-register strand alignment, whereas FPtr has one strand out of register with respect to the other two strands (cf. Figure 7 and 8, Chapter II). According to the high-resolution structure of HIV-1 gp41 [1, 2], the most likely fusion peptide topology would be an in-register trimer, and it is possible that this arrangement is a structural requirement for enhanced fusogenicity. In order to study the most

biologically relevant system, we improved our synthetic strategy and created an FPtr with an in-register strand arrangement. Our kinetic analyses in this chapter were made on the new version of FPtr. With the in-register trimer, we found that the rate of vesicle fusion induced by FPtr was substantially higher than the rate of vesicle fusion induced by FPdm and FPmn.

Also, we increased the length of the C-terminal lysine sequence from three to six lysines in order to reduce peptide aggregation. Analytical ultracentrifugation has shown that the FPmn, FPdm, and FPtr studied in this chapter do not self-associate in an aqueous solution at concentrations similar to those of the stock solutions used for fusion assays (cf. Chapter III).

MATERIALS AND METHODS

Peptides. Monomeric, dimeric, and trimeric HIV-1 fusion peptides were synthesized as described in Chapter II. In particular, FPtr is made as an in-register trimer by method 2, which is different from the out-of-register trimer used in Chapter IV. All three peptide constructs included 6 C-terminal lysines (cf. Chapter III). The amino acid sequences of FPmn, PFdm, and FPtr are displayed in Figure 23.

Figure 23. Amino acid sequences of FP constructs in the kinetic analysis of fusion reaction.

Preparation of large unilamellar vesicles (LUVs). Lipids and cholesterol were purchased from Avanti (Alabaster, AL). LUVs were prepared with one of the two compositions: (1) "LM3" – 1-palmitoyl-2-oleoyl-*sn*-glycero-3-phosphocholine (POPC), 1-palmitoyl-2-oleoyl-*sn*-glycero-3-phosphoethanolamine (POPE), 1-palmitoyl-2-oleoyl-*sn*-glycero-3-[phospho-L-serine] (POPS), sphingomyelin, phosphatidylinositol (PI) and cholesterol in a 10:5:2:2:1:10 mol ratio. (2) "PC/PG" – 1-palmitoyl-2-oleoyl-*sn*-glycero-3-phosphocholine (POPC) and 1-palmitoyl-2-oleoyl-*sn*-glycero-3-[phospho-*rac*-(1-glycerol)] (POPG) in a 4:1 mol ratio. LM3 reflects the approximate lipid headgroup and cholesterol composition of host cells of the HIV-1 virus [3] and PC/PG has been a common composition used in studies of FPs. In addition, solid state NMR structural measurements are consistent with predominant β strand conformation for LM3-associated FPs and with predominant helical conformation for PC/PG-associated FPs (cf. Chapter VII). For either composition, ten percent of the LUVs were prepared with an additional 2 mol% of the fluorescent lipid *N*-(7-nitro-2,1,3-benzoxadiazol-4-yl)-phosphatidylethanolamine (*N*-NBD-PE) and 2 mol% of the quenching lipid *N*-(lissamine Rhodamine B sulfonyl)-phosphatidylethanolamine (*N*-Rh-PE).

Large unilamellar vesicles (LUVs) of 100 nm diameter were prepared by extrusion [4] using a procedure described in Chapter IV.

Peptide Concentration Quantitation. Peptide concentrations were quantitated by 280-nm absorbance. We used 6000 $M^{-1}cm^{-1}$, 12000 $M^{-1}cm^{-1}$, and 18000 $M^{-1}cm^{-1}$ as the extinction coefficient for FPmn, FPdm, and FPtr, respectively. The reproducibility of an absorbance measurement was ± 0.010 a.u. or typically ± 2%.

Stopped-flow Fluorescence Assay and Analysis. In this assay, fluorescence was recorded on a stopped-flow fluorimeter (Applied Photophysics SX.18MV-R, Surrey, UK) using excitation and emission wavelengths of 465 and 530 nm, respectively. In the instrument, one syringe contained a mixture of labeled and unlabeled LUVs at 1:9 ratio and 300 μM total lipid concentration, and the other syringe contained FPmn, FPdm, or FPtr at 3, 2, or 1 μM concentration, respectively, as determined from 280 nm absorbance. The buffer in each syringe solution was 5 mM HEPES pH 7 with 0.01% NaN_3. Time zero in the assay was set by the ~5 ms mixing of the two solutions and fluorescence was then measured every second for ~1000 s. The temperature of the system was set to a value specified between 25 and 40 °C.

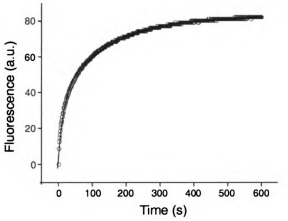

Figure 24. Fluorescence data and fitting for FPdm-induced PC/PG lipid mixing at 37 °C. The step-like features at longer times are due to the digitization of the data.

As displayed in Figure 24, fluorescence data F(t) in arbitrary units were fitted with equation 1:

$$F(t) = F_0 + F_1(1 - e^{-k_1 t}) + F_2(1 - e^{-k_2 t}) \quad (1)$$

where F_0, F_1, F_2, k_1, and k_2 are fitting parameters. F_0 represents the fluorescence intensity prior to mixing the LUV and FP solutions. The fluorescence increase after mixing was modeled as the sum of a fast buildup with overall fluorescence change F_1 and rate constant k_1, and a slow buildup with overall fluorescence change F_2 and rate constant k_2. Fitting was much poorer with a single buildup model. In a single data set, the best-fit values of F_1 and F_2 are generally comparable, and the best-fit $k_1 \sim 10\ k_2$. The fast component likely represents the lipid mixing induced by initial interaction of FPs with membranes and the associated k_1 rate constants are listed as the rate constants k in Table 1. The origin of the slow component in fluorescence buildup is not yet understood.

Temperature-dependence of The Fusion Rate. In an Arrhenius model, $k=Ae^{-E_a/RT}$ and the variations in rate constants would have contributions from differences in activation energy E_a and differences in pre-exponential factor A [5]. To quantify these contributions, assays and kinetic analyses were carried out over a temperature range of

25-40 °C. As an example, Figure 25 plots the natural log of FPtr-induced fast fusion rate vs. temperature. According to the Arrhenius equation, a linear relationship exists between ln$k$ and 1/T:

$$\ln k = \ln A - E_a/RT \quad (2)$$

$$A = (e^2 k_B T/h) e^{\Delta^{\ddagger}S^{\circ}/R} \quad (3)$$

In the Arrhenius model, the activation energy (E_a) represents the energy barrier for lipid mixing. The pre-exponential factor (A) is related to the frequency of collision of reactants and probability of favorably oriented collision. Their values can be calculated from the slope and y-intersection of the Arrhenius plot, respectively. $\Delta^{\ddagger}S^{\circ}$ is the change of entropy from the initial state to the transition state of the fusion reaction, and its value could be calculated from the A value using equation 3 [5].

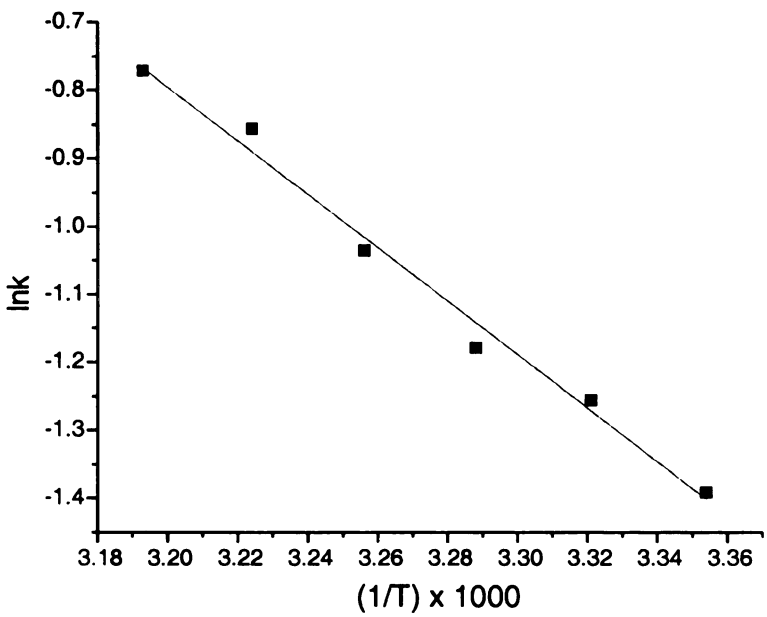

Figure 25. Arrhenius plot for FPtr-induced LM3 fusion (fast component).

RESULTS

Rate of Fusion. Figure 26 displays the stopped-flow fluorescence data for FP-induced (a) LM3 and (b) PC/PG lipid mixing. In the assays, [FPmn]=2[FPdm]=3[FPtr] and the strand concentration was constant among the different constructs. The long-time changes in fluorescence for both LM3 and PC/PG are ordered $\Delta F_{mn}<\Delta F_{dm}<\Delta F_{tr}$, which suggests that the oligomeric constructs induce more vesicle fusion than FPmn. Because an increased fusion rate is an important FP effect in viral/target cell fusion, the kinetics of the stopped-flow fluorescence data were analyzed to determine the variation of fusion rate with FP construct. In a single data set, the initial increase in fluorescence could be modeled by a dominant fast exponential buildup, while at longer time, there was an additional contribution from a slower buildup. The data were fitted with equation 1 and the fitting results for FP-induced LM3 and PC/PG vesicle fusion at 37°C are listed in Table 2. The fast component likely represents the lipid mixing induced by initial interaction of FPs with membranes and the values of its rate are presented as k_1. The values of slow fluorescence build up rates are presented as k_2. For both PC/PG and LM3 vesicles, $k_{tr}>k_{dm}>k_{mn}$ with $k_{1\text{-}tr}\sim 40k_{1\text{-}mn}$ for LM3 and $k_{1\text{-}tr}\sim 15k_{1\text{-}mn}$ for PC/PG. Thus, there is very significant correlation of the fusion rate with both the oligomeric topology enforced by C-terminal cross-linking and with the number of FP strands in the construct.

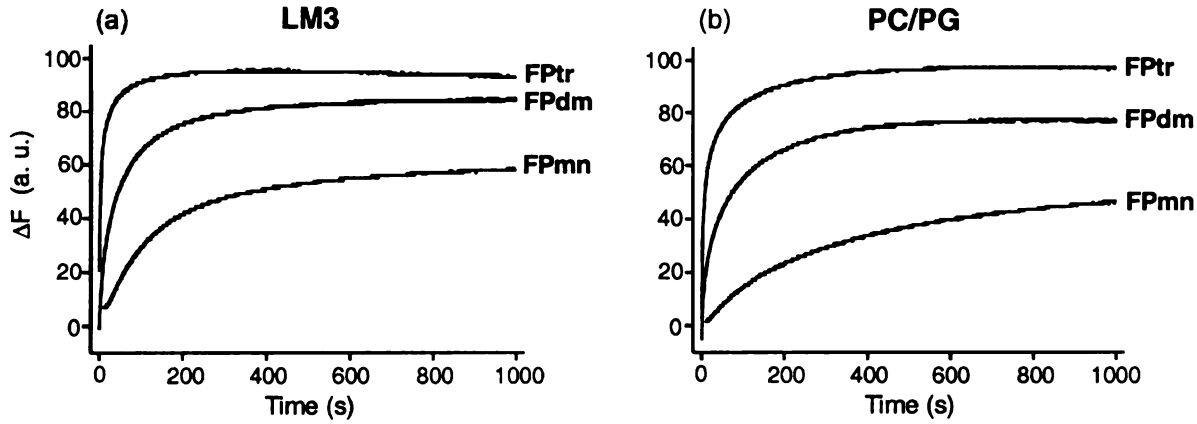

Figure 26. Stopped-flow fluorescence data for FP-induced lipid mixing in (a) LM3 and (b) PC/PG vesicles at 37 °C and [total lipid] = 150 μM, [FPmn] = 1.5 μM, [FPdm] = 0.75 μM, and [FPtr] = 0.50 μM.

Table 2. Fitting Results for FP-induced Vesicle Fusion According to Equation 1.

	LM3			PC/PG		
	FPmn	FPdm	FPtr	FPmn	FPdm	FPtr
k_1 (10^{-3} s^{-1})	11	76	430	13	63	190
k_2 (10^{-3} s^{-1})	3	11	40	3	7	11
F_1 (10^{-3} a.u.)	98	90	123	29	80	145
F_2 (10^{-3} a.u.)	60	119	51	92	116	89
F_0 (10^{-3} a.u.)	-612	-604	-612	-422	-464	-457

The listed k and F values are at 37°C. Each k value has ±20% uncertainty and each F value has ±10% uncertainty.

Temperature-dependence of Fusion Rate. We examined the temperature dependence of reaction rate by obtaining the *k* values at 25°C, 28°C, 31°C, 35°C, 37°C, and 40°C. Figure 27 and 28 display k_1 and k_2 Arrhenius plots and linear fits for some of the plots. Arrhenius plots of the data yielded values of E_a and lnA for FP-induced lipid mixing in LM3 and PC/PG. As presented in Table 3, the values of E_a and lnA are similar for FPtr-induced fusion of either LM3 or PC/PG LUVs, and in PC/PG, $E_{a\text{-}tr}<E_{a\text{-}dm},E_{a\text{-}mn}$ and $A_{tr}<A_{dm},A_{mn}$. Thus, the changes in E_a and A appear to have competing effects on the magnitude of k. The entropy of activation $\Delta S^{\ddagger}$ at 37°C was approximately calculated with the transition-state theory expression $\Delta S^{\ddagger}=R[\ln(Ah/k_BT)-2]$ where R, h, and k_B are the standard physical constants [5]. It is not yet clear why $\Delta S^{\ddagger}<0$ for all constructs and why $\Delta S_{tr}^{\ddagger}<\Delta S_{dm}^{\ddagger},\Delta S_{mn}^{\ddagger}$. The PC/PG k_2 Arrhenius plots were also linear with trends $E_{a\text{-}tr} < E_{a\text{-}dm} < E_{a\text{-}mn}$ and $\ln A_{tr} < \ln A_{dm} < \ln A_{mn}$, which are similar to the trends observed for the PC/PG k_1 Arrhenius plots. We do not yet understand the non-linearity of the Arrhenius plots for FPmn and FPdm-induced fusion of LM3 LUVs.

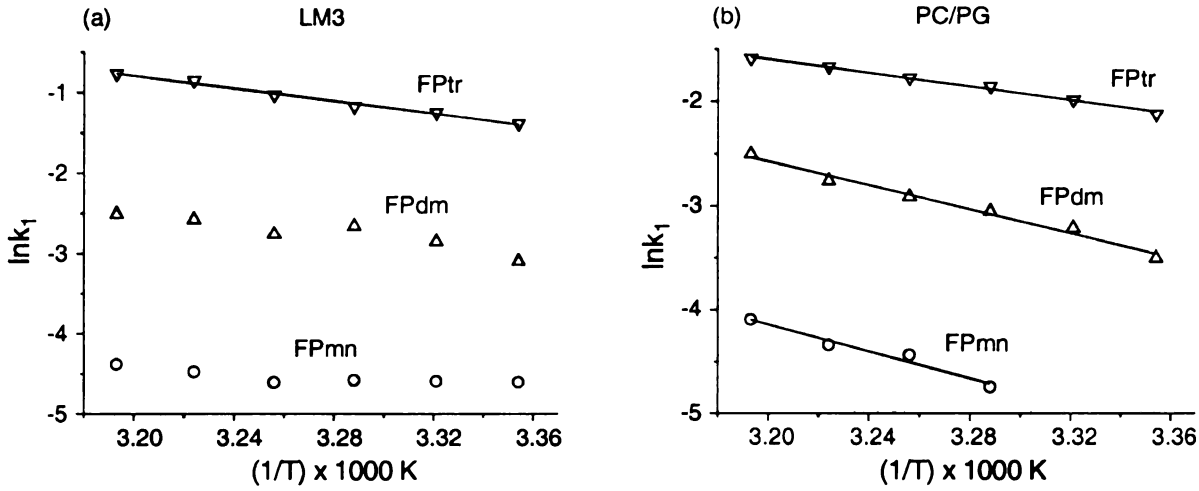

Figure 27. Arrhenius plots for the fast component of FP-induced lipid mixing in (a) LM3 and (b) PC/PG.

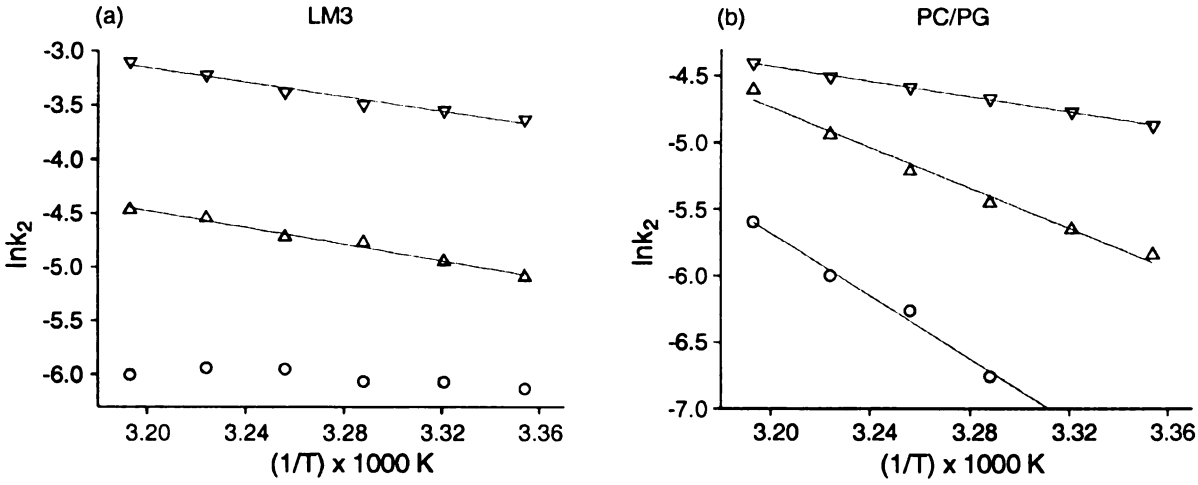

Figure 28. Arrhenius plots for the slow component of FP-induced lipid mixing in (a) LM3 and (b) PC/PG.

Table 3. Kinetic Parameters of FP-induced Vesicle Fusion.

	LM3			PC/PG		
	FPmn	FPdm	FPtr	FPmn	FPdm	FPtr
k (10^{-3} s^{-1})	11	76	430	13	63	190
E_a(kJ/mol)	n.d.	n.d.	33(2)	54(7)	48(3)	27(1)
lnA	n.d.	n.d.	12(1)	17(3)	16(1)	9(1)
$\Delta S^{\ddagger}$(J/mol-K)	n.d.	n.d.	-160	-120	-130	-190

The listed k and $\Delta S^{\ddagger}$ values are at 37°C. Each k value has ±20% uncertainty and the fitting uncertainties in E_a and lnA are given in parentheses. Because of significant deviations from linearity, the Arrhenius plots for FPmn and FPdm in LM3 are not presented.

DISCUSSION

In summary, enforcement of the trimeric biological FP strand topology by cross-linking reduces E_a and increases the fusion rate by a factor of 15-40. The effect is observed both for LM3 and for PC/PG fusion in which the membrane-associated FPs have dominant β strand and helical conformations, respectively (cf. Chapter VII). For FPdm or FPtr in either conformation, one reason for the fusogenic enhancement may be placement of the apolar N-terminal regions of strands on one end of the oligomer and placement of the more polar C-terminal regions of strands on the other end of the oligomer. FPtr likely has the largest apolar volume which may correlate with the greatest membrane disruption and fusion rate for this construct. Fusion may also be enhanced by the larger localized free energy released upon membrane binding of multiple FP strands in FPdm and FPtr. We note that enhanced fusion has also been observed with influenza protein constructs which likely contain FPs in the biologically relevant trimeric topology [6, 7].

For both PC/PG and LM3 vesicles, $k_{tr}>k_{dm}>k_{mn}$. In addition, $E_{a\text{-}tr}$ (LM3) ~ $E_{a\text{-}tr}$ (PC/PG), $\ln A_{tr}$ (LM3) ~ $\ln A_{tr}$ (PC/PG). In PC/PG vesicle fusion, $E_{a\text{-}tr} < E_{a\text{-}dm}$, $E_{a\text{-}mn}$ & $A_{tr} < A_{dm}$, A_{mn}. These trends suggest that E_a and A play competing roles in affecting k values.

We set up a simplified model to interpret our data. In this model, vesicle fusion occurs in a two-step process:

Step1: $P + V \rightarrow PV$ rate constant k_B

Step2: $PV + PV \rightarrow A$ rate constant k_F

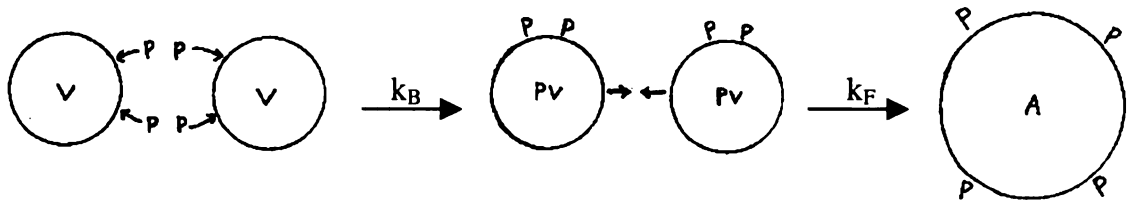

Figure 29. Collision model for vesicle fusion.

where P stands for the fusion peptide, V stands for the unfused vesicle, PV stands for the unfused vesicle with bound peptide, and A stands for the fused vesicle product.

We consider the maximum rates of the two reactions which are determined by diffusion-limited collision rates [8].

$$d[PV]/dt = k_B[P][V] \leq k_D^{P\text{-}V}[P][V] \quad (4)$$

$$d[A]/dt = k_F[PV]^2 \leq k_D^{PV\text{-}PV}[PV]^2 \quad (5)$$

In general, the diffusion-limited rate constant k_D for collision between particles A and B can be described by [8]:

$$k_D = 2k_BT(r_A + r_B)^2/ 3\eta(T)r_Ar_B \quad (6)$$

where k_B is Boltzmann's constant, T is the temperature of reaction, $\eta(T)$ is the temperature-dependent viscosity of the solution, and r_A and r_B are the radii of the two particles. In our model, the radii of V and PV are ~ 500 Å which are determined by our sample preparation methods. In equation 4, we assign particle A as V and particle B as P, while in equation 5, particles A and B are both PV. For equation 4, r_B is given by the effective hydrodynamic radius (r_H) of the fusion peptide [9]:

$$r_H = [3VM_r/(4\pi N_A)]^{1/3} + r_w \qquad (7)$$

where V is the specific volume of the fusion peptide, M_r is the molecular mass of the peptide, N_A is Avogadro constant, and r_w is the thickness of a hydration layer. Assuming the specific volume V = 0.73 cm^3/g and a hydration layer r_w = 2.4 Å [9], the radius of FPtr is ~ 16 Å.

Steinfeld et al. gives a typical k_D value of 6×10^9 $M^{-1}s^{-1}$ for collisions at 300 K with r_A and r_B equal to 2 Å [8]. Using this number and our values for r_A and r_B, $k_D^{P\text{-}V}$ is ~ 50×10^9 $M^{-1}s^{-1}$, and $k_D^{PV\text{-}PV}$ is ~ 6×10^9 $M^{-1}s^{-1}$. In the fusion assay, at FPtr:lipid mole ratio of 1:300, the initial concentrations for different species are: $[P]_0 = 5 \times 10^{-7}$ M, and $[V]_0 = 1.5 \times 10^{-9}$ M (using an estimated 100,000 lipid molecules per vesicle). In a model in which step 1 occurs much more rapidly than step 2, the initial rates $d[PV]_0/dt \approx k_B[P]_0[V]_0$, and $d[A]_0/dt \approx k_F [PV]_0^2 \approx k_F [V]_0^2$. Using $k_B = k_D^{P\text{-}V}$ and $k_F = k_D^{PV\text{-}PV}$, we calculate $(d[PV]_0/dt)/(d[A]_0/dt])$, which is predicted by our model to be $\gg 1$.

$$\begin{aligned}(d[PV]_0/dt)/(d[A]_0/dt]) &= k_B[P]_0[V]_0/\, k_F[PV]_0^2 \\ &= k_D^{P\text{-}V}[P]_0[V]_0/\, k_D^{PV\text{-}PV}[V]_0^2 \\ &= k_D^{P\text{-}V}[P]_0/\, k_D^{PV\text{-}PV}[V]_0 \\ &= 2.5 \times 10^3\ s^{-1}/\, 9\ s^{-1} \approx 300 \end{aligned} \qquad (8)$$

The result supports our model, and suggests that the second step is the rate-limiting step in the fusion process.

The fastest experimentally observed fusion rate is ~ 0.4 s^{-1} and is for FPtr-induced LM3 fusion (cf. Table 2). This is slower than the calculated PV-PV collision rate (~ 9 s^{-1}) and suggests that ~ 5% of the PV-PV collisions lead to fusion.

This two-step model provides some insights of the fusion process. Under our experimental conditions, the predicted P-V collision rate is significantly greater than the PV-PV collisions rate, and suggests that peptides first bind to vesicles and then vesicles fuse. In addition, the diffusion-limited rate of the rate-limiting step is 9 s^{-1}, which is much faster than the fastest experimental fusion rate (0.4 s^{-1}) and suggests that relatively few PV-PV collisions lead to fusion. A possible explanation is that the surface of the unfused vesicles are not fully covered with fusion peptides, and that the intervesicle contacts in a large number of collisions do not occur at FP binding sites. This idea is supported by the following calculations of the vesicle surface area and the FPtr surface area on the vesicle. The surface area of an LM3 vesicle with radius 500 Å is:

$$A_V = 4\pi r^2 = 4\pi(500\ \text{Å})^2 \approx 3 \times 10^6\ \text{Å}^2$$

If we consider FPtr as a sphere when it binds with the vesicle, the cross-sectional area of the sphere can be calculated using r_H ~ 16 Å for FPtr,

$$A_F = \pi r_H^2 \approx 800\ \text{Å}^2$$

At FPtr:lipid mole ratio of 1:300 and 100,000 lipid molecules per vesicle, there would be ~100,000/300 ≈ 300 FPtr bound with one vesicle. The fractional surface area of FPtr on an LM3 vesicle would be:

$$300 \times 800\ \text{Å}^2 / 3 \times 10^6\ \text{Å}^2 \approx 0.08$$

The result suggests that only 8% of the vesicle surface is covered with FPtr molecules. These data support a model in which only PV-PV collisions at FP binding sites would lead to fusion. This is consistent with the small value of experimentally observed fusion rate (~ 0.4 s^{-1}) relative to the PV-PV collision rate (~ 9 s^{-1}).

Besides the fractional surface area, the membrane-insertion topology of the different fusion peptide constructs may also affect the fusion rate. r_H for FPmn is ~ 12 Å and r_H for FPdm is ~ 15 Å. At a 1:100 FP strand to lipid mole ratio, their corresponding fractional surface coverage are ~ 0.15 and 0.12, respectively. If the peptide surface coverage was the only factor in determining the fusion rate, we would expect faster fusion rate for FPmn- and FPdm-induced vesicle fusion comparing to FPtr-induced vesicle fusion. However, the experimental results of $k_{tr}>k_{dm}>k_{mn}$ with $k_{l\text{-}tr}$ ~ 15-40 $k_{l\text{-}mn}$ suggests that FPtr may adopt a conformation which facilitates membrane fusion more efficiently than FPmn and FPdm. The membrane-insertion topology of FPtr could be in-register parallel strand arrangement or "splayed helix pyramid" [10], which may be correlated with the greatest membrane disruption (cf. Chapter VII).

Another interesting topic is the dependence of fusion rate on fusion peptide and vesicle concentration. We observed an approximately linear relationship between [FPdm] and FPdm-induced LM3 fusion rate. We also observed an approximately quadratic dependence of FPmn-induced LM3 fusion rate on [FPmn] (cf. Chapter IV, Figure 22). We hypothesize that the actual fusion rate constant k_F is determined by the product of k_D and a fusion factor f,

$$k_F = k_D \times f \qquad (9)$$

where $f < 1$.

If we consider that fusion peptides first bind to the surface of vesicles at a fast rate, then increasing fusion peptide concentration would result in increasing the surface density of fusion peptides, but not appreciably change $k_D^{PV\text{-}PV}$. The observed increase in fusion rate with higher fusion peptide concentration would be a result of increasing f, and is likely related to the greater membrane disruption associated with higher fusion peptide concentration. The preliminary data on the orders of reaction of FP were obtained using a regular fluorimeter with an acquisition delay of ~ 1 s, and it would be interesting to investigate the [FP] dependence of fusion rate for FPmn-, FPdm-, and FPtr-induced fusion using a stopped-flow fluorimeter, which has a much shorter acquisition delay (~ 5 ms). Because fluorescence intensity builds up rapidly after mixing FP with vesicles, the stopped-flow fluorimeter would provide the short-time fluorescence data which are essential for more accurate kinetic analysis.

Equation 5 predicts that the fusion rate would have a quadratic dependence of [PV]. This hypothesis can be tested by further experiments in which the variation of fusion rates with lipid concentrations are examined. The model predicts that there would be a quadratic relationship between fusion rate and [lipid], because of the linear correlation between [lipid] and [PV].

REFERENCE

1. Caffrey, M., Cai, M., Kaufman, J., Stahl, S. J., Wingfield, P. T., Covell, D. G., Gronenborn, A. M., and Clore, G. M. (1998) *EMBO J. 17*, 4572-84.

2. Weissenhorn, W., Dessen, A., Harrison, S. C., Skehel, J. J., and Wiley, D. C. (1997) *Nature 387*, 426-30.

3. Aloia, R. C., Tian, H., and Jensen, F. C. (1993) *Proc. Natl. Acad. Sci. U. S. A. 90*, 5181-5.

4. Hope, M. J., Bally, M. B., Webb, G., and Cullis, P. R. (1985) *Biochim. Biophys. Acta 812*, 55-65.

5. McQuarrie, D. A., and Simon, J. D. (1997) *Physical Chemistry: A Molecular Approach*, University Science Books, Sausalito, CA.

6. Epand, R. F., Macosko, J. C., Russell, C. J., Shin, Y. K., and Epand, R. M. (1999) *J. Mol. Biol. 286*, 489-503.

7. Lau, W. L., Ege, D. S., Lear, J. D., Hammer, D. A., and DeGrado, W. F. (2004) *Biophys. J. 86*, 272-284.

8. Steinfeld, J. I., Francisco, J. S., and Hase, W. L. (1999) *Chemical Kinetics and Dynamics*, Prentice-Hall, Upper Saddle River, NJ.

9. Cavanaugh, J., Fairbrother, W. J., Palmer, A. G., and Skelton, N. J. (1996) *Protein NMR Spectroscopy Principles and Practice*, Academic Press, San Diego.

10. LeDuc, D. L., Shin, Y. K., Epand, R. F., and Epand, R. M. (2000) *Biochemistry 39*, 2733-9.

CHAPTER VI

ELECTRON MICROSCOPY

BACKGROUND

Besides the fluorescence assay, we applied transmission electron microscopy (TEM) to assess the effect of the synthetic HIV-1 fusion peptides on membrane fusion.

TEM relies on a focused beam of electrons to examine objects on a very fine scale and produces magnified images of up to > 100,000 times the original object size. Therefore it is suitable for visualizing small particles including viruses, proteins, and liposomes. In the study of viral membrane fusion, TEM has been employed to characterize the structural features of fusion intermediates [1,2] and the aggregation/fibrilization of fusion peptides interacting with membranes [3]. In addition, TEM has provided direct evidence that a synthetic construct of the HIV-1 fusion peptide induces vesicle fusion [4]. Despite the broad application of TEM in studying viral membrane fusion, there has been no TEM data to date that directly compares the fusogenicity of monomeric HIV-1 fusion peptide and its oligomeric analogs.

In the present study, FPmn, FPdm and FPtr were added to LM3 and PC/PG vesicles. Negative stain TEM images of the FP-vesicle samples and pure vesicle samples were obtained. Our results evidenced that synthetic HIV-1 fusion peptides induce vesicle fusion. This agrees with Nieva et al.'s report [4], where TEM showed that a membrane-incorporated HIV-1 fusion pepide induces fusion of vesicles. In particular, our TEM data demonstrated much larger aggregates of fused vesicles in the samples containing FPtr and FPdm compared to samples containing FPmn. Therefore, TEM provided direct evidence for the enhanced fusogenicity of oligomeric fusion peptides.

MATERIAL AND METHODS

Sample Preparation. LUVs of LM3 and PC/PG were prepared in a similar procedure as described in Chapter IV and V [5], except that no fluorescent lipids were added. FPmn, FPdm, and FPtr were similar to what have been used in Chapter V. Peptides were dissolved in 5 mM pH 7 HEPES buffer and the concentrations were ~ 100, 50 and 30 μM for FPmn, FPdm, and FPtr, respectively. Peptide and LUV were mixed and gently vortexed ~ 15 minutes prior to negative staining and ~ 30 minutes prior to being viewed from the electron microscope. Two types of sample were prepared using 1 mM and 150 μM lipid concentration. In all the samples, the peptide strand-to-lipid mol ratio was 1:100.

Negative Staining. Negativly charged dyes containing heavy atoms commonly derived from molybdenum, uranium, or tungsten are added to TEM samples in order to increase the contrast between the objects and their background. This approach is called negative staining, which is a simple technique for routine examination of structures. They are commonly used to visualize the edges of protein complexes, macromolecules and cells in suspension. The stain we used in the present work was 1% uranyl acetate.

During staining, a small drop of the peptide/vesicle mixture was deposited on the carbon coated grid, allowed to settle for approximately one minute, blotted dry if necessary, and then covered with a small drop of the stain (1% uranyl acetate). After a few seconds, this drop is also blotted dry, and the sample is ready for viewing.

Transmission Electron Microscopy (TEM). Samples were observed using a JEOL (Japan Electron Optics Laboratories) 100CXII microscope at an accelerating voltage of 100 kv. TEM images were obtained at 5,000 – 100,000 magnification.

RESULTS

Figures 30, 31 display the TEM images of LM3 vesicles at lipid concentration 0.15 mM and 1 mM, respectively. No fusion peptides were added. The average vesicle size is ~ 100 nm in the 0.15 mM LM3 sample (cf. Figure 30) and is ~ 400 nm in the 1 mM sample (cf. Figure 31). The origin of the different vesicle sizes in the two samples is not known. In both samples all vesicles are unilamellar, and the majority of vesicles are unfused.

Figures 32, 34, and 36 display the TEM images of 0.15 mM LM3 in the prescence of FPmn, FPdm and FPtr, respectively. The FP strand to lipid molar ratios were 1:100. In the FPmn-LM3 sample (cf. Figure 32), fused vesicles with diameter of ~ 500 nm co-exist with unfused vesicles of ~ 100 nm. The number of fused vesicles is significantly less than that of unfused ones. In the FPdm-LM3 sample (cf. Figure 34), most vesicles are fused. The average size of aggregations is ~ 500 nm. The image of the FPtr-LM3 sample is dominated by vesicle aggregations bigger than 500 nm (cf. Figure 36). A comparison of these images clearly indicates that as the oligomerization state of FP increases, the size and number of aggregated/fused vesicles increase. FPs at higher oligomerization state are appreciably more fusogenic than FPs in the lower oligomerization state.

Figures 33, 35, and 37 display the TEM images of 1 mM LM3 with FPmn, FPdm, and FPtr, respectively. Similar trend of fusogenicity as observed in the 0.15 mM FP-LM3 samples are also found in these 1 mM LM3 samples. Increasing fusogenicity is associated with higher oligomerization states. In the FPmn-LM3 sample (cf. Figure 33), the majority of vesicles are unfused. Their sizes range from ~ 100 nm to ~ 300 nm. In the FPdm-LM3 sample (cf. Figure 35), significant amounts of vesicles are fused. The aggregates of fused

vesicles are approximately 200-500 nm in size. In FPtr-LM3 sample (Figure 37), the vesicle aggregates are ≥ 2 um. Since the vesicles are more concentrated in these samples, it is easier to find fused vesicles in the TEM images, and the aggregates seem to be bigger than those in the 0.15 mM samples.

Figures 38 and 39 display the TEM images of PC/PG vesicles at lipid concentration 0.15 mM and 1 mM, respectively. No fusion peptides were added. The majority of vesicles are unfused with a few exceptions. The vesicle sizes range from ~ 100 nm to 300 nm.

Figures 40, 42, and 44 display the TEM images of 0.15 mM PC/PG in the presence of FPmn, FPdm, and FPtr, respectively. Figures 41, 43, and 45 displayed the TEM images of 1 mM PC/PG with FPmn, FPdm, and FPtr, respectively. Similar to the trend observed in the FP-LM3 samples, larger aggregates of fused vesicles are present in the samples containing higher oligomerization states of FPs.

DISCUSSION

TEM data for LM3 and PC/PG vesicles with addition of FPmn, FPdm, and FPtr demonstrate that higher oligomerization states of FPs are associated with greater fusion catalyzing activity. Specifically, FPtr is the most fusogenic construct among the three peptides. This observation provides direct evidence for the enhanced fusogenicty of trimeric fusion peptide.

Our TEM data were obtained under the same peptide/lipid molar ratio as in the fluorescence assay described in Chapter IV and V. In particular, the TEM images for LM3 and PC/PG at lipid concentration 0.15 mM were obtained using the same vesicle

and peptide solutions as used in the kinetic analysis described in Chpater V. As the fluorescence assay established that FPtr possesses the greatest fusogenicity, a similar finding using TEM further confirms the point. We could conclude that fusion peptide trimerization plays an important role in membrane fusion.

Using electron microscopy, at least two groups have observed that fusion peptides form large fibrillar aggregates in neutral pH PBS or saline buffered D_2O where fusion of HIV virion occurs [3,4]. However, under our fusion peptide concentration and buffer composition, no fibrils or aggregated fusion peptides were identified. This may be because our data were obtained at a much lower peptide concentration than the other researchers, i.e. at 0.0015 mM or 0.01 mM fusion peptide concentration, while Nieva [4] used 0.1 mM fusion peptide and Karamov [3] used 0.5 mM. Karamov has suggested that fusogencitiy of fusion peptides are correlated with their potential to form long filaments in aqueous solution. On the contrary, our results do not support the direct correlation between fusogencity and the HIV-1 fusion peptide's ability to form fibrillar aggregates.

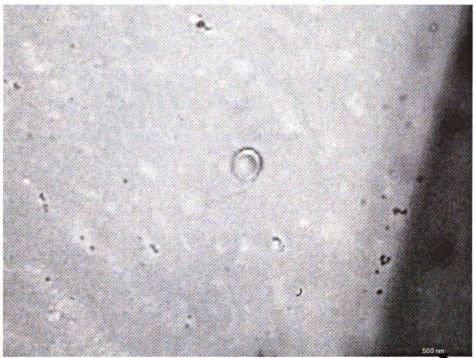

Figure 30. 0.15 mM LM3 (Magnification = 40,000)

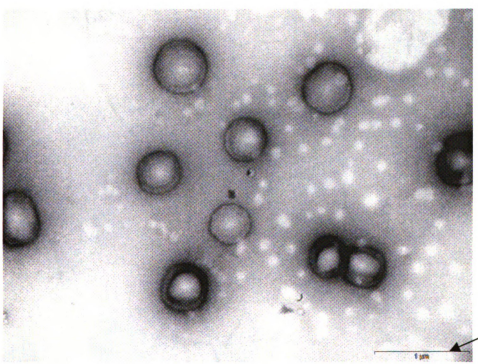

Figure 31. 1 mM LM3 (Magnification = 27,000)

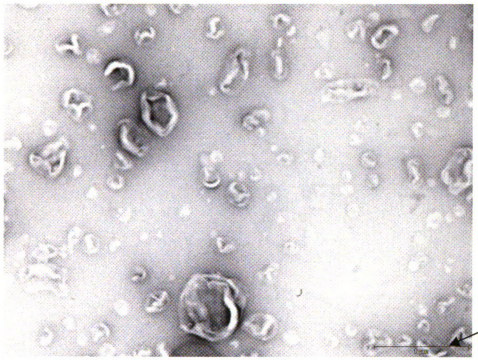

Figure 32. 0.15 mM LM3 + 0.0015 mM FPmn (Magnification = 27,000)

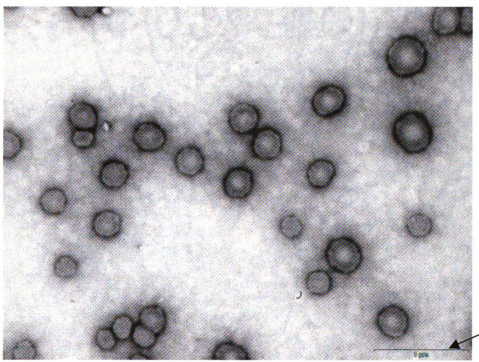

Figure 33. 1 mM LM3 + 0.01 mM FPmn (Magnification = 27,000)

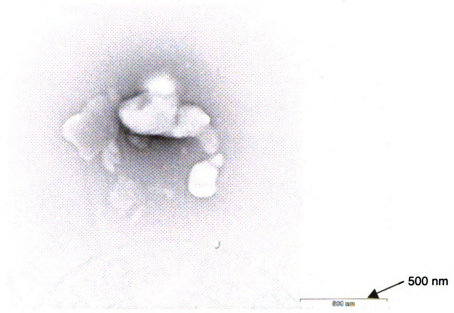

Figure 34. 0.15 mM LM3 + 0.00075 mM FPdm (Magnification = 50,000)

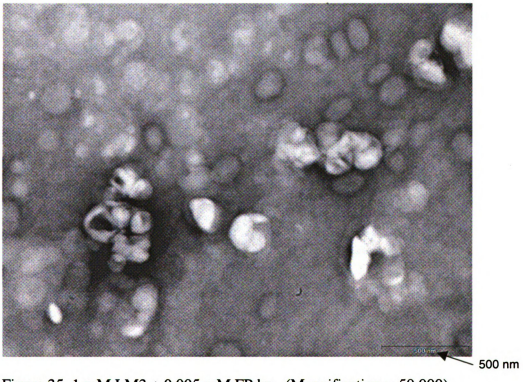

Figure 35. 1 mM LM3 + 0.005 mM FPdm (Magnification = 50,000)

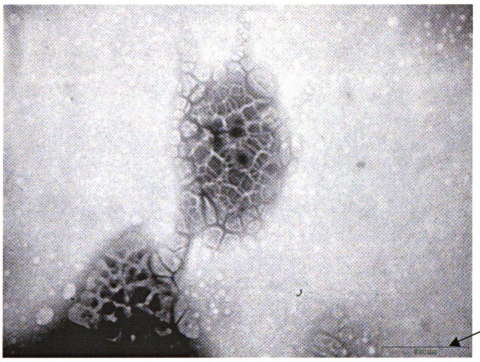

Figure 36. 0.15 mM LM3 + 0.0005 mM FPtr (Magnification = 50,000)

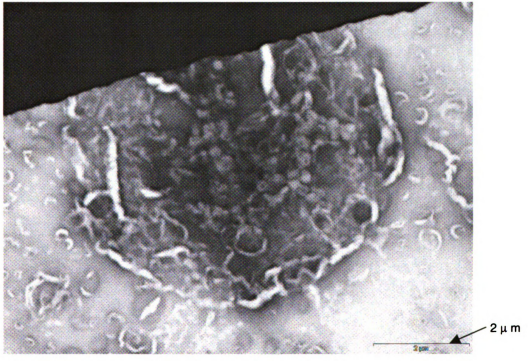

Figure 37. 1 mM LM3 + 0.0033 mM FPdm (Magnification = 14,000)

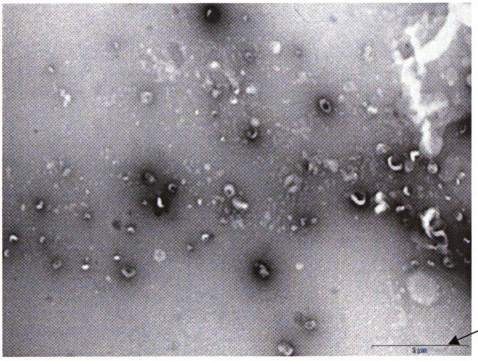

Figure 38. 0.15 mM PC/PG (Magnification = 14,000)

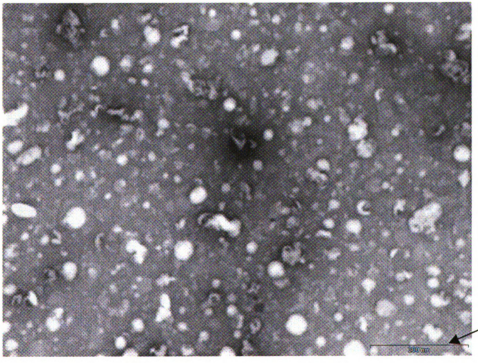

Figure 39. 1 mM PC/PG (Magnification = 14,000)

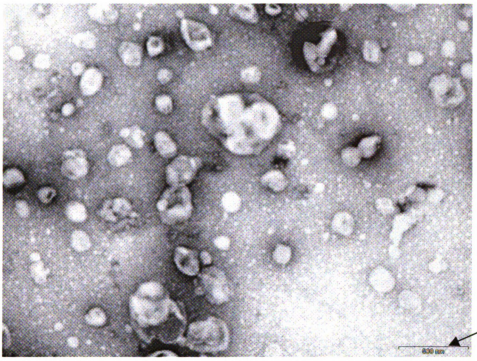

Figure 40. 0.15 mM PC/PG + 0.0015 mM FPmn (Magnification = 40,000)

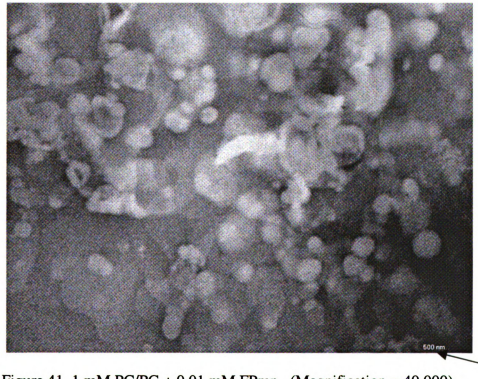

Figure 41. 1 mM PC/PG + 0.01 mM FPmn (Magnification = 40,000)

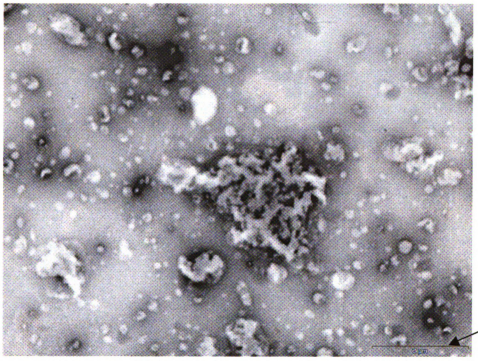

Figure 42. 0.15 mM PC/PG + 0.00075 mM FPdm (Magnification = 14,000)

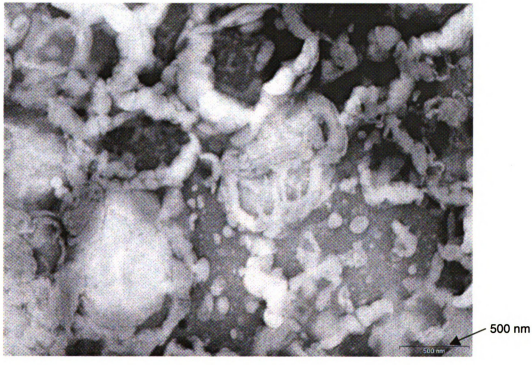

Figure 43. 1 mM PC/PG + 0.005 mM FPdm (Magnification = 40,000)

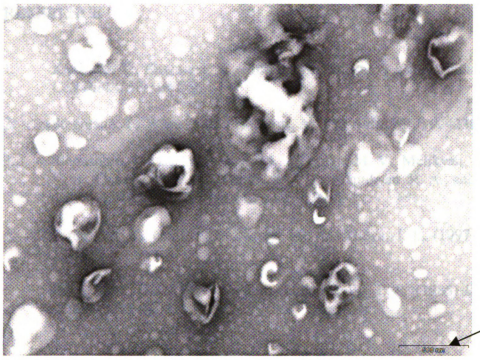

Figure 44. 0.15 mM PC/PG + 0.0005 mM FPtr (Magnification = 40,000)

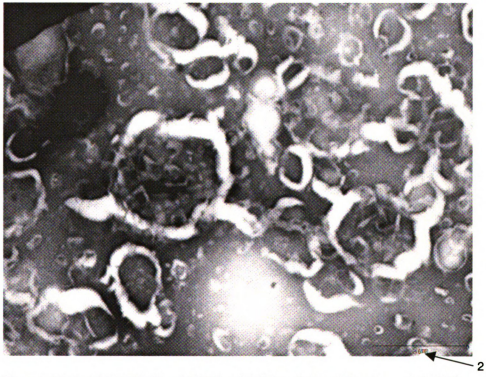

Figure 45. 1 mM PC/PG + 0.0033 mM FPtr (Magnification = 14,000)

REFERENCE

1. Kanaseki, T., Kawasaki, K., Murata, M., Ikeuchi, Y., and Ohnishi, S-i. (1997) *J. Cell Biol. 137*, 1041-56.

2. Stegmann, T., White, J. M., Helenius, A. (1990) *EMBO J. 9*, 4231-41.

3. Slepushkin, V. A., Andreev, S. M., Sidorova, M. V., Melikyan, G. B., Grigoriev, V. B., Chumakov, V. M., Grinfeldt, A. E., Manukyan, R. A., and Karamov, E. V. (1992) *AIDS Res. Hum. Retroviruses. 8*, 9-18.

4. Pereira, F. B., Goni, F. M., Muga, A., and Nieva, J. L. (1997) *Biophys. J. 73*, 1977-86.

5. Hope, M. J., Bally, M. B., Webb, G., and Cullis, P. R. (1985) *Biochim. Biophys. Acta 812*, 55-65.

CHAPTER VII

REDOR CHEMICAL SHIFT MEASUREMENTS TO PROBE THE SECONDARY STRUCTURE OF MEMBRANE-BOUND HIV-1 FUSION PEPTIDE CONSTRUCTS

BACKGROUND

The three dimensional structure of membrane-bound fusion peptide is essential for understanding its function in fusion catalysis. The low solubility of fusion peptide complicates the preparation of quality X-ray crystals. Therefore, X-ray crystallography is not an appropriate technique to probe fusion peptide structure. Solution NMR is not very suitable, either. Although the structure of fusion peptide solublized in detergent could be determined by solution NMR [1, 2], it is difficult to study the fusion peptide virtually immobilized in lipid membranes using solution NMR because of the lack of rapid molecular tumbling.

Solid state NMR has some advantages relative to the conventional techniques in detecting atomic-resolution structure of proteins in membrane environments. Unlike X-ray crystallography, solid state NMR does not require crystals; and unlike solution NMR, macromolecules do not have to truncate [3] [4].

Solid state NMR employs magic angle spinning (MAS) as a major approach to examine the structure of membrane proteins embedded in unoriented bilayer samples. MAS is defined as mechanically rotating the sample at an axis tilted at 54.7° relative to an external magnetic field. In these experiments, structural information can be obtained by measuring the dipolar interaction between coupled pairs of rare-spin spin-1/2 nuclei, because the dipolar coupling strength is inversely proportional to the cube of the internuclear distance. Solid-state NMR techniques for heteronuclear dipolar interaction measurements have been well developed. Examples include dipolar exchange-assisted recoupling (DEAR) [5], transfer-echo double-resonance (TEDOR) [6], and rotational-echo double-resonance (REDOR) [7] [8] techniques.

As a simple and versatile heterodipolar recoupling technique, REDOR filters the MAS signals of selectively labeled nuclei from the background signal of natural abundance isotopes. In the present work, REDOR was employed to perform chemical shift measurements which probe the secondary structure of the N-terminal region of our synthesized fusion peptide constructs. Based on the experimental correlation between secondary structure and NMR chemical shift [9], we investigated the local secondary structure in the vicinity of Phe-8 using its ^{13}C carbonyl carbon chemical shift.

The REDOR measurements were made on the consensus 23-residue HIV-1 fusion peptide sequence, AVGIGALFLGFLGAAGSTMGARS, and its cross-linked analogs. It has been demonstrated that the N-terminal and central region of the fusion peptide inserts into the target membrane during fusion [10] [11] [12]. Our central interest is to investigate the secondary and tertiary structure of these fusion peptide analogues in their membrane-bound states.

In the literature, there have been conflicting experimental data regarding the secondary structure of membrane-bound HIV-1 fusion peptide from CD, infrared, solution NMR, fluorescence, and ESR experiments [1, 13-23]. Evidence for both helical and β structures exists. Different conformations may arise from the differences in peptide sequence, lipid composition, sample preparation, or hydration level.

In our group, Yang et al. have reported a predominantly β strand structure of the fusion peptide N-terminal and central region when it is associated with membranes whose lipid headgroup and cholesterol composition is close to that of the host cell of the HIV-1 virus [24]. Moreover, REDOR experiments [12] probing the ^{13}C-^{15}N proximity between neighboring FP strands strongly support a structural model in which oligomeric β strands

are held together by inter-peptide hydrogen bonding. This experiment revealed equal population of fusion peptide in parallel and antiparallel strand arrangements. In the parallel alignment, the oligomeric strands are approximately in-register. Also, C-terminal fraying is detected in the parallel arrangement which is consistent with a reasonable biophysical model in which the apolar N-terminal and central regions of the oligomer insert into the membrane while the polar C-terminal region is outside the membrane (cf. Figure 49 (a)).

The gp41 soluble ectodomain structure consists of three gp41 subunits associating as an in-register helical coiled-coil, which ends just a few residues C-terminal of the fusion peptide. It has been postulated that at least three fusion peptides insert into the target membrane during fusion [25, 26]. In these contexts, it is attractive that a fusion peptide population was indeed observed with an approximately in-register parallel strand arrangement. This arrangement seems a natural extension of the soluble ectodomain oligomeric structure, and this arrangement also has a distinct apolar region of the fusion peptide oligomer which could penetrate into the membrane and catalyze fusion [12].

In the present study, we mimicked the trimeric topology of the HIV-1 fusion peptide and used solid-state NMR REDOR chemical shift measurements to probe the N-terminal secondary structure of individual strands in FPmn, FPdm, and FPtr embedded in LM3 and PC/PG bilayer membranes. Our result is consistent with a model in which the interacting fusion peptide strands adopt a β strand structure in LM3 and a helical structure in PC/PG. We hypothesized that the enhanced fusogencity of oligomeric fusion peptides in LM3 may be partly due to their preference for parallel strand arrangement.

METHODS

Solid State NMR Sample Preparation.

(1) Fusion Peptide in LUVs. Samples were typically prepared using 5 mM HEPES buffer (pH 7) which also contained 0.01% NaN_3. Between 0.05 and 0.4 μmol FPmn-F8CL9N, FPdm-F8CL9N, or FPtr-F8CL9N (cf. Figure 46) were mixed with LUVs containg 15 ~ 40 μmol LM3 or PC/PG lipids in a total volume of ~ 4 ml or 36 ml, and the mixture were kept at room temperature overnight to ensure maximum peptide/lipid binding. The peptide/lipid mixtures were then ultracentrifuged at 100,000g for 4 to 5 hours so that the membrane and associated peptide pelleted. The peptide/lipid pellet formed after ultracentrifugation was transferred by spatula to a 4 mm or 6 mm diameter magic angle spinning (MAS) NMR rotor.

Figure 46. Amino acid sequences of FPmn-, FPdm-, and FPtr-F8CL9N. Each peptide strand has a ^{13}C carbonyl carbon label at Phe-8 and an ^{15}N amide nitrogen label at Leu-9.

(2) FPmn in DPC. 0.5 μmol of FPK3W was dissolved in 250 μL 5 mM pH 7 HEPES buffer. DPC (dodecylphosphocholine) powder of ~ 50 μmol was added to the peptide solution. The sample was gently vortexed was for 1 hour. Subsequently the sample was frozen in liquid nitrogen and stored in a – 4 °C freezer.

Solid State NMR Spectroscopy. The rotational-echo double-resonance (REDOR) filtering technique relies on the heteronuclear dipolar interation between bonded spin ½ nuclei pairs. In our labeling approach, the peptide had a ^{13}C label at the Phe-8 carbonyl carbon and an ^{15}N label at the directly bonded Leu-9 amide nitrogen. In REDOR experiments, we took two ^{13}C spectra, one with N^{15} π pulses, and one without ^{15}N π pulses (cf. Figure 47).

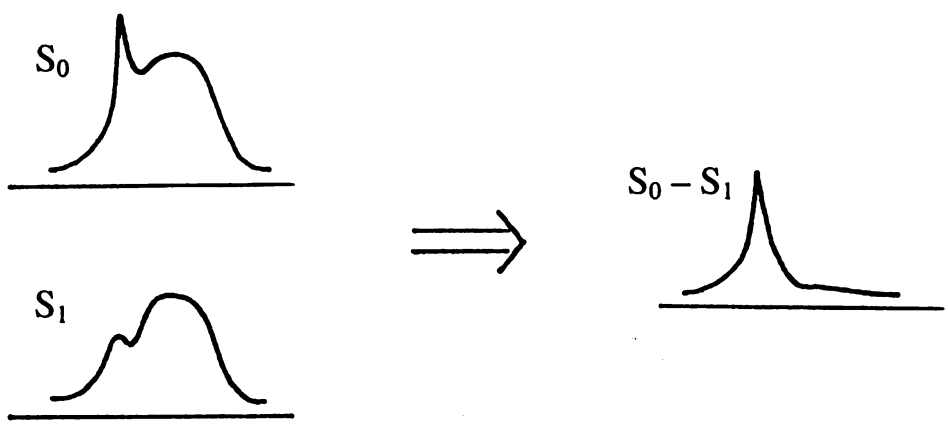

Figure 47. REDOR subtraction. S_0, S_1, and S_0-S_1 represents the full spectrum, reduced spectrum, and difference spectrum, respectively.

In the first spectrum (S_0), the ^{13}C signal arises from both the labeled carbonyl carbon and natural abundance ^{13}C in the protein and lipids. When taking the second spectrum (S_1), we apply two ^{15}N π pulses per MAS rotor period to the N channel. Because of the dipolar coupling between the carbonyl carbon of Phe-8 and its directly bonded amide nitrogen of Leu-9, the ^{13}C signal from Phe-8 carbonyl carbon is attenuated [27], while the ^{13}C signal from the protein backbone and lipids will remain unchanged. If we subtract the S_1 from

the S_0, the difference spectrum ($S_0 - S_1$) will be the signal from the Phe-8 carbonyl ^{13}C. In this way, the background from natural abundance ^{13}C is filtered out. The chemical shift of the difference spectrum can then be used to assess the distribution of local secondary structures in the vicinity of Phe-8.

There exists an experimental correlation between peptide secondary structure and NMR chemical shift [9]: For peptide or protein carbonyl carbons, helical secondary structure correlates with downfield (higher ppm) chemical shifts while extended β structure correlates with upfield (lower ppm) chemical shifts. This correlation is the basis of our interpretation of the NMR spectra.

Experiments were done on a 9.4 T spectrometer (Varian Infinity Plus) using a triple resonance MAS probe. Spacers were placed in a 4 mm or 6 mm diameter rotor so that the sample was in the central 2/3 volume of the coil length, and the ^{13}C and ^{15}N RF fields in the NMR probe circuit were reduced by at most 10% from their maximum values in the rotor center. The NMR detection channel was tuned to ^{13}C at 100.8 MHz, the decoupling channel was tuned to ^{1}H at 400.8 MHz, and the third channel was tuned to ^{15}N at 40.6 MHz. Experiments were carried out using a MAS frequency of 8000 Hz and the spinning frequency was stabilized to ± 2 Hz. A single spectrum was the average of 80,000 – 120,000 scans.

NMR spectra were taken using a REDOR filter of the ^{13}C–^{15}N dipolar interaction so that the Phe-8 carbonyl was the only signal observed in the ^{13}C-detected REDOR difference spectrum [7, 28]. Between 1 and 2 ms of cross-polarization at 50 kHz was followed by a 1-ms REDOR dephasing period and then direct ^{13}C detection. A single 50 kHz ^{13}C refocusing π pulse was placed at the center of the dephasing time and ^{1}H TPPM

decoupling of 70 kHz (6 mm rotor) or 100 kHz (4 mm rotor) was applied during both dephasing and detection [29]. The ^{13}C transmitter frequency was set to 155 ppm, and the ^{15}N frequency was near the isotropic peptide amide resonance (115 ppm). For the S_1 acquisition, the dephasing time contained a 40 kHz ^{15}N π pulse at the middle and end of each rotor period, while the S_0 acquisition did not contain these pulses. XY-8 phase cycling was used for the ^{15}N pulses [30, 31]. During the dephasing period, pulses were not actively synchronized to the rotor phase. To obtain optimal compensation of B_0, B_1, and spinning frequency drifts, S_0 and S_1 FID values were acquired alternately. The recycle delay was 1 s.

Chemical shifts were referenced to the methylene carbon resonance of adamantane (38.2 ppm). At room temperature and at 0 °C, ^{13}C NMR signals were attenuated, presumably because of slow motion. Hence, most measurements were made at −50 °C where the samples are rigid and the ^1H T_1 is < 1 s. With sufficient signal averaging time, spectra can also be obtained at room temperature and are similar to those observed at −50 °C except that some of the lines are narrower.

RESULTS

Figure 48 (a-c) are REDOR difference spectra of FPmn-, FPdm-, and FPtr-F8CL9N associated with LM3 bilayer membrane. Figure 48 (d) displays a REDOR difference spectrum of FPtr-F8CL9N associated with PC/PG bilayer membrane. Figure 48 (e) displays a REDOR difference spectrum of FPKKK associated with DPC micelle. For samples (a) – (e), the FP strand-to-lipid mol ratio were all approximately 1:100. The (a) – (e) spectra were each derived from the difference between the S_0 and the S_1 free-

induction decays (FID) and included 50 Hz line broadening. Because of the specific isotopic labeling and use of the REDOR difference, natural abundance signals are filtered out and only the signal from the labeled Phe-8 is detected in each spectrum.

For (a) – (c), the spectra are very similar and consist of a single line centered at 171 ppm with 2.3 ~ 2.5 ppm linewidth (full-width at half-maximum (FWHM)). This strong similarity suggests that the three membrane-bound peptides have similar structures in the vicinity of Phe-8. According to the chemical shift correlation table [9], a carbonyl carbon chemical shift of 171 ppm corresponds to β strand structure. These results are consistent with previous experiment [12] where LM3-associated structure in the vicinity of Phe-8 for FP23 and FPKKK has been demonstrated to adopt β strand conformation. In Figure 48 (b), the FPdm spectrum shows partial resolution of three components, which is not apparent in the displayed FPmn and FPtr spectra. However, we have also observed these components in spectra of some other FPmn samples and hence conclude that they are not uniquely related to FPdm.

In Figure 48 (d), the REDOR spectrum of FPtr associated with PC/PG bilayer membrane in a 1:100 peptide strand-to-lipid ratio yields a sharp line with a chemical shift peak at 176 ppm, which corresponds to helical structure in the vicinity of Phe-8.

In Figure 48 (e), the REDOR spectrum of FPKKK (F8CL9N) in frozen detergent DPC yields a sharp line with a chemical shift peak at 176 ppm, corresponding to helical structure. This observation is consistent with the results from solution NMR which show that FPmn is predominantly helical in detergent [1, 2].

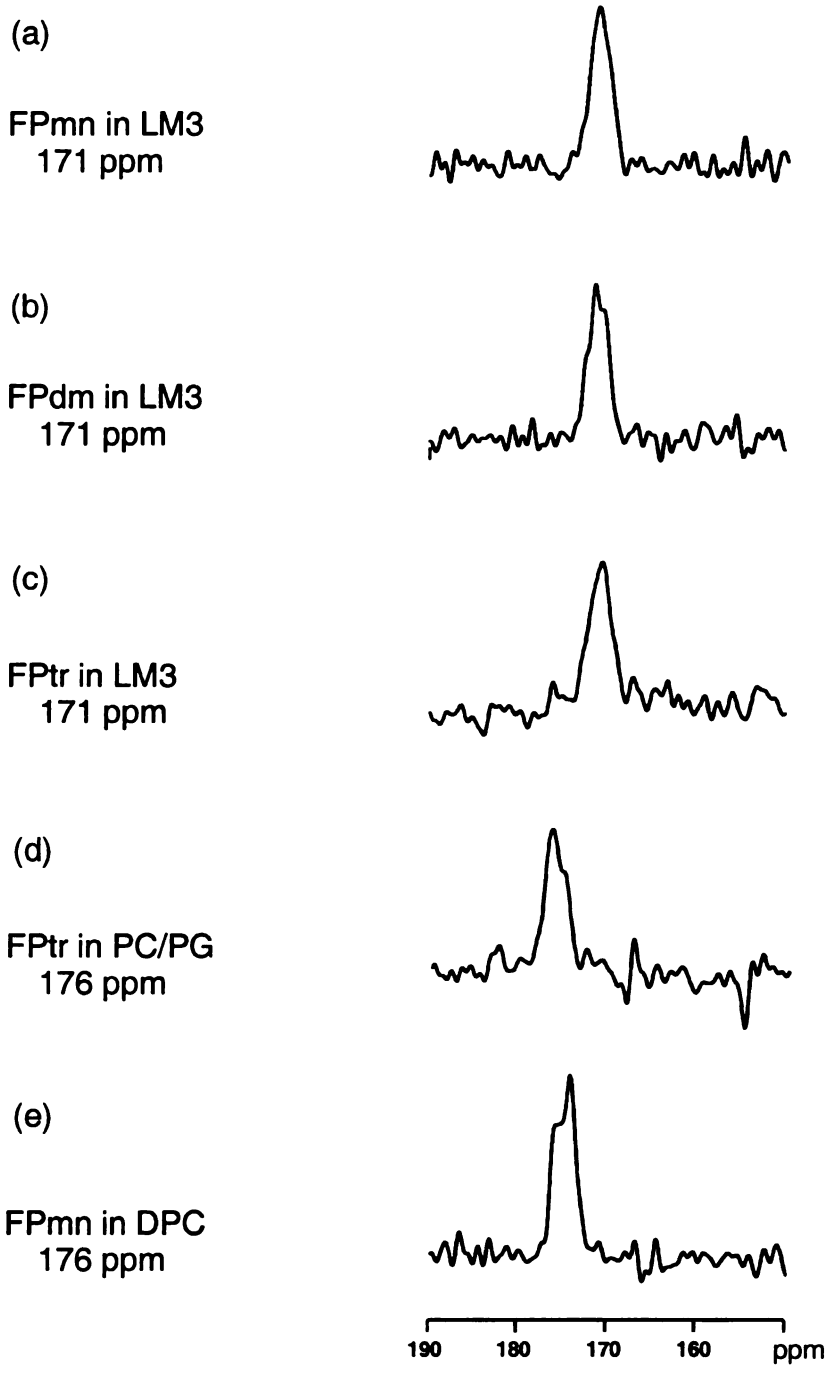

Figure 48. REDOR-filtered $S_0 - S_1$ difference spectra for (a) FPmn, (b) FPdm, (c) FPtr associated with LM3, (d) FPtr associated with PC/PG, and (e) FPmn associated with DPC micelle. All the peptides have ^{13}C carbonyl carbon label at Phe-8 and ^{15}N amide nitrogen label at Leu-9. Sample (a) contained 0.4 μmol FPKKKW and LUVs made from 40 μmole LM3 lipids. Sample (b) contained 0.2 μmol $(FPCKKKW)_2$ and LUVs made from 40 μmole LM3 lipids. Sample (c) contained 0.05 μmol FPtr and LUVs made from 15 μmole LM3 lipids. Sample (d) has 0.05 μmol FPtr and LUVs made from 15 μmole PC/PG lipids. Sample (e) contained 0.5 μmol of FPK3W and 50 μmol of DPC dissolved in 250 μL 5 mM HEPES buffer. The displayed spectra are dominated by the Phe-8 carbonyl signals.

DISCUSSION

We observed ~ 171 ppm ^{13}C chemical shift for FPmn-, FPdm-, and FPtr-F8CL9N associated with LM3 bilayer membrane and ~ 176 ppm ^{13}C chemical shift for FPtr-F8CL9N associated with PC/PG. The result for LM3-associated FP constructs is consistent with a model in which the N-termini of multiple fusion peptide strands insert into an LM3 membrane in a β strand conformation, and the result for PC/PG membranes is consistent with a model in which the N-termini of multiple fusion peptide strands insert into a PC/PG membrane in a helical conformation. The different secondary structures for the FP constructs embedded in different lipid bilayers indicated that the peptides' conformation is dependent on the membrane's lipid and cholesterol composition.

We examined the correlation between the secondary structure of the oligomeric fusion peptide constructs and their enhanced fusogenicity. We first considered the LM3-associated FPs that adopt β strand conformation. Additional solid-state NMR REDOR studies have shown that there are both parallel and antiparallel arrangements of strands for LM3-associated FPmn [12]. For FPdm and FPtr, their C-terminal cross-linking topology suggests parallel strand arrangement, since the C-terminal chemical bonds would likely enforce a parallel alignment for the multiple peptide strands. Furthermore, it is possible that the parallel alignment is more fusogenic than the antiparallel alignment. For the parallel alignment, the apolar N-terminal regions of two or more peptide strands could insert into the hydrophobic interior of the membrane, which could be more disruptive to the membrane than a single peptide strand (cf. Figure 49 (a)). This particular insertion topology is less likely with the antiparallel arrangement in which the polar and apolar ends of strands would be on the same side of the oligomer (cf. Figure 49 (b)).

Thus, FPmn, which has a mix of both parallel and antiparallel alignments, would be less fusogenic than FPdm and FPtr. The actual strand arrangement of the membrane-associated cross-linked peptides will be investigated by solid state NMR inter-strand distance measurements and other experimental methods.

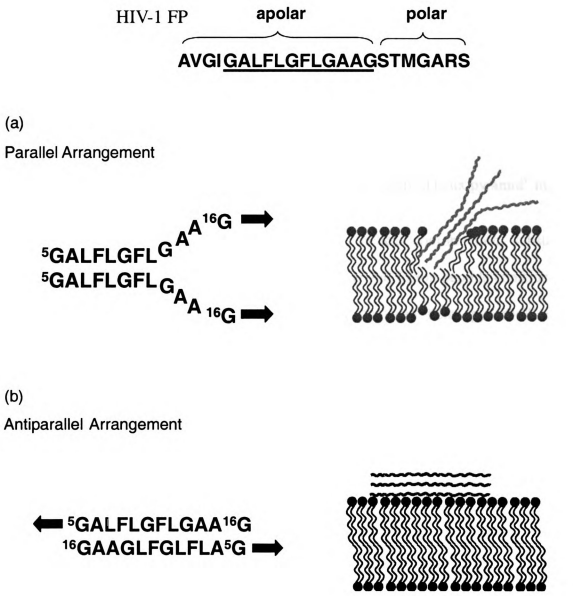

Figure 49. Peptide oligomerization and membrane insertion models for (a) parallel strand arrangement and (b) antiparallel strand arrangement. The arrows indicate the peptide direction from N-terminus to C-terminus while the numbers label the indices of individual residues.

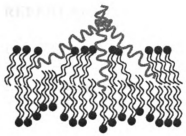

Figure 50. Membrane insertion topology according to the "splayed helix pyramid" model.

In PC/PG where the fusion peptide adopts helical conformation, substantial fusogenic enhancement was also observed for oligomerized fusion peptide constructs. In order to explain this phenomenon, I suggest the "splayed helix pyramid" model developed from influenza FHA2 fusion peptide trimerization by LeDuc et al. [32]. In this model, three N-terminal fusion peptides form a trimer, with each strand being a helix and inserting into the target cell membrane at an angle of ~ 65° from the bilayer normal (cf. Figure 50). The insertion topology resembles the shape of a pyramid, with the C-termini of the three helices in close proximity. I think that FPtr could adopt the "splayed helix pyramid" structure in PC/PG. The insertion of three FP strands into the bilayer would cause more membrane disruption than the insertion of one or two FP strands, and would correlate with higher fusogenicity.

It should be noted that in the solid-state NMR experiments, the peptide structure is observed after vesicle fusion has occurred. It is also possible that fusion requires a transient structure that is different from the NMR structure observed at the end state of fusion.

REFERENCE

1. Chang, D. K., Cheng, S. F., and Chien, W. J. (1997) *J. Virol. 71*, 6593-602.

2. Chang, D. K., Cheng, S. F., and Trivedi, V. D. (1999) *J. Biol. Chem. 274*, 5299-309.

3. Griffin, R. G. (1998) *Nat. Struct. Biol. NMR Suppl.*, 508-12.

4. Marassi, F. M., and Opella, S. J. (1998) *Curr. Opin. Struct. Biol. 8*, 640-8.

5. Sachleben, J. R., Frydman, V., and Frydman, L. (1996) *J. Am. Chem. Soc. 118*, 9786-9787.

6. Hing, A. W., Vega, S., and Schaefer, J. (1992) *J. Magn. Reson. 96*, 205-209.

7. Gullion, T., and Schaefer, J. (1989) *J. Magn. Reson. 81*, 196-200.

8. Gullion, T., and Schaefer, J. (1989) in *Advances in Magnetic Resonance* (Warren, W. S., Ed.) pp 57-83, Academic Press, New York.

9. Wishart, D. S., Sykes, B. D., and Richards, F. M. (1991) *J. Mol. Biol. 222*, 311-33.

10. Durrer, P., Galli, C., Hoenke, S., Corti, C., Gluck, R., Vorherr, T., and Brunner, J. (1996) *J. Biol. Chem. 271*, 13417-21.

11. Yang, J., Parkanzky, P. D., Khunte, B. A., Canlas, C. G., Yang, R., Gabrys, C. M., and Weliky, D. P. (2001) *J. Mol. Graph. Model. 19*, 129-35.

12. Yang, J., and Weliky, D. P. (2003) *Biochemistry 42*, 11879-11890.

13. Kliger, Y., Aharoni, A., Rapaport, D., Jones, P., Blumenthal, R., and Shai, Y. (1997) *J. Biol. Chem. 272*, 13496-505.

14. Slepushkin, V. A., Andreev, S. M., Sidorova, M. V., Melikyan, G. B., Grigoriev, V. B., Chumakov, V. M., Grinfeldt, A. E., Manukyan, R. A., and Karamov, E. V. (1992) *AIDS Res. Hum. Retroviruses 8*, 9-18.

15. Gordon, L. M., Curtain, C. C., Zhong, Y. C., Kirkpatrick, A., Mobley, P. W., and Waring, A. J. (1992) *Biochim. Biophys. Acta 1139*, 257-74.

16. Chang, D. K., Chien, W. J., and Cheng, S. F. (1997) *Eur. J. Biochem. 247*, 896-905.

17. Rafalski, M., Lear, J. D., and DeGrado, W. F. (1990) *Biochemistry 29*, 7917-22.

18. Pereira, F. B., Goni, F. M., Muga, A., and Nieva, J. L. (1997) *Biophys. J. 73*, 1977-86.

19. Mobley, P. W., Waring, A. J., Sherman, M. A., and Gordon, L. M. (1999) *Biochim. Biophys. Acta 1418*, 1-18.

20. Peisajovich, S. G., Epand, R. F., Pritsker, M., Shai, Y., and Epand, R. M. (2000) *Biochemistry 39*, 1826-33.

21. Martin, I., Defrise-Quertain, F., Decroly, E., Vandenbranden, M., Brasseur, R., and Ruysschaert, J. M. (1993) *Biochim. Biophys. Acta 1145*, 124-33.

22. Martin, I., Schaal, H., Scheid, A., and Ruysschaert, J. M. (1996) *J. Virol. 70*, 298-304.

23. Taylor, S. E., Desbat, B., Blaudez, D., Jacobi, S., Chi, L. F., Fuchs, H., and Schwarz, G. (2000) *Biophys. Chem. 87*, 63-72.

24. Yang, J., Gabrys, C. M., and Weliky, D. P. (2001) *Biochemistry 40*, 8126-37.

25. Caffrey, M., Cai, M., Kaufman, J., Stahl, S. J., Wingfield, P. T., Covell, D. G., Gronenborn, A. M., and Clore, G. M. (1998) *EMBO J. 17*, 4572-84.

26. Weissenhorn, W., Dessen, A., Harrison, S. C., Skehel, J. J., and Wiley, D. C. (1997) *Nature 387*, 426-30.

27. Gullion, T. (1998) *Conc. Magn. Reson. 10*, 277-289.

28. Yang, J., Parkanzky, P. D., Bodner, M. L., Duskin, C. A., and Weliky, D. P. (2002) *J. Magn. Reson. 159*, 101-110.

29. Bennett, A. E., Rienstra, C. M., Auger, M., Lakshmi, K. V., and Griffin, R. G. (1995) *J. Chem. Phys. 103*, 6951-6958.

30. Gullion, T., Baker, D. B., and Conradi, M. S. (1990) *J. Magn. Reson. 89*, 479-484.

31. Gullion, T., and Schaefer, J. (1991) *J. Magn. Reson. 92*, 439-442.

32. LeDuc, D. L., Shin, Y. K., Epand, R. F., and Epand, R. M. (2000) *Biochemistry 39*, 2733-9.

CHAPTER VIII

DEUTERIUM SOLID STATE NMR EVIDENCE FOR MEMBRANE BILAYER CURVATURE INDUCED BY THE HIV-1 FUSION PEPTIDE

BACKGROUND

Many experiments have suggested that the rate and efficiency of membrane fusion is modulated by the curvature properties of these membranes [1]. In the present work, we investigated the influence of a synthetic HIV-1 fusion peptide analog on the phospholipid membrane morphology. We used ^{2}H-NMR spectroscopy to probe the interaction of these peptides with model bilayer membranes similar in composition to those of host cells of the virus. ^{2}H-NMR spectra of the LM3 bilayer membrane system in the presence and absence of HIV fusion peptide were obtained to probe the specific effect of fusion peptide on lipid motion and structure, with the goal of relating observed changes to the fusion process. Our results suggest that the addition of fusion peptide promotes the formation of curvature in the lipid membranes.

1. Membrane Morphology

The curvature of biological and model membranes are determined by the bilayer arrangement of the phospholipid. This bilayer contains two opposing monolayers (cf. Figure 51, bilayer). In a membrane bilayer comprised of two identical monolayers, any curvature would lead to structural instability. Hence the bilayer has no tendency to curve. Different from this kind of bilayer curvature, each monolayer has an intrinsic curvature. This intrinsic curvature can be defined as the shape of the monolayer when it had attained its most stable structure, i.e. when the head groups were hydrated with water and the terminal methyl groups were surrounded with a nonpolar solvent [2, 3]. If both monolayers adopted the intrinsic curvature, they would bend in similar direction (assuming that the two monolayer have similar chemical composition), leading to

separation of the two monolayers. (cf. intrinsic curvature in Figure 49). Thus, the intrinsic curvature would cause instability in the bilayer structure [2].

Figure 51 [2]. (Left) Diagrammatic sketch of phospholipid arrangements. The bilayer is the arrangement of phospholipids commonly found in biological and model membranes. (Right) The hexagonal phase (H_{II}).

Generally there are two types of intrinsic monolayer curvature strain: negative curvature strain and positive curvature strain (cf. Figure 51, 52). When the membrane lipids have smaller cross-sectional area at the headgroup and larger cross-sectional area at the acyl chain, the membrane tends to have negative curvature strain. On the other hand, positive curvature strain occurs when the membrane lipids have large, well-hydrated, or repelling head groups and a smaller cross section at the acyl chain.

Hydrophobic substances such as hydrocarbons, diacyglycerols [2], and some viral fusion peptides can promote negative curvature strain. When the negative monolayer curvature rises to certain extent, the bilayer will convert to the hexagonal (H_{II}) phase. The left panel of Figure 51 displays the cross-section of a single hexagonal phase cylinder. This cylinder has a hydrophobic outlayer and is surrounded by other identical

cylinders in a hexagonal packing array with the structure extending perpendicular to the plane of the page (cf. Figure 51 right panel).

Positive curvature strain could be enhanced by detergents. When positive monolayer curvature strain becomes too large, the bilayer membrane forms micelles (cf. Figure 52).

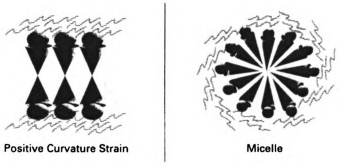

Figure 52. [3] Diagrammatic sketch of positive curvature strain (left) and micelle (right).

It has been suggested that viral fusion peptides promote membrane fusion by inducing negative curvature strain in the membranes [4]. Studies on influenza fusion peptide [5, 6], SIV fusion peptide [7, 8] and HIV fusion peptide [9] have demonstrated correlation between fusogenicity of these peptides and their ability to promote the formation of inverted hexagonal phase (H_{II}), which has a high degree of negative curvature [3].

These observations are consistent with the "stalk/TMC" fusion model [10, 11]. In this model, membrane fusion begins with the "stalk" intermediate, in which the contacting (cis) monolayers acquire negative curvature (cf. Figure 53). It has been proposed that fusion peptide may promote the formation of "stalk" intermediate by inducing negative curvature [1]. From "stalk", the membrane will proceed through a

series of morphological rearrangements that will lead to fusion pore formation.

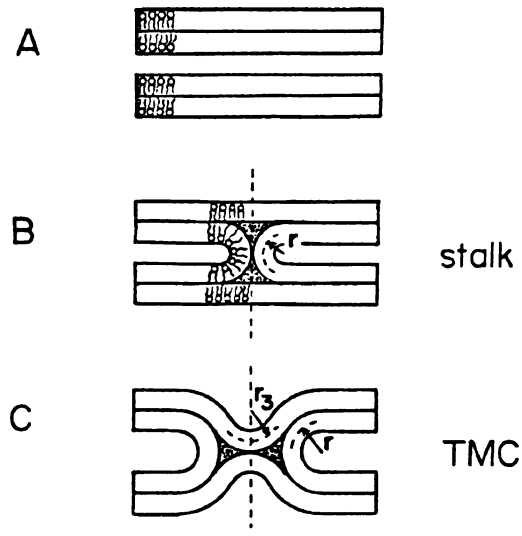

Figure 53 [10, 11]. Scheme for membrane fusion and inverted phase formation. (A) Two juxtaposed bilayers join to form the stalk, hemifusion intermediate (B), followed by a transmembrane contact (TMC) intermediate (C), which will lead to fusion pore formation during membrane fusion.

In our work, we studied the influence of synthetic HIV-1 fusion peptides on model bilayer membranes whose lipid headgroup and cholesterol composition are similar to that of the host cell of HIV-1 virus. The membrane structure and dynamics of the membrane lipids are probed by ^{2}H-NMR.

2. ^{2}H-NMR for Fusion Peptide Effect on Membrane Structure & Dynamics

2.1. ^{2}H Pake Doublet Powder Spectrum

Local structural information on fluid bilayer membranes could be obtained from the ^{2}H-NMR Pake powder pattern spectra [12] [13], which are usually acquired using a "Solid Echo" NMR pulse sequence which minimizes distortions in spectrum [14]. Figure 54 displays a Pake doublet powder spectrum:

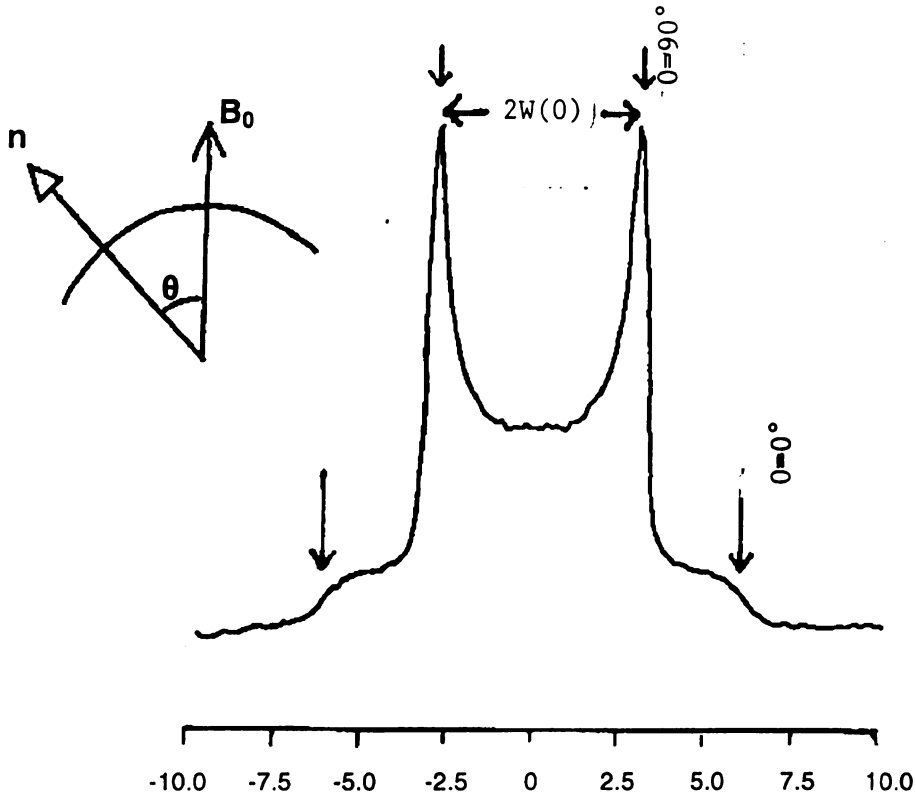

Figure 54. The experimental Pake doublet ^{2}H-NMR powder spectrum for DPPC-d_2 deuterated in the α-position of the phosphocholine (PC) polar head group. It is obtained as the Fourier transform of the quadrupolar echo signal [15].

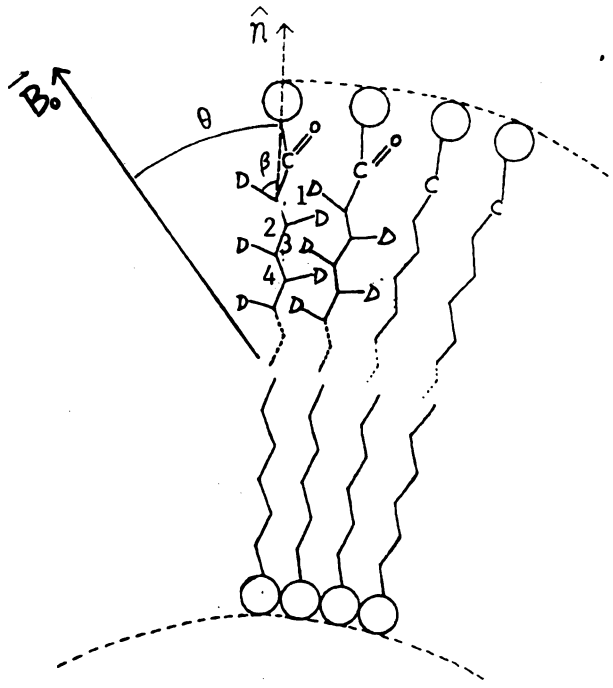

Figure 55. Model for the bilayer lipid membrane in the external magnetic field B_0. n is the bilayer local membrane normal. Each carbon position is numbered as 1, 2, 3, ...

For fluid membranes, the ^{2}H-NMR spectrum of a deuteron on a C-^{2}H bond of the membrane lipid is a doublet with a splitting $2\omega(\theta)$ [15], where θ (cf. Figure 55) is the angle between the external magnetic field and the bilayer normal. On the bilayer, the phospholipid molecules rotate rapidly about the surface normal, such that:

$$\omega(\theta) = \left| \delta_Q S_{CD} \left(3\cos^2 \theta - 1 \right) / 2 \right| \qquad (1)$$

where δ_Q (125 kHz) is ½ times the largest (θ=0°) NMR splitting in a sample containing rigid C-^{2}H, and S_{CD} is the orientational order parameter defined by:

$$S_{CD} = < \left(3\cos^2\beta - 1 \right) / 2 >_{\text{fast motions}} \qquad (2)$$

< > stands for the average over fast motion, and β is the angle between the C-^{2}H bond and the bilayer normal. S_{CD} varies between 0 and 1. These extrema correspond to rapid

isotropic motion and no motion, respectively. In Figure 54, the separation of peaks corresponding to $\theta = 90°$ in the powder spectrum yields the magnitude of the order parameter $|S_{CD}|$. According to equation 1:

$$S_{CD} = \omega(90°) / 62.5 \text{ kHz} \quad (3)$$

The shape of the Pake doublet spectrum indicates the fluidity of the lipid membrane [15]. A smaller splitting in the Pake powder pattern ($|S_{CD}|$) is a sign of more conformational freedom in the bilayer membranes. The observation of a Pake doublet spectrum with $|S_{CD}| < 0.5$ for a methylene deuteron on an acyl chain in a lipid bilayer is associated with the type of rapid axially symmetric motion characteristic of a fluid bilayer [15]. These motions include: (1) Transitions between different molecular conformations (often referred to as 'trans-gauche isomerizaton' in the case of acyl chains); and (2) rotations of the molecules around the bilayer normal.

In our experiment, the Pake powder spectra of side-chain ^2H-labeled phospholipid (DMPC-d54 cf. Figure 56) bilayer membranes are obtained in the presence and absence of HIV-1 fusion peptide. The ^2H quadrupolar splittings in the Pake patterns are compared to study the fusion peptide effect on different regions of the lipid bilayer

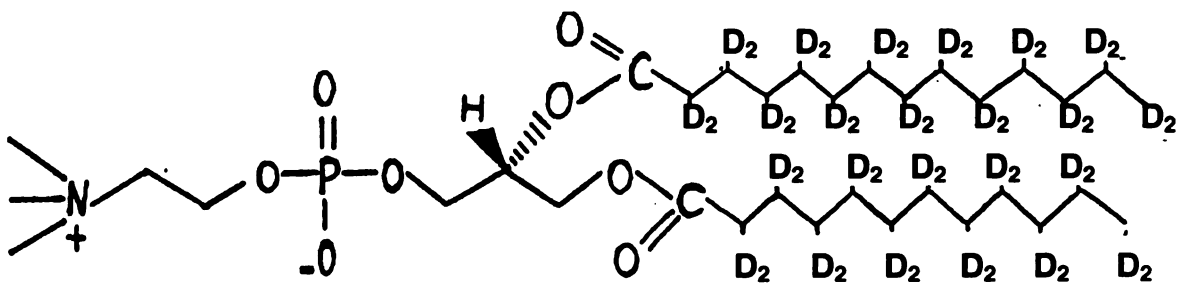

Figure 56. 2-Dimyristoyl-d54-sn-Glycero-3-Phosphocholine (DMPC-d54).

2.2. Relaxation-time Measurements

In NMR spectroscopy, the classical motion of the nuclear moment $\boldsymbol{\mu}$ in an applied magnetic field $\mathbf{B_0}$ can be understood as a rotation of the direction of $\boldsymbol{\mu}$ in a cone with its axis along $\mathbf{B_0}$. This is called Larmor precession [16], whose angular velocity is $-\gamma\mathbf{B_0}$ (γ, magnetogyric ratio, is a constant for a given nucleus). The corresponding Larmor frequency ω_0, is

$$\omega_0 = \left|\gamma/2\pi\right| B_0 \tag{4}$$

Any system with a magnetic moment will give Larmor precession. For an NMR sample containing many identical molecules, each having one magnetic nucleus, the total magnetic moment $\mathbf{M}$ of the sample is the vector sum of the individual nuclear moments $\boldsymbol{\mu}$:

$$\mathbf{M} = \sum \boldsymbol{\mu} \tag{5}$$

Therefore, the total magnetic moment $\mathbf{M}$ will be the resultant of the Larmor precession of each nuclear magnetic moment.

In addition to Larmor precession, the total magnetic moment $\mathbf{M}$ is also affected by the internal realignment of individual nuclear spins with the magnetic field $\mathbf{B_0}$. When the sample is placed in $\mathbf{B_0}$, its magnetization changes from 0 to $\mathbf{M_0}$, the thermal equilibrium value. The process for the magnetic moment to approach thermal equilibrium is referred to as relaxation. In Bloch equations that describe motion of the magnetic moment [17], the components of $\mathbf{M}$ decay to $\mathbf{M_0}$ exponentially, with the components of $\mathbf{M}$ parallel (M_z) and perpendicular (M_x, M_y) to $\mathbf{M_0}$ approaching their equilibrium values M_0 and 0 with different time constants T_1 and T_2.

$$M_z(t)-M_z(0)=[M_z(0)-M_0]\exp(-t/T_1) \tag{6}$$

$$M_x(t) = M_x(0)\exp(-t/T_2),\ M_y(t) = M_y(0)\exp(-t/T_2) \quad (7)$$

T_1 and T_2 are relaxation times [17]. T_1 describes the energy flow between the nuclear spin system and the other degrees of freedom of the system know as 'lattice', and is therefore named the spin-lattice relaxation time. It is also named the longitudinal relaxation time. T_2 describes the relaxation of M_x and M_y to 0. T_2 relaxation is caused by the direct interaction between the spins of different nuclei without energy transferred to the lattice, and is thus named the spin-spin relaxation time, or transverse relaxation time.

The T_1 relaxation processes are sensitive to relatively fast dynamical molecular motions characteristic of correlation times $\tau_1 \leq \omega_0^{-1}$ [18], where ω_0 may lie between a few MHz and about 500 MHz, depending on the magnetic field and nucleus being studied [15]. The fast motions that contribute to T_1 include transitions between different molecular conformations and rotations of the molecules around the bilayer normal [15]. T_2 is very sensitive to slow motions with correlation time $\tau_2 \gg \omega_0^{-1}$ [18]. The slow motions that contribute to T_2 in are interpreted as associated with molecular diffusion along curved membrane surfaces [18].

Relaxation-time measurements provide information on thermally driven molecular and membrane motions. In our experiments, ^2H spin-lattice relaxation (T_1) and spin-spin relaxation times (T_2) are determined at different peptide:lipid ratios to investigate the fusion peptide effect on the dynamic properties of membrane lipids.

MATERIALS AND METHODS

Materials. Dimyristoyl-sn-glycero-3-phosphocholine (DMPC), 1-palmitoyl-2-oleoyl-sn-glycero-3-phosphocholine (POPC), 1-palmitoyl-2-oleoyl-sn-glycero-3-

phosphoethanolamine (POPE), 1-palmitoyl-2-oleoyl-sn-glycero-3-[phospho-L-serine] (POPS), phosphatidylinositol (PI), sphingomyelin, and cholesterol were purchased from Avanti Polar Lipids, Inc. (Alabaster, AL). The Micro BCA™ protein assay was obtained from Pierce (Rockford, IL). N-2-hydroxyethylpiperazine-N'-2-ethanesulfonic acid (HEPES) was obtained from Sigma. All other reagents were analytical grade.

Peptides. FP23 peptides corresponding to the 23 N-terminal residues (AVGIGALFLGFLGAAGSTMGARS) of the LAV_{1a} strain of HIV-1 gp41 were synthesized as their C-terminal amides using a peptide synthesizer (ABI 431A, Foster City, CA) equipped for FMOC chemistry. A similar FP23KKK peptide was synthesized by combining the FP23 sequence with three C-terminal lysines. A 26 amino acid polypeptide melittin (GIGAVLKVLTTGLPALISWIKRKRQQ) is also synthesized. Melittin represents about 50 % of bee venom and its major function is to cause dissolution or destruction of natural and artificial lipid membranes [19].

Lipid Preparation. Samples were prepared using a lipid/cholesterol mixture which reflects the approximate lipid and cholesterol content of host cells of the HIV-1 virus [20]. The lipid mixture, denoted "LM3-DMPCdac" had DMPC, POPE, POPS, sphingomyelin, PI and cholesterol in a 10:5:2:2:1:10 mole ratio. DMPC was perdeuterated along the acyl sidechains. Another mixture, denoted "LM3" had POPC, POPE, POPS, sphingomyelin, PI and cholesterol in a 10:5:2:2:1:10 mole ratio was also prepared. Lipid and cholesterol powders were dissolved together in chloroform. The chloroform was removed under a stream of nitrogen followed by overnight vacuum pumping. Lipid dispersions were formed by addition of water or buffer containing 0.01% NaN_3 followed by homogenization with freeze-thaw cycles. Large unilamellar vesicles

(LUVs) of 100 nm diameter were prepared by extrusion [21]. In this approach, lipid dispersions were extruded ~ 30 times through two stacked 0.1 μm polycarbonate filters (Avestin, Inc., Ottawa, ON, Canada).

Static NMR Sample Preparation. Samples were prepared in two different ways. Method (1): Peptide and lipid (either dispersion or 100 nm diameter LUV) were mixed in 36 mL of 5 mM HEPES buffer (pH 7.0) which also contained 0.03% NaN_3. The mixtures were kept at room temperature overnight and then ultracentrifuged at 130,000 × g for four hours at 15 °C to pellet the peptide-lipid complex. Using the BCA assay, it was shown that the peptide binds quantitatively to lipid under these conditions and unbound peptide does not pellet [22]. The peptide/lipid pellet formed after ultracentrifugation was transferred by spatula to a NMR tube. Method (2): Peptide and lipid were mixed in 0.5 – 1 mL of aqueous solution and kept at room temperature overnight. Peptide-lipid complex was then transferred to an NMR tube. The peptide binding to lipid was nearly quantitative under these conditions [22].

Static NMR Experiment. Experiments were done on a 9.4 T spectrometer (Varian VXR or Varian Infinity Plus, Palo Alto, CA) using a Varian single resonance probe. The NMR detection channel was tuned to ^2H. The RF field was about 40 kHz. The quadrupolar echo sequence $(\pi/2) - \tau_1 - (\pi/2) - \tau_2 -$ acquire [23] was used to minimize effects from probe ring-down. The phase of the first $\pi/2$ pulse was x and the phase of the second $\pi/2$ pulse alternated between y and –y. Each $\pi/2$ pulse was 6.7 μs. τ_1 was 50 μs, and τ_2 was 40 μs. The recycle delay was 1 s.

T_1 Measurement. To determine the ^2H T_1, a $(\pi)_x - d_1$ inversion-recovery module [23] was inserted before the echo sequence, and the variation of the acquired signal was measured as a function of d_1. In the pulse sequence:

$$\pi - d_1 - (\pi/2) - \tau_1 - (\pi/2) - \tau_2 - \text{acquire}$$

a π pulse inverts the magnetization from $\mathbf{M_{z0}}$ to $-\mathbf{M_{z0}}$. This is followed by spin-lattice relaxation during d_1, when the magnetization tends towards its equilibrium value $\mathbf{M_{z0}}$ according to equation 6. The NMR signal is acquired after the quadrupolar echo sequence. The signal intensity is plotted as a function of recovery time d_1. Figure 57 displays an array of lipid mixture ^2H-NMR spectra with varied d_1 from 0 to 0.4 s. At short recovery time d_1 the signal will appear negative. At long times, full recovery is obtained. At some intermediate time the signal will be zero.

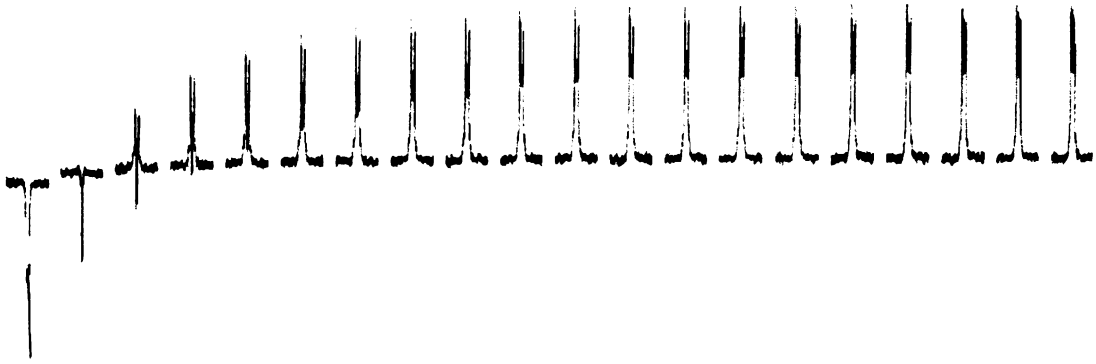

Figure 57. An array of lipid mixture ^2H-NMR spectra with varied d_2 from 0 to 0.4 s.

T_1 was determined by fitting the inversion-recovery data to the equation:

$$I(d_1) = I_i + \Delta I(1 - e^{-d_1/T_1}) \quad (8)$$

where $I(d_1)$ is the measured echo intensity, and I_i (the initial echo intensity), ΔI (the difference between the equilibrium and initial echo intensities), and T_1 (the longitudinal relaxation time) are fitting parameters.

T_2 Measurement. Taking the natural log of both sides of equation 7 yields:

$$\ln M_y = \ln M_{y0} - t/T_2 \quad (9)$$

Using the solid echo pulse sequence: $(\pi/2) - \tau_1 - (\pi/2) - \tau_2 -$ acquire, the decay of the acquired signal was measured as a function of synchronous increment of τ_1 and τ_2. T_2 can be determined by plotting the natural log of peak height (lnI) as a function of the total echo time, 2τ, where τ is the time from the end of the second $\pi/2$ pulse to the echo formation. The data were fit with the equation:

$$\ln[I(2\tau)] = \ln[I(0)] - 2\tau/T_2 \quad (10)$$

where $I(2\tau)$ is the measured echo intensity, and $I(0)$ (the initial signal intensity) and T_2 (the transverse relaxation time) are fitting parameters.

RESULTS AND DISCUSSION

Static Lipid NMR Spectra. Figure 58 displays ^2H NMR spectra of various static samples containing lipid or lipid plus peptide. All spectra were taken at 35 °C. In (a – e), the samples contained LM3-DMPCdac dispersions with FP23:lipid mole ratios of (a) 0, (b) 1:33, and (c) 1:10, and melittin:lipid mole ratios of (d) 1:33 and (e) 1:10. The (a), (c – e) samples were made by method (2) and the (b) sample was made by method (1). A sample with a composition identical to the (b) sample but made by method (2) gave a

spectrum similar to the displayed (b) spectrum (data not shown). Thus, the spectra appear to be approximately independent of whether sample preparation was done by method (1) or (2). In addition, the ^{31}P NMR spectra of the (a – c) samples are similar to those of LM3 samples, indicating that lipid phase is independent of whether the choline lipid is DMPC or POPC [24].

Each ^{2}H spectrum in (a – e) is a superposition of individual Pake powder patterns of the ^{2}H along the DMPC acyl chain. Each methylene position experiences a different amount of motion and thus has a different quadrupolar splitting. The motion increases and the quadrupolar splitting decreases as one moves from the phospholipid headgroup to the tail. As displayed in (a – c), there were minor changes in the ^{2}H NMR spectra with addition of fusion peptide. Relative to a pure LM3-DMPCdac sample, there appear to be some small increases in quadrupolar splittings with bound fusion peptide which are in the range of 1 – 3% for the 1:33 sample and 2 – 5% for the 1:10 sample. This is consistent with slightly less chain motion in the presence of peptide. In addition, the features that define the sharp "horns" of individual Pake patterns are broader in the presence of peptide, which is consistent with a more heterogeneous distribution of lipid motion.

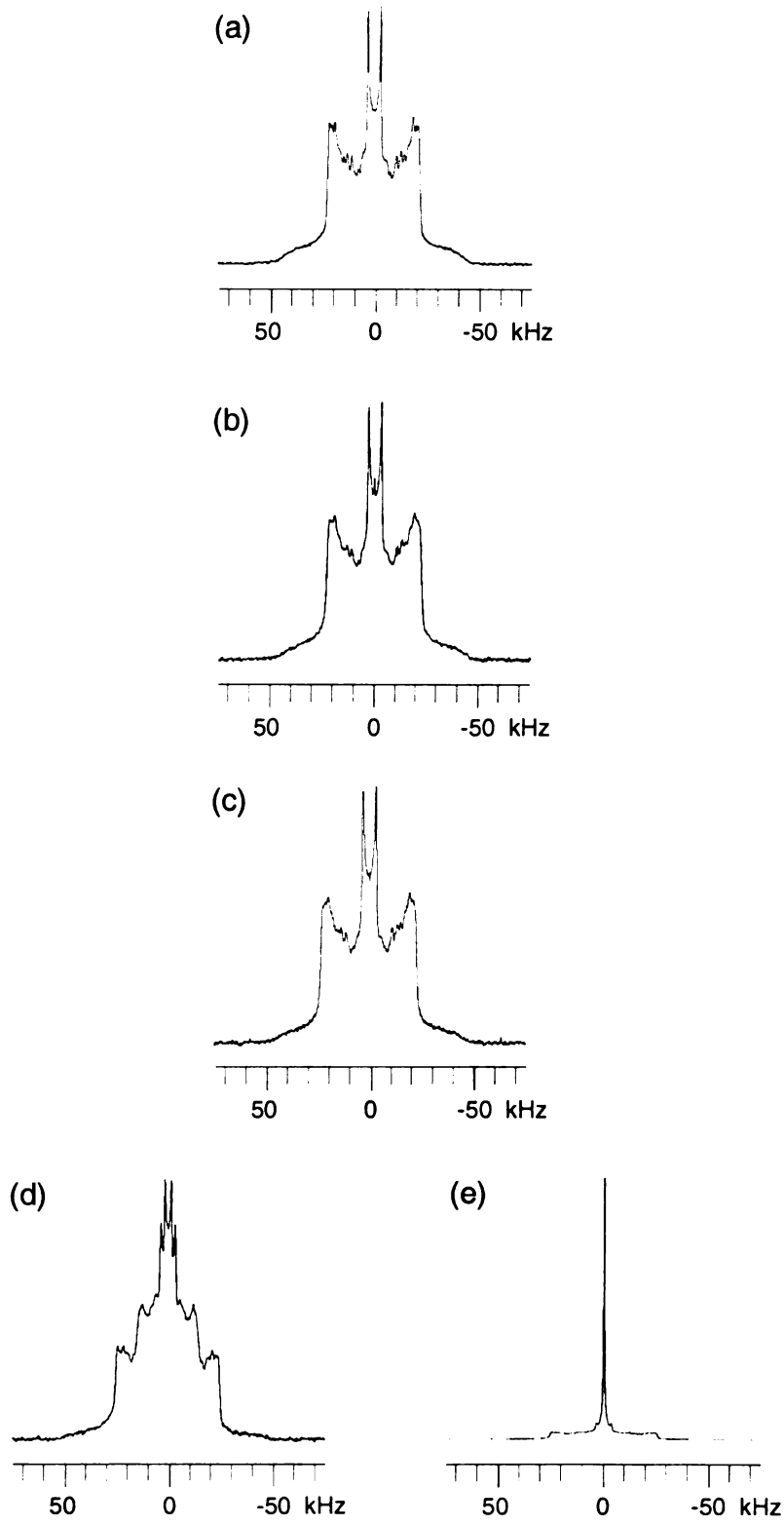

Figure 58. ^{2}H spectra of unoriented samples. All spectra were taken at 35°C. The ^{2}H spectra of an LM3-DMPCdac sample is presented in (a). Similar spectra are presented for

FP23:LM3-DMPCdac at (b) 1:33 and (c) 1:10 peptide lipid ratios and for melittin:LM3-DMPCdac at (d) 1:33 and (e) 1:10 peptide:lipid ratios. The (a) and (c)-(e) samples were made by method (2) and (b) sample was made by method (1). Each (a)-(e) spectrum was processed with 150 Hz line broadening and is the sum of 4000-6000 scans.

In large contrast, melittin induces a narrow isotropic ^2H feature which has ~ 200 Hz full-width at half-maximum (FWHM) linewidth and which is shifted about 300 Hz upfield of the ^2H_2O resonance. This feature is likely associated with formation of micelles which undergo fast isotropic reorientation.

The (a – e) spectra indicate that the HIV-1 fusion peptide and melittin have very different effects on the same lipid distribution, which reflects the different biological function of the two peptides. The role of fusion peptide is to induce viral/target cell membrane fusion. It is essential for the viral and target cell membrane to remain intact during fusion pore formation so that the cell could maintain its biological function after fusion. Therefore, the fusion peptide should not disrupt the equilibrium structure of the lipid membrane. Our NMR results indicate that in the presence of fusion peptide the membranes remain as a bilayer with slightly less chain motion and a more heterogeneous distribution of lipid motion. On the other hand, one of the major biological functions of melittin is to cause cell lysis (dissolution or destruction of cell membrane)[19], which is consistent with the observed micellization of lipids in the presence of melittin. Other investigators have also observed this effect of melittin in different lipid systems [19].

^2H T_1 and T_2 measurements. Measurements were made on LM3-DMPCdac dispersions containing no fusion peptide, and for dispersions containing 1:33, and 1:10 FP23:lipid ratios. The 1:33 sample was made by method (2) and the pure dispersion and 1:10 samples were made by method (1). For each of our spectra, we measured the

intensities of "outer" and "inner" features, as is visually shown in the Figure 59 (a). The intensity of the outer feature is mostly due to the ^2H close to the headgroups while the inner feature is mostly due to the ^2H in the terminal methyl group. The outer feature intensity was measured relative to the spectrum baseline while the inner feature intensity was measured relative to the approximate baseline intensity of the non-methyl deuteron transitions.

Figure 59 (b) displays the outer feature inversion-recovery data for the three samples. The best-fit relaxation times for these and other data sets are presented in Table 4. Within our fitting uncertainties, there is no difference between the outer feature T_1 values of the different samples. There are also not significant differences between the inner feature T_1 values of the different samples. The relative uncertainties of the inner feature T_1 values are greater than those of the outer feature values, in part because of the difficulty of determining the inner feature baseline.

Figure 59 (c) displays plots of the outer feature data for the three different samples and the best-fit T_2 values are presented in Table 4. There appears to be a 10 – 15% reduction in the outer feature T_2 with addition of fusion peptide. There is probably not a significant difference between the outer feature T_2 values of the 1:10 and 1:33 samples. The inner feature intensity data are qualitatively the same for the three samples. However, for these data, a plot of $\ln[I(2\tau)]$ vs. 2τ is non-linear, probably because of inaccuracy in baseline intensity subtraction. Thus, it is not reasonable to fit the inner feature data to equation 10.

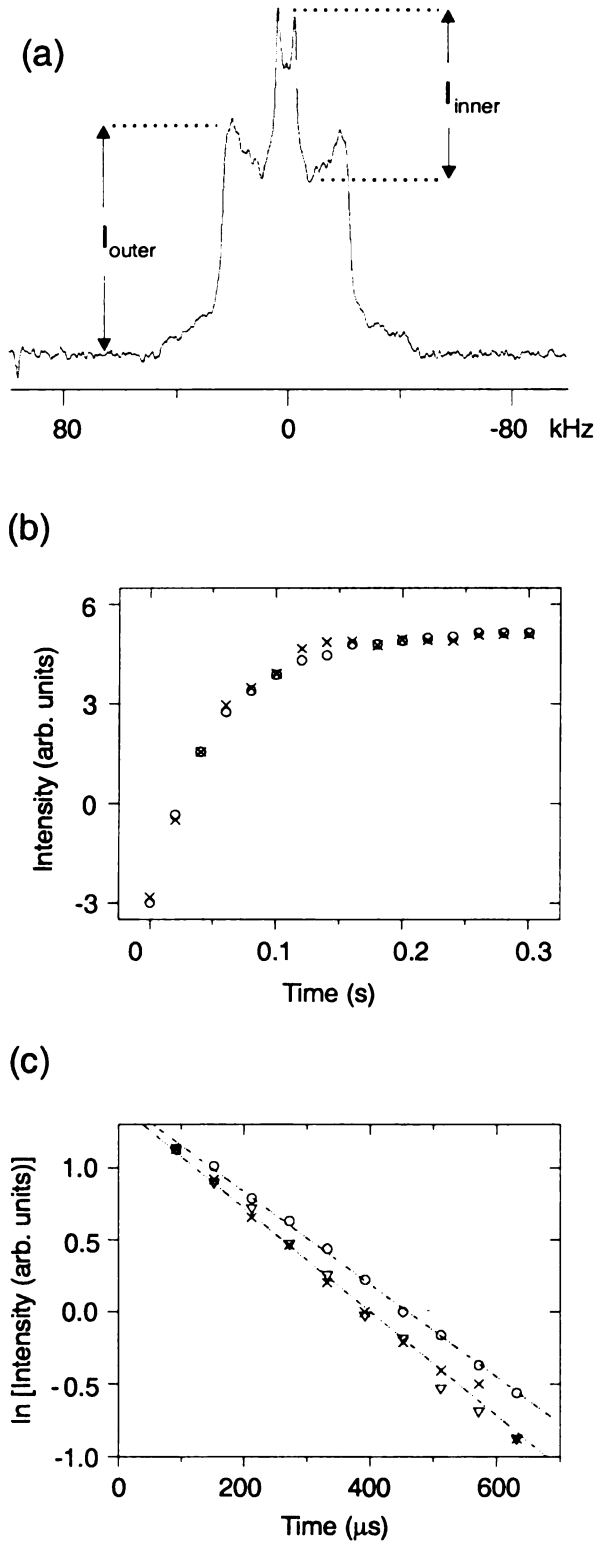

Figure 59. ^2H relaxation data. (a) Measurements of outer and inner intensities. I_{outer} is measured between the horns of the outer Pake pattern and the spectrum baseline. I_{inner} is measured between the horns of the inner Pake pattern and an approximate baseline from

the outer Pake pattern. (b) T_1 inversion recovery data of the outer Pake pattern. The pure LM3 (circles) and 1:10 FP23:LM3 (crosses) intensities are plotted as a function of d_1. There is little difference between LM3, 1:10 FP23:LM3 and 1:33 FP23:LM3 (data not shown). (c) T_2 data of the outer Pake pattern. The pure LM3 (circles), 1:33 FP23:LM3 (triangles) and 1:10 FP23:LM3 (crosses) data are plotted as a function of 2τ. In addition, the best-fits are shown for the LM3 and 1:10 FP23:LM3 samples. Addition of the peptide causes a 10 – 15% reduction in T_2.

Table 4. Lipid T_1 and T_2 Relaxation Times for Various Peptide:lipid Ratios

Nucleus	Peptide: Lipid Ratio*	Lipid Mixture	T_1 (s) #		T_2 (μs) #
^2H	0	LM3-DMPCdac	Outer	0.053 (0.001)	327 (10)
			Inner	0.34 (0.01)	794 (53)
	1:33	LM3-DMPCdac	Outer	0.050 (0.002)	268 (5)
			Inner	0.32 (0.06)	794 (84)
	1:10	LM3-DMPCdac	Outer	0.051 (0.002)	294 (10)
			Inner	0.31 (0.06)	709 (50)

* All fusion peptide in these samples was FP23KKK.

Relaxation time measurements reported as value (error).

CONCLUSION

We applied deuterium NMR to hydrated lipid membranes with bound HIV-1 fusion peptide. The lipid headgroup composition reflected the composition of the host cells of the virus. Phosphocholine lipid deuterated along its acyl chains was incorporated into the membranes. Our ^{2}H-NMR spectra are consistent with a predominant bilayer structure in the presence of bound fusion peptide and this differs from the work of other investigators who observed a significant component of isotropic phase [25]. This difference is likely due to the different lipid compositions used in the various studies.

The broadening of the "horns" of the individual Pake patterns in our ^{2}H spectra are consistent with a more heterogeneous distribution of lipid motion. The increase in quadrupolar splittings is consistent with a slight decrease in the motion of the acyl chains, possibly due to the insertion of the peptide into the membrane.

We noticed no significant change in the ^{2}H T_1 relaxation times with the addition of fusion peptide, however the ^{2}H and T_2 times decreased with the addition of fusion peptide. T_1 is sensitive to fast molecular motions including transitions between different molecular conformations and rotation around the bilayer normal. Our data for T_1 suggest that insertion of fusion peptide into the bilayer membrane does not significantly affect these molecular motions.

We interpret the decrease in T_2 as a result of more curvature in the bilayer membrane induced by insertion of fusion peptide. T_2 is strongly influenced by diffusion of phospholipid molecules along the membrane surface [18]. At our experimental temperature, the phospholipids could diffuse along the membrane surface. During diffusion, the ^{2}H spin on the C-^{2}H bond in the phospholipid acyl chain will experience

some fluctuation in the quadrupolar field due to variation of the C-^{2}H bond angle with respect to the external magnetic field B_0 (cf. Figure 55). Fluctuations in the quadrupolar field are essential for relaxation [26]. If the phospholipid was moving along a planar surface, the angle between the C-^{2}H bond and the external field B_0 would remain approximately the same during diffusion. As a result, there would be little fluctuation in the quadrupolar field experienced by the ^{2}H spin, and therefore, slower relaxation. When the phospholipid moves along a curved surface, the angle between the C-^{2}H bond with the external field B_0 will change, causing greater fluctuation in the quadrupolar field experienced by the ^{2}H spin. Thus, there is a correlation between the curvature in the membrane and field fluctuation, which might then explain the faster relaxation and shorter T_2 in the presence of fusion peptide.

Taken together, these lipid NMR results support a model in which the peptide acts as a fusion catalyst by inducing membrane curvature and reducing the energies of high-energy, highly curved fusion intermediates.

REFERENCE

1. Epand, R. M. E., R. F. (2000) *Biopolymers 55*, 358-363.

2. Epand, R. M., Shai, Y., and Segrest, J. P. (1995) *Biopolymers (Pept. Sci.) 37*, 319-338.

3. Epand, R. M. (1998) *Biochim. Biophys. Acta 1376*, 353-368.

4. Epand, R. M. (1997) *Biochem. Soc. Trans. 25 (3)*, 1073-1079.

5. Epand, R. M. a. E., R. F. (1994) *Biochem. Biophys. Res. Commun. 202*, 1420-1425.

6. Colotto, A. E., R. M. (1997) *Biochemistry 36*, 7644-7651.

7. Epand, R. F., Martin, I., Ruysschaert, J.-M. and Epand, R. M. (1994) *Biochem. Biophys. Res. Commun. 205*, 1938-1943.

8. Colotto, A., Martin, I., Ruysschaert, J.-M., Sen, A., Hui, S. W. and Epand, R.M. (1996) *Biochemistry 35*, 980-989.

9. Peisajovich, S. G., Epand, R. F., Pritsker, M., Shai, Y., and Epand, R. M. (2000) *Biochemistry 39*, 1826-33.

10. Siegel, D. P. (1993) *Biophys. J. 65*, 2124-2140.

11. Siegel, D. P. a. E., R. M. (1997) *Biophys. J. 73*, 3089-3111.

12. Davis, J. H. (1983) *Biochim. Biophys. Acta 737*, 117-171.

13. Schmidt-Rohr, K., and Spiess, H. W. (1994) *Multidimensional Solid-state NMR And Polymers*, Academic Press Limited, San Diego.

14. Davis, J. H., Jeffrey, K. R., Bloom, M., Valic, M. I., and Higgs, T. P. (1976) *Chem. Phys. Lett. 42*, 390-394.

15. Bloom, M., Evans, E., and Mouritsen, O. (1991) *Q. Rev. Biophys. 24*, 293-397.

16. Harris, R. K. (1983) *Nuclear Magnetic Resonance Spectroscopy, a Physicalchemical View*, Pitman Books Limited. London, UK. Section 1-6.

17. Harris, R. K. (1983) *Nuclear Magnetic Resonance Spectroscopy, a Physicochemical View*, Pitman Books Limited, London, UK. Section 3-2.

18. Bloom, M., and Sternin, E. (1987) *Biochemistry 26*, 2101-2105.

19. Dufourc, E. J., Smith, I. C., and Dufourcq, J. (1986) *Biochemistry 25*, 6448-55.

20. Aloia, R. C., Tian, H., and Jensen, F. C. (1993) *Proc. Natl. Acad. Sci. U. S. A. 90*, 5181-5.

21. Hope, M. J., Bally, M. B., Webb, G., and Cullis, P. R. (1985) *Biochim. Biophys. Acta 812*, 55-65.

22. Yang, J., Gabrys, C. M., and Weliky, D. P. (2001) *Biochemistry 40*, 8126-37.

23. Harris, R. K. (1983) *Nuclear Magnetic Resonance Spectroscopy, a Physicochemical View*, Pitman Books Limited, London, UK. Section 3-12.

24. Wasniewski, C., Canlas, C. G., and Weliky, D. P. Unpublished experiments.

25. Schanck, A., Peuvot, J., and Brasseur, R. (1998) *Biochem. Biophys. Res. Commun. 250*, 12-14.

26. Harris, R. K. (1983) *Nuclear Magnetic Resonance Spectroscopy, a Physicochemical View*, Pitman Books Limited, London, UK. Section 3-15.

CHAPTER IX

BINDING ASSAY

BACKGROUND

For fusion assay and solid-state NMR structural measurements, it is important to examine the binding strength of peptide to lipid. In fusion assays, our aim was to assess the correlation between numbers of strand in each peptide constructs and fusogenicity. In order to make a fair comparison, we need to determine whether all the peptide constructs bind quantitatively, or at least comparably to membranes. In solid-state NMR measurements, the NMR signals are observed for fusion peptide in all types of environment, i.e. membrane-bound or free. Since we are particularly interested in the structure of membrane-bound peptide, the contribution from the free peptide must be eliminated. Also, when we used ^{2}H NMR to probe the change of membrane morphology as a function of fusion peptide to lipid ratio, we need to verify quantitative binding of the fusion peptide with lipid membranes. Otherwise, the putative peptide to lipid ratio would not reflect their actual values.

For solid-state NMR samples, Yang et al. [1] demonstrated that there is strong binding between FPmn and LM3 bilayer membrane. Yang et al. estimated the percentage of binding by comparing the initial peptide concentration to that found in the supernatant after addition of lipid and subsequent centrifugation. The BCA assay was used to determine peptide concentration. During preparation of FPmn (FP or FPKKK) NMR samples at 10 μM peptide and 1 mM lipid, BCA data showed little peptide in the centrifugation supernatant [2]. As a control experiment, BCA assay measurement showed that in the absence of LM3, FPmn did not pellet under centrifugation. Taken together, these observations suggest quantitative association of FPmn with LM3.

For FPdm, BCA assay measurements also showed that it did not pellet under the ultracentrifugation conditions used to make the solid-state NMR samples in the absence of LM3 [3].

We did not directly test the binding affinity of FPdm and FPtr to LM3 and PC/PG membranes. However, there was approximately the same NMR signal per scan for the FPmn, FPdm, and FPtr sample (cf. Figure 48, Chapter VII), which is consistent with comparable (quantitative) membrane binding for the three peptide constructs.

For samples made under the conditions of the fusion assay (1.5 μM FPmn or 0.75 μM FPdm and 150 μM lipid), peptide binding was not accurately measured because of large background signals in the BCA assay from HEPES and uncentrifuged lipid. In this chapter, we describe the attempts to assess the binding strength of FPmn, FPdm, and FPtr to LM3 and PC/PG under fusion assay conditions.

METHODS

Binding Assessments Based on Centricon Separation of Free Peptide from Membrane-bound Peptide. In this experiment, we measured the binding of 1.5 μM FPmn (FPGCK6W) solution to 150 μM LM3, which are similar to the concentrations used in the fusion assays described in Chapter IV and V.

Solutions containing both FP and LM3 vesicles and reference solutions containing either LM3 vesicles or FP were prepared. We denoted the mixture as FP+L, and the two references as L and FP, respectively. These solutions were centrifuged on a Sorvall Ultracentrifuge (Newtown, CT) with a SW25.1 rotor (100,000 × g, 300 minutes). Supernatants were collected and lyophilized. The lyophilized supernatant for FP+L, L,

and FP were re-dissolved in 1.2 ml H_2O, and their 280-nm absorbance were measured. Next, the 1.2 ml solutions of FP+L, L, and FP were each placed in the top compartments of Centricons YM-10 (Millipore, MA) and were centrifuged on a Sorvall RC-5B centrifuge (Newton, CT) with a GSA rotor (14,000 × g, 300 – 420 minutes). Because the Centricon YM-10 is equipped with a membrane filter between the top and bottom compartments and is designed to sieve any particles greater than 10,000 Dalton, FPmn bound with LM3 vesicles or LM3 vesicles will not pass through the filter, since the mass of an LM3 vesicle (~ 100,000 lipid molecules per vesicle) is ~ 42,000,000 Dalton whereas unbound FPmn (M.W.~ 3000 g/mol) will pass through the filter. Therefore, separation of the membrane-bound peptide from unbound peptide can be achieved.

The 280-nm absorbance of the Centricon filtrate from FP+L, L, and FP were recorded and denoted as $A_{(FP+L)}$, $A_{(L)}$, and $A_{(FP)}$, respectively. The percentage of unbound peptide is calculated with the equation:

$$\text{Percent of Unbound FPmn} = [A_{(FP+L)} - A_{(L)}]/ A_{(FP)} \quad (1)$$

In this calculation, the percentage of unbound peptide is determined by dividing the difference of 280-nm absorbance of FP+L and L filtrate by the absorbance of pure FP filtrate. The reason to subtract the absorbance of L from FP+L is to correct for the background resulting from the lipids which has passed through the Centricon filter.

Binding Assessments Based on Fluorescence Energy Transfer. FPmn, FPdm, and FPtr all contain a Trp residue at the C-terminus of each fusion peptide strand. Their amino acid sequences are displayed in Figure 60. Fluorescence resonance energy transfer between the tryptophan (donor) and fluorescently labeled phospholipid (acceptor) was used to characterize the binding of the peptides with lipid vesicles. Binding of the

Figure 60. Amino acid sequences of FP constructs in the binding assessments.

peptides to the NBD-labeled vesicles puts the donor and acceptor in proximity such that excitation of the Trp in the peptide leads to an increase in the emission of the NBD-lipid.

In this experiment, LM3 and PC/PG vesicles were prepared. The LM-3 mixture had POPC, POPE, POPS, sphingomyelin, PI and cholesterol in a 10:5:2:2:1:10 mole ratio. The PC/PG mixture had POPC and POPG in a 4:1 mole ratio. In both LM3 and PC/PG lipid mixture, 2 mol % of N-NBD-PE lipids were added. Lipid and cholesterol powders were dissolved together in chloroform. The chloroform was removed under a stream of nitrogen followed by overnight vacuum pumping. Lipid dispersions were then formed with addition of 5 mM pH 7 HEPES buffer. After homogenization of the dispersion with ten freeze-thaw cycles, LUVs were prepared by extrusion through a polycarbonate filter with 100 nm diameter pores [4]

Fluorescence was recorded using 4 nm bandwidth using an Instruments S. A. Fluoromax-2 (Edison, NJ) spectrofluorimeter operating at excitation and emission wavelengths of 290 nm and 530 nm, respectively. A siliconized glass cuvette was used with continuous stirring in a thermostated cuvette holder. Measurements were carried out at 37 °C with ~ 2 ml of 150 μM LUV in H_2O. Peptide solution (FP strand concentration =

100 μM) was titrated into the liposome solution and the change in fluorescence of the sample was monitored during the titration.

RESULTS

Binding Assessments Based on Centricon Separation of Membrane-bound Peptide from Unbound Peptide. FPmn (FPGCK6W) was mixed with LM3 vesicles in 12 ml H_2O. The concentration of FPmn and LM3 were 1.5 and 150 μM, respectively. Two reference solutions were prepared: 1.5 μM FPmn solution and 150 μM LM3 solution. The sample and references were denoted as FP+L, FP, and L, respectively. For simplicity, all three solutions were made in H_2O instead of 5 mM pH 7 HEPES buffer. The ultracentrifuged supernatant of FP+L, FP, and L were lyophilized and re-dissolved in 1.2 ml H_2O. The 280-nm absorbance for the re-dissolved FP+L, L, and FP were 1.075, 1.060, and 0.101, respectively. The large absorbance of FP+L and L was due to light scattering from unpelleted lipids. Each of three solutions was placed in the top compartment of Centricon YM-10 and was centrifuged under a spinning force of 14,000 × g for 4 – 6 hours until most of the top solution went through the Centricon membrane into the bottom compartment of the Centricon. The 280-nm absorbance of the filtrates of FP+L, L, and FP, were 0.061, 0.052, and 0.053, respectively. Therefore we calculated the percentage of unbound peptide according equation 1:

Percent of Unbound FPmn = (0.061 – 0.052)/0.053 = 17 %

The experiment was repeated and the 280-nm absorbances of the filtrate of FP+L, L, and FP were 0.048, 0.049, and 0.045, respectively. The percentage of unbound FPmn = (0.048 – 0.049)/0.045 ~ 0 %. These results are consistent with approximately

quantitative binding of FPmn with LM3 bilayer membrane under the fusion assay conditions.

Since the result could be confounded by the possibility that the lipids that have already adhered to the Centricon filter may block unbound peptide, we did two control experiments. First, we re-centrifuged the FP filtrate (280-nm absorbance = 0.053) through the Centricon which had been used for centrifuging FP+L under similar spinning condition. The 280-nm absorbance of the re-centrifuged filtrate was 0.032. Comparing to the initial absorbance of 0.053, the result indicated that ~ 60 % (0.032/0.053) of free fusion peptide could pass through a Centricon contaminated with LM3 lipids. The other control experiment we did was to filter an FP solution with a 280-nm absorbance of 0.124 through a clean Centricon filter under similar centrifuging condition. The absorbance of the filtrate was 0.076, which means only ~ 60 % (0.076/0.124) of FP passed through the clean filter as well. Therefore, we concluded that LM3 lipids adhered to the Centricon filter would not change the filter's capability to trap unbound FP compared to a clean Centricon filter. In either case ~ 40% of free FP will be hold by the filter.

This approach was only successful for assessing membrane binding strength of FPmn. It was not suitable for measuring lipid affinity of FPdm and FPtr. Due to the oligomeric FPs' larger size and possibly higher affinity with the Centricon membrane, they could not pass through the centricon filter in the absence of lipids. As a result, separation of free oligomeric fusion peptide from membrane-bound peptide was not successful.

Binding Assessments Based on Fluorescence Energy Transfer. Titration of FPmn, FPdm, and FPtr to LM3 and PC/PG vesicles containing 2 mol % *N*-NBD-PE as

fluorescent acceptor resulted in an increase in the NBD fluorescence emission [5]. The fluorescence increase is interpreted as the result of energy transfer from the tryptophan (donor) on the peptides to the NBD (acceptor) on the lipid. Following each titration, the NBD fluorescence increased and then leveled off after 200 - 1500 seconds (depending on the different peptide used). This was recorded and the average fluorescence intensity in the platform was calculated. For each peptide, the average value of stabilized fluorescence intensity after each titration was plotted as a function of FP strand concentration. The profiles of FPmn, FPdm, and FPtr associated with LM3 and PC/PG are displayed in Figure 61 and 62, respectively. The fluorescence profiles for FPmn, FPdm, and FPtr are nearly identical in Figure 61, which indicates similar LM3 binding affinity for the three peptide constructs. In Figure 62, the patterns of fluorescence increase are also very similar for FPmn, FPdm, and FPtr, with the fluorescence of FPdm somewhat higher than that of FPmn and FPtr, suggesting the binding affinity of FPdm to PC/PG may be a little higher than the other two peptides. The fluorescence curve for FPtr is slightly higher than that of FPmn in Figure 62 (a). However, the FPtr profile is almost identical to that of FPmn in Figure 62 (b). Therefore we could not conclude that the binding strength of FPtr to PC/PG is higher than that of FPmn to PC/PG.

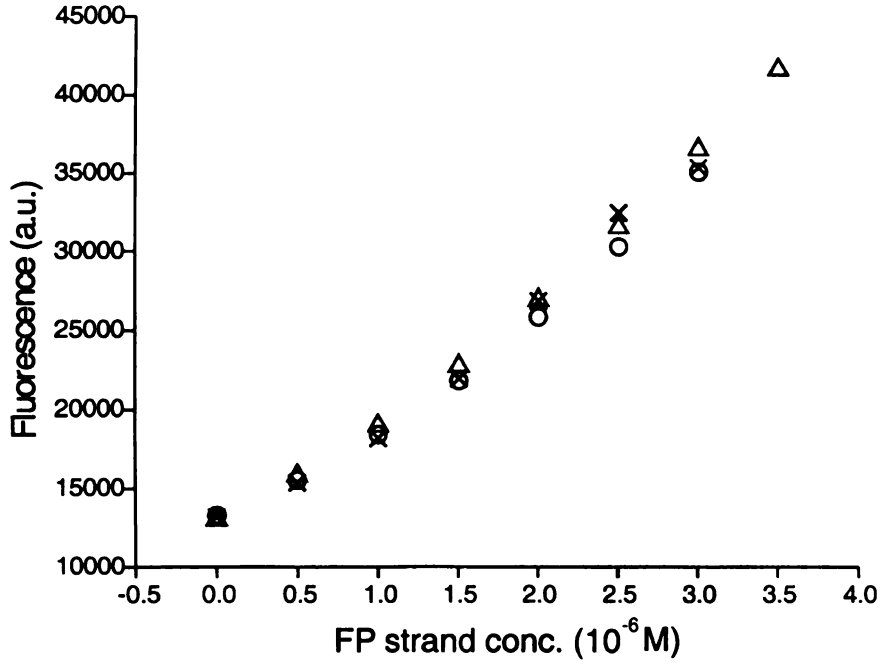

Figure 61. Titration of FPmn, FPdm, and FPtr with LM3/NBD-PE LUV (98:2 mol %) as monitored by fluorescence. Fluorescence emission were measured for LUV at 150 μM in 5 mM pH 7 HEPES buffer with increasing amounts of added peptide, and the fluorescence intensities in the range of 526 – 534 nm were integrated and plotted as a function of fusion peptide strand concentration. Fluorescence data were obtained in two consecutive experiments. The average values of the two measurements were used in the plot. ×, FPmn; Δ, FPdm; ○, FPtr.

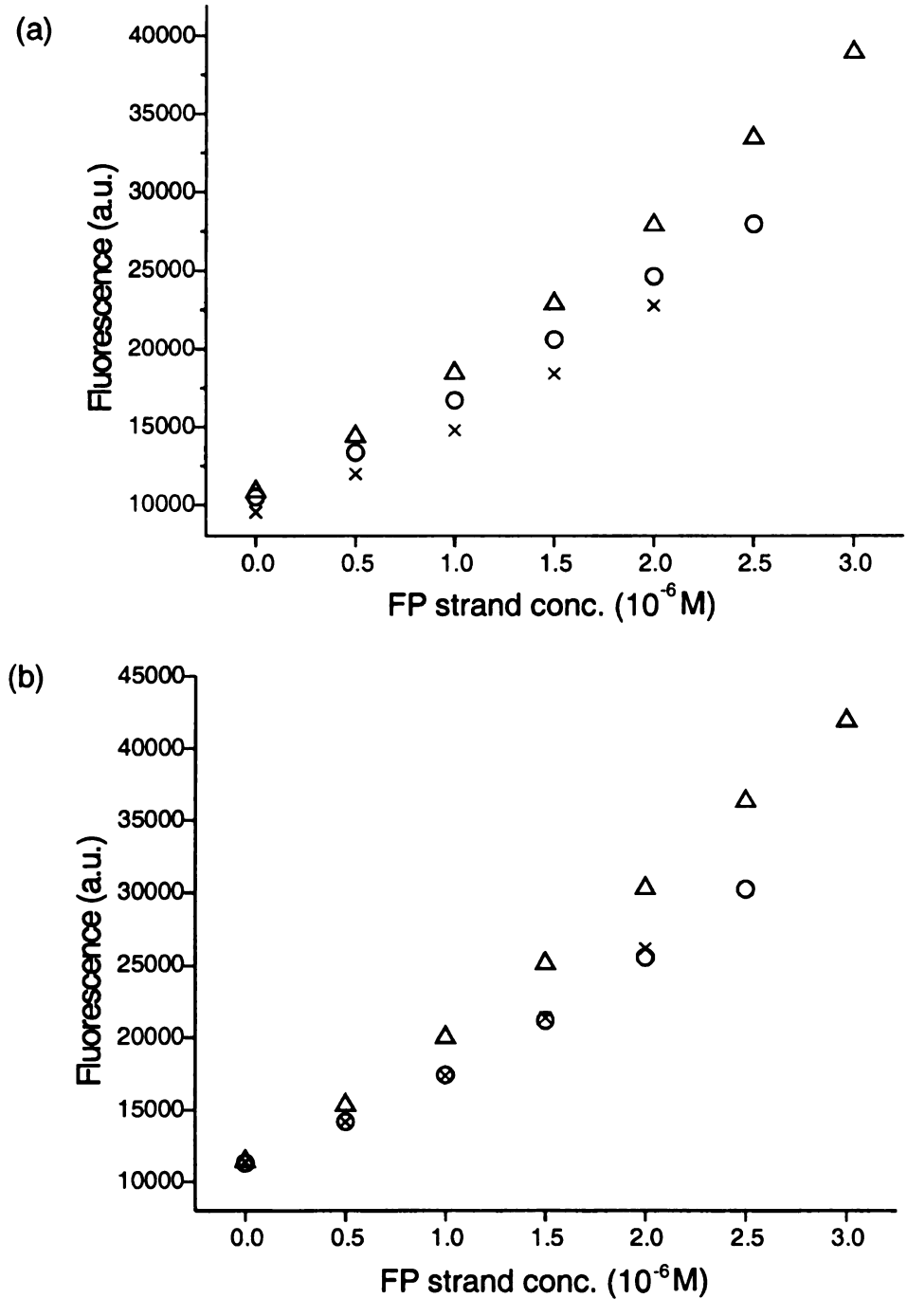

Figure 62. Titration of FPmn, FPdm, and FPtr with PCPG/NBD-PE LUV (98:2 mol %) as monitored by fluorescence obtained under similar condition in two sets of experiment (a, b). Fluorescence emission was measured for LUV at 150 μM in 5 mM pH 7 HEPES buffer with increasing amounts of added peptide, and the fluorescence intensities in the range of 526 – 534 nm were integrated and plotted as a function of fusion peptide strand concentration. ×, FPmn; Δ, FPdm; ○, FPtr.

DISCUSSION

With Centricon separation of free peptide from membrane-bound ones, we have determined that the binding of FPmn (FPGCK6W) to LM3 is 83 – 100% under fusion assay conditions. Based on fluorescence resonance energy transfer from Trp residue in the membrane-bound peptide to NBD-labeled lipids, we determined that the binding strength of FPmn, FPdm, and FPtr to LM3 bilayer membrane are approximately equal. The PC/PG lipid affinity of FPdm seemed to be slightly higher than that of FPmn and FPtr.

It is possible that the overall concentration of cross-linked fusion peptide in LM3 could be higher than that of FPmn because of higher lipid affinity of the cross-linked peptide, and this higher affinity could be an additional reason for the enhanced fusogenicty of the oligomeric fusion peptides, in addition to the higher local peptide concentration achieved with cross-linking. Our observations in this chapter point against different affinities of the different peptides to LM3. For PC/PG, FPdm has a little higher affinity to PC/PG lipids than FPmn or FPtr. However, the fusion activities are ordered FPtr > FPdm > FPmn so there is not a direct conclusion between binding affinity and fusogenicity. Interestingly, the affinity of the peptides for PC/PG and LM3 appear to be about the same, and may be due to the comparable hydrophobicity and charges of PC/PG and LM3 bilayers.

In related studies, other investigators have studied the lipid binding and fusogenicities of peptides that contained between 16 and 70 of the N-terminal residues of gp41 [6, 7]. Longer peptides had higher fusogenicities, but at 0.1 μM peptide concentration there were negligible differences in the lipid affinities of the different

peptides. These data are similar to the different fusogenicities and comparable binding that we observed for FPmn, FPdm, and FPtr.

REFERENCE

1. Yang, J., Gabrys, C. M., and Weliky, D. P. (2001) *Biochemistry 40*, 8126-37.

2. Yang, J., Prorok, M., Castellino, F. J., and Weliky, D. P. (2004) *Biophys. J. 87*, 1951-1963.

3. Yang, R., Yang, J., and Weliky, D. P. (2003) *Biochemistry 42*, 3527-3535.

4. Hope, M. J., Bally, M. B., Webb, G., and Cullis, P. R. (1985) *Biochim. Biophys. Acta 812*, 55-65.

5. Lau, W. L., Ege, D. S., Lear, J. D., Hammer, D. A., and DeGrado, W. F. (2004) *Biophys. J. 86*, 272-284.

6. Peisajovich, S. G., Epand, R. F., Pritsker, M., Shai, Y., and Epand, R. M. (2000) *Biochemistry 39*, 1826-33.

7. Sackett, K., and Shai, Y. (2002) *Biochemistry 41*, 4678-85.

CHAPTER X

SUMMARY AND WORK IN PROGRESS

The overall goal of this research is to understand some aspects of the HIV-1 fusion peptide-induced viral/target cell membrane fusion. My specific aim is to study the effect of fusion peptide oligomerization on its fusion catalyzing activity. The motivation of my project is to test the hypothesis that during fusion at least three fusion peptides insert into the target cell membrane with their C-termini in close proximity and that fusion peptide trimerization may be a structural requirement for HIV-1 viral/target cell fusion. Evidences for the significance of trimerization include high-resolution structure of trimerized viral envelope proteins [1, 2], findings of multiple trimers and corresponding high local fusion peptide concentration at the fusion site [3-5], and mutational studies [6]. Despite the importance of fusion peptide oligomerization, there is not a high-resolution structure to date for the fusion peptide domain in its membrane-inserted form because (1) its hydrophobicity impairs the high protein solubility required by X-ray crystallography and (2) the fast molecular tumbling required by solution NMR could not be satisfied due to immobilization of the fusion peptide by membrane lipids. Therefore we thought it would be interesting to study the membrane-insertion structure of HIV-1 fusion peptide as a trimer with three fusion peptide strands chemically cross-linked at their C-termini. We also thought it would be interesting to compare the fusogenicity of the trimeric fusion peptide with previously studied monomeric fusion peptide. These goals were achieved through peptide design/synthesis, analytical ultracentrifugation, fusion assay, electron microscopy, and solid-state NMR techniques.

In our approach, a series of monomeric and oligomeric peptides have been synthesized and are derived from the region of the HIV envelope glycoprotein that mediates membrane fusion during infection. Three major products are denoted as FPmn,

FPdm, and FPtr. Each contains the original fusion peptide sequence plus 3-6 extra lysines at the C-terminus to increase solubility and inhibit self-association of the peptide constructs. FPmn was synthesized with an automatic peptide synthesizer. FPdm was formed by cross-linking two monomeric fusion peptides through C-terminal cystine di-sulfide bond. An in-register trimer, FPtr, was created by cross-linking three monomeric fusion peptide through C-terminal lysine side-chains. Because fusion peptides contain many bulky, nonpolar amino acid residues, they tend to self-associate and form aggregates in aqueous solution. Since our aim was to study the correlation between numbers of strand in each construct with their relative fusogenicity, it is crucial to know that these peptide constructs do not aggregate in aqueous solution prior to interaction with the membrane. Analytical ultracentrifugation results demonstrated that at the peptide concentrations similar to those of the stock solution of fusion assays, the three peptide constructs' experimental fitted masses were close to their theoretical monomer masses. This indicated that there was no appreciable higher order aggregation in the assay buffer.

Fusogenicity of FPmn, FPdm, and FPtr were compared in a fusion assay in which the increase in NBD fluorescence due to lipid mixing induced by the fusion peptide constructs was monitored as a function of time. In the two vesicle systems (LM3 and PC/PG) that we have used, the long time changes of fluorescence were ordered $\Delta F_{tr} > \Delta F_{dm} > \Delta F_{mn}$, which indicated that oligomeric fusion peptides induced more vesicle fusion.

Because an increased fusion rate is likely the most important fusion peptide effect on viral/target cell fusion, the kinetics of the fluorescence data were analyzed to determine the variation of fusion rate with different constructs. In a single data set, the

initial fluorescence was modeled by a dominant, fast exponential build-up representing the lipid mixing induced by the initial interaction of fusion peptide with membranes. At longer times, there was an additional contribution from a slower build-up whose origin has not yet been understood. For both LM3 and PC/PG fusion, the fast fluorescence build-up rates were ordered $k_{tr}>k_{dm}>k_{mn}$, with $k_{tr}\sim40k_{mn}$ for LM3 and $k_{tr}\sim15k_{mn}$ for PC/PG. These findings suggest that the cross-linked peptides induce both a greater final extent and a more rapid rate of fusion than their non-cross-linked analogs.

We also studied the temperature dependence of fusion rate. Fluorescence data were obtained at five temperatures between 25 ~ 40°C and lnk was plotted over 1/T according to the Arrhenius equation. From the Arrhenius plot, activation energies, E_a, and pre-exponential factors, A were calculated for LM3 and PC/PG vesicle fusion induced by FPmn, FPdm, and FPtr. The trends in the data were: (1) $E_{a\text{-}tr}$ (LM3) ~ $E_{a\text{-}tr}$ (PC/PG), $\ln A_{tr}$ (LM3) ~ $\ln A_{tr}$ (PC/PG); and (2) for PC/PG vesicle fusion, $E_{a\text{-}tr} < E_{a\text{-}dm}$, $E_{a\text{-}mn}$ & $A_{tr} < A_{dm}$, A_{mn}. We did not obtain the E_a and A values for LM3 fusion induced by FPmn and FPdm since the Arrhenius plots for these two cases were not linear.

In addition to the fusion assay, images from transmission electron microscope also provided evidence for a strong correlation between C-terminal cross-linking and enhanced fusogenicity. In order to establish a structure-function relationship for the oligomeric fusion peptides, we used solid-state NMR REDOR chemical shift measurements to determine the secondary structure of FPmn, FPdm, and FPtr in their membrane-inserted forms. Previous solid-state NMR results in this group have demonstrated that in LM3 at peptide/lipid ratio $\geq$ 0.010, the N-terminal and central regions of the peptide adopt a nonhelical β strand structure [7]. In Figure 48 (a-c) of

Chapter VII, the 1-D solid-state NMR spectra for the Phe-8 carbonyl are very similar for LM3-associated FPmn, FPdm, and FPtr, which suggests that FPdm and FPtr also forms a β strand at this residue. Additional solid-state NMR REDOR studies have shown that there is ~ 50% fusion peptide population of LM3-associated FPmn which adopts an approximately in-register parallel strand arrangement [8]. In the contexts that cross-linked fusion peptides are significantly more fusogenic than their non-cross-linked analogs, this finding is interesting because the in-register parallel strand arrangement is likely to be a reasonable extension of the known ectodomain oligomeric structure and this arrangement also has a distinct apolar region of the fusion peptide oligomer which could insert into the membrane and catalyze fusion [8]. The other 50 % of FPmn associated with LM3 was found to adopt antiparallel strand arrangement. It does not seem clear to us how the oligomer could insert into the membrane with this type of strand arrangement. Therefore, LM3-associated FPdm and FPtr with their in-register parallel β strand conformation enforced by their C-terminal cross-linking would be more fusogenic than FPmn, which has a mix of both parallel and antiparallel alignment.

For PC/PG-associated fusion peptides, Figure 48 (d) indicates that PC/PG-associated FPtr adopts helical structure. The "splayed helix pyramid" model may explain the enhanced fusogenicity for the helical-structured fusion peptide trimer [9].

In addition to studying the secondary structure of membrane-bound fusion peptide by solid-state NMR chemical shift measurement, we applied ^{2}H solid-state NMR to probe the fusion peptide effect on ^{2}H labled membrane lipids. Our results are consistent with a model in which the addition of fusion peptide promotes the formation of curvature in the lipid membranes.

In summary, the present research demonstrated a strong correlation between C-terminal cross-linking and enhanced fusogenicity of the HIV-1 fusion peptide. The fusion enhancement effect of trimeric HIV-1 fusion peptides may be due to the following reasons:

(1) Placement of apolar N-terminal regions on one end of the oligomer may facilitate membrane insertation.

(2) Larger apolar volume relative to FPmn and the consequent greater membrane disruption and fusion rate.

(3) Larger free energy released upon membrane binding of multiple FP strands.

Our observations using various experimental techniques are consistent with the hypothesis that trimerization of fusion peptide may be a structural requirement for viral/target cell membrane fusion. The topology achieved through C-terminal cross-linking should be similar to the fusion peptide topology thought to exist in the fusogenic form of HIV-1 gp41.

Because it is possible to obtain FPtr in ~ 1 μmol quantities and because it has negligible self-association in aqueous solution, it should be possible to study its structural and motional properties in aqueous, detergent, and membrane environments with a variety of biophysical methods. These studies should provide further insight into its enhanced fusion rate. The synthetic approach should also be applicable to fusion peptides from other viruses and perhaps to other membrane-associated peptides derived from proteins of known oligomeric stoichiometry.

There are many remaining questions including the actual strand arrangement of FPdm and FPtr associated with LM3 membranes. When we tried to correlate the peptide

constructs' membrane-bound structure with their enhanced fusogenicity, we hypothesized that both FPdm and FPtr would prefer parallel strand arrangement in LM3. This assumption is based on the C-terminal cross-linking topology of FPdm and FPtr, in which the covalent bond would be likely to enforce a parallel arrangement for the multiple peptide strands. However, we have not yet obtained experimental evidence for this assumption. Work in progress in this group involves solid-state NMR measurements of the inter-strand distance for FPdm and FPtr. One possible approach would be to form the FPdm by cross-linking equal amount of two types of fusion peptide monomer: one has [^{13}C] carbonyl label at Phe 8, and the other has [^{15}N] amide label at Phe 8. If the two peptides strands adopt an in-register parallel β arrangement in FPdm, the hydrogen bonding between the two strands can be detected using ^{13}C – ^{15}N distance measurement. For FPtr, a radio frequency-driven dipolar recoupling (RFDR) experiment [10] will be employed to probe the inter-strand distance based on homonuclear dipolar coupling between ^{13}C labeled carbonyl carbon on each strand.

REFERENCE

1. Weissenhorn, W., Dessen, A., Harrison, S. C., Skehel, J. J., and Wiley, D. C. (1997) *Nature 387*, 426-30.

2. Caffrey, M., Cai, M., Kaufman, J., Stahl, S. J., Wingfield, P. T., Covell, D. G., Gronenborn, A. M., and Clore, G. M. (1998) *EMBO J. 17*, 4572-84.

3. Munoz-Barroso, I., Durell, S., Sakaguchi, K., Appella, E., and Blumenthal, R. (1998) *J. Cell Biol. 140*, 315-23.

4. Bentz, J. (2000) *Biophys. J. 78*, 227-45.

5. Bentz, J. (2000) *Biophys. J. 78*, 886-900.

6. Freed, E. O., Delwart, E. L., Buchschacher, G. L., Jr., and Panganiban, A. T. (1992) *Proc. Natl. Acad. Sci. U. S. A. 89*, 70-4.

7. Yang, J., Gabrys, C. M., and Weliky, D. P. (2001) *Biochemistry 40*, 8126-37.

8. Yang, J., and Weliky, D. P. (2003) *Biochemistry 42*, 11879-11890.

9. LeDuc, D. L., Shin, Y. K., Epand, R. F., and Epand, R. M. (2000) *Biochemistry 39*, 2733-9.

10. Bennett, A. E., Ok, J. H., Griffin, R. G., and Vega, S. (1992) *J. Chem. Phys. 96*, 8624-8627.